BioMed Research International

Cell/Tissue Microenvironment Engineering and Monitoring in Tissue Engineering, Regenerative Medicine, and In Vitro Tissue Models

Guest Editors: Nihal Engin Vrana, Vasif Hasirci, Garrett Brian McGuinness, and Albana Ndreu-Halili

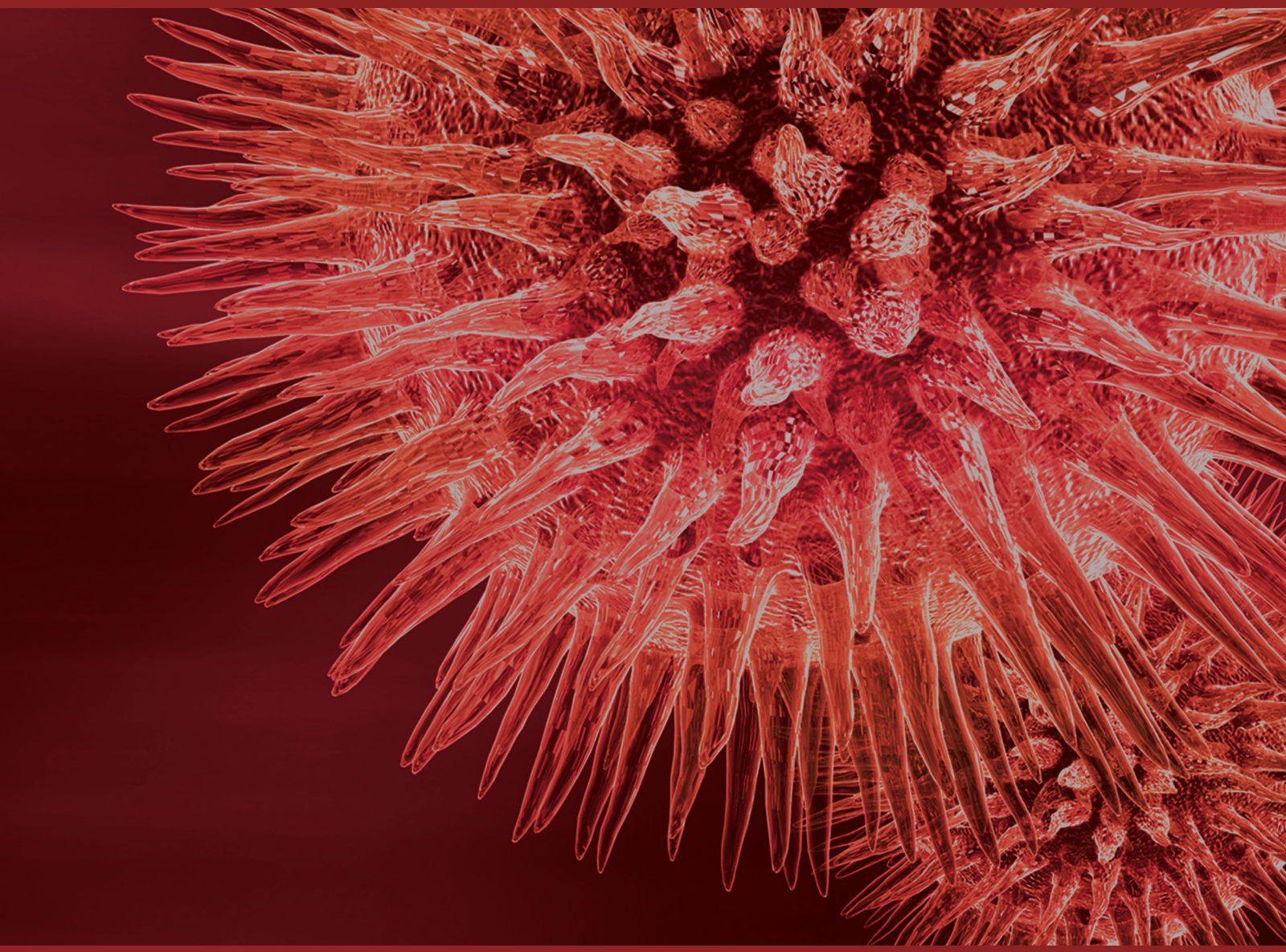

Cell/Tissue Microenvironment Engineering and Monitoring in Tissue Engineering, Regenerative Medicine, and In Vitro Tissue Models

BioMed Research International

Cell/Tissue Microenvironment Engineering and Monitoring in Tissue Engineering, Regenerative Medicine, and In Vitro Tissue Models

Guest Editors: Nihal Engin Vrana, Vasif Hasirci, Garrett Brian McGuinness, and Albana Ndreu-Halili

Contents

Cell/Tissue Microenvironment Engineering and Monitoring in Tissue Engineering, Regenerative Medicine, and In Vitro Tissue Models, Nihal Engin Vrana, Vasif Hasirci, Garrett Brian McGuinness, and Albana Ndreu-Halili
Volume 2014, Article ID 951626, 2 pages

Cell Microenvironment Engineering and Monitoring for Tissue Engineering and Regenerative Medicine: The Recent Advances, Julien Barthes, Hayriye Özçelik, Mathilde Hindié, Albana Ndreu-Halili, Anwarul Hasan, and Nihal Engin Vrana
Volume 2014, Article ID 921905, 18 pages

The ECM-Cell Interaction of Cartilage Extracellular Matrix on Chondrocytes, Yue Gao, Shuyun Liu, Jingxiang Huang, Weimin Guo, Jifeng Chen, Li Zhang, Bin Zhao, Jiang Peng, Aiyuan Wang, Yu Wang, Wenjing Xu, Shibi Lu, Mei Yuan, and Quanyi Guo
Volume 2014, Article ID 648459, 8 pages

The Effect of Autologous Activated Platelet Rich Plasma (AA-PRP) Injection on Pattern Hair Loss: Clinical and Histomorphometric Evaluation, V. Cervelli, S. Garcovich, A. Bielli, G. Cervelli, B. C. Curcio, M. G. Scioli, A. Orlandi, and P. Gentile
Volume 2014, Article ID 760709, 9 pages

The Study of the Frequency Effect of Dynamic Compressive Loading on Primary Articular Chondrocyte Functions Using a Microcell Culture System, Wan-Ying Lin, Yu-Han Chang, Hsin-Yao Wang, Tzu-Chi Yang, Tzu-Keng Chiu, Song-Bin Huang, and Min-Hsien Wu
Volume 2014, Article ID 762570, 11 pages

Characterization of Silk Fibroin Modified Surface: A Proteomic View of Cellular Response Proteins Induced by Biomaterials, Ming-Hui Yang, Shyng-Shiou Yuan, Tze-Wen Chung, Shiang-Bin Jong, Chi-Yu Lu, Wan-Chi Tsai, Wen-Cheng Chen, Po-Chiao Lin, Pei-Wen Chiang, and Yu-Chang Tyan
Volume 2014, Article ID 209469, 13 pages

Hindawi Publishing Corporation
BioMed Research International
Volume 2014, Article ID 951626, 2 pages
http://dx.doi.org/10.1155/2014/951626

Editorial

Cell/Tissue Microenvironment Engineering and Monitoring in Tissue Engineering, Regenerative Medicine, and In Vitro Tissue Models

Nihal Engin Vrana,[1,2] Vasif Hasirci,[3] Garrett Brian McGuinness,[4] and Albana Ndreu-Halili[5]

[1] *Protip SAS, 8 Place de l'Hôpital, 67000 Strasbourg, France*
[2] *Institut National de la Santé et de la Recherche Médicale (INSERM), UMR-S 1121, "Biomatériaux et Bioingénierie", 11 rue Humann, 67085 Strasbourg Cedex, France*
[3] *Department of Biological Sciences and BIOMATEN, CoE Biomaterials and Tissue Engineering, Middle East Technical University, Biotechnology Research Unit Building, 06800 Ankara, Turkey*
[4] *Mechanical and Manufacturing Engineering, Centre for Medical Engineering Research, Dublin City University, Dublin 9, Ireland*
[5] *Department of Computer Engineering, Epoka University, Tirana 1039, Albania*

Correspondence should be addressed to Nihal Engin Vrana; e.vrana@protipmedical.com

Received 16 July 2014; Accepted 16 July 2014; Published 26 August 2014

In any engineered system, the understanding of the properties and interactions between the system components is of utmost importance for a successful outcome. The main components in engineered tissues are the cells, the materials used in construction of scaffolds, soluble or immobilized bioactive agents, and physical and chemical stimuli presented by the environment. As most of the mammalian tissues are constructed by bringing together repeating units of microscale complex tissue structures, understanding and control of all these components would provide the tissue engineers the capability to overcome clinical challenges as well as to develop technologies for high fidelity tissue models suitable for pharmacology, toxicology, and disease modelling applications.

As tissue engineering and regenerative medicine fields mature, the level of information about how cells interact with the surrounding scaffold materials and/or other cells has increased, too. Cell microenvironment, which can be defined as the sum of all the stimuli that stem from the neighborhood of a cell and have direct or indirect effects on a given cell, has become an important consideration in exerting more control over the interactions of the cells with engineered structures.

Another important aspect of tissue engineering and regenerative medicine is their temporal nature. An engineered tissue is actively remodelled over a period of time either in vitro or in vivo and currently our ability to influence this process in order to interfere with the sequence of events to achieve better regeneration is limited. However, developments in noninvasive monitoring methods and biosensor systems have begun to provide the necessary tools for tissue engineers to have real-time information about engineered tissues.

This special issue set out to demonstrate the current developments and future perspectives in the use of cell microenvironment engineering and monitoring in producing functional tissues. Several investigators contributed original research or review articles about the different aspects of cell microenvironment. M.-H. Yang et al. (2014) focused on a natural biomaterial, silk fibroin, and analyzed its interaction with fibroblasts. They used proteomic approaches to understand the interaction of the cells with the substrate formed by silk fibroin in the presence of carbon nanotubes. V. Cervelli et al. (2014) demonstrated the importance of the introduction of bioactive agents in the cell microenvironment in a clinical

setting in the specific example of the treatment of male pattern hair loss. They have used platelet rich plasma (PRP) injections to the scalp and observed a significant increase in hair density, epithelial thickness, and number of hair follicles.

W.-Y. Lin et al. (2014) studied another important aspect of cell microenvironment, namely, the effect of dynamic mechanical stress/strain conditions. They have developed a system which can apply cyclic compressive stress to chondrocytes at physiologically relevant levels. They have shown that the application of stress has a direct effect on the chondrocyte metabolic activity and glycosaminoglycan secretion. Another aspect of cartilage tissue engineering, the extracellular matrix/chondrocyte interactions, was reviewed by Gao et al. (2014), where they focused on the signaling pathways that are active during chondrogenesis. In another review paper, Barthes et al. (2014) gave a comprehensive description of cell microenvironment and how each component can be used to direct cellular activity for tissue engineering applications, together with the current developments in the monitoring of artificial tissues.

The advances in tissue engineering not only established it as a field where solutions to serious clinical problems can be developed but also as a growing area where enabling technologies such as organ-on-a-chip systems for pharmacological purposes can be devised. In order to have models accurately mimicking artificial organs, it is important to have a good grasp of the specific microenvironments pertaining to each tissue type. We believe engineering of the cell microenvironment will be an important part of future tissue engineering activities.

Nihal Engin Vrana
Vasif Hasirci
Garrett Brian McGuinness
Albana Ndreu-Halili

Hindawi Publishing Corporation
BioMed Research International
Volume 2014, Article ID 921905, 18 pages
http://dx.doi.org/10.1155/2014/921905

Review Article

Cell Microenvironment Engineering and Monitoring for Tissue Engineering and Regenerative Medicine: The Recent Advances

Julien Barthes,[1] Hayriye Özçelik,[1] Mathilde Hindié,[2] Albana Ndreu-Halili,[3] Anwarul Hasan,[4,5,6] and Nihal Engin Vrana[1,7]

[1] *Institut National de la Santé et de la Recherche Médicale (INSERM) UMR-S 1121, "Biomatériaux et Bioingénierie", 11 rue Humann, 67085 Strasbourg Cedex, France*
[2] *Equipe de Recherche sur les Relations Matrice Extracellulaire-Cellules, Université de Cergy-Pontoise, 2 Avenue Adolphe Chauvin, 95302 Cergy Pontoise, France*
[3] *Department of Computer Engineering, Epoka University, Tirana, Albania*
[4] *Biomedical Engineering and Department of Mechanical Engineering, American University of Beirut, Beirut 1107 2020, Lebanon*
[5] *Center for Biomedical Engineering, Department of Medicine, Brigham and Women's Hospital, Harvard Medical School, Cambridge, MA 02139, USA*
[6] *Harvard-MIT Division of Health Sciences and Technology, Massachusetts Institute of Technology, Cambridge, MA 02139, USA*
[7] *Protip SAS, 8 Place de l'Hôpital, 67000, Strasbourg, France*

Correspondence should be addressed to Nihal Engin Vrana; e.vrana@protipmedical.com

Received 23 April 2014; Accepted 15 June 2014; Published 20 July 2014

Academic Editor: Vasif Hasirci

In tissue engineering and regenerative medicine, the conditions in the immediate vicinity of the cells have a direct effect on cells' behaviour and subsequently on clinical outcomes. Physical, chemical, and biological control of cell microenvironment are of crucial importance for the ability to direct and control cell behaviour in 3-dimensional tissue engineering scaffolds spatially and temporally. In this review, we will focus on the different aspects of cell microenvironment such as surface micro-, nanotopography, extracellular matrix composition and distribution, controlled release of soluble factors, and mechanical stress/strain conditions and how these aspects and their interactions can be used to achieve a higher degree of control over cellular activities. The effect of these parameters on the cellular behaviour within tissue engineering context is discussed and how these parameters are used to develop engineered tissues is elaborated. Also, recent techniques developed for the monitoring of the cell microenvironment *in vitro* and *in vivo* are reviewed, together with recent tissue engineering applications where the control of cell microenvironment has been exploited. Cell microenvironment engineering and monitoring are crucial parts of tissue engineering efforts and systems which utilize different components of the cell microenvironment simultaneously can provide more functional engineered tissues in the near future.

1. What is Cell Microenvironment?

Tissue engineering and regenerative medicine fields aim to produce artificial tissues or whole organs for both clinical applications and drug testing, disease models, and cell based biosensors. Even though there are several methods to approach tissue engineering, whether scaffold/biomaterial based approaches, utilization of decellularized natural materials, or scaffold-free methods, presence of the cellular component is inevitable [1]. As the advances in the different fields of biology demonstrated well that cells are highly sensitive to their environment, it can be said that the control over cell microenvironment is a fundamental aspect of tissue engineering and regenerative medicine.

Cell microenvironment is constituted by factors that directly affect conditions around a cell or group of cells which have direct or indirect effect on cell behavior via biophysical, biochemical, or other routes. When considered for a single cell *in vivo*, cell microenvironment is composed of (i) extracellular matrix (ECM), (ii) homotypic or heterotypic cells surrounding the single cell, (iii) cytokines, hormones, and other bioactive agents around the cells due to autocrine,

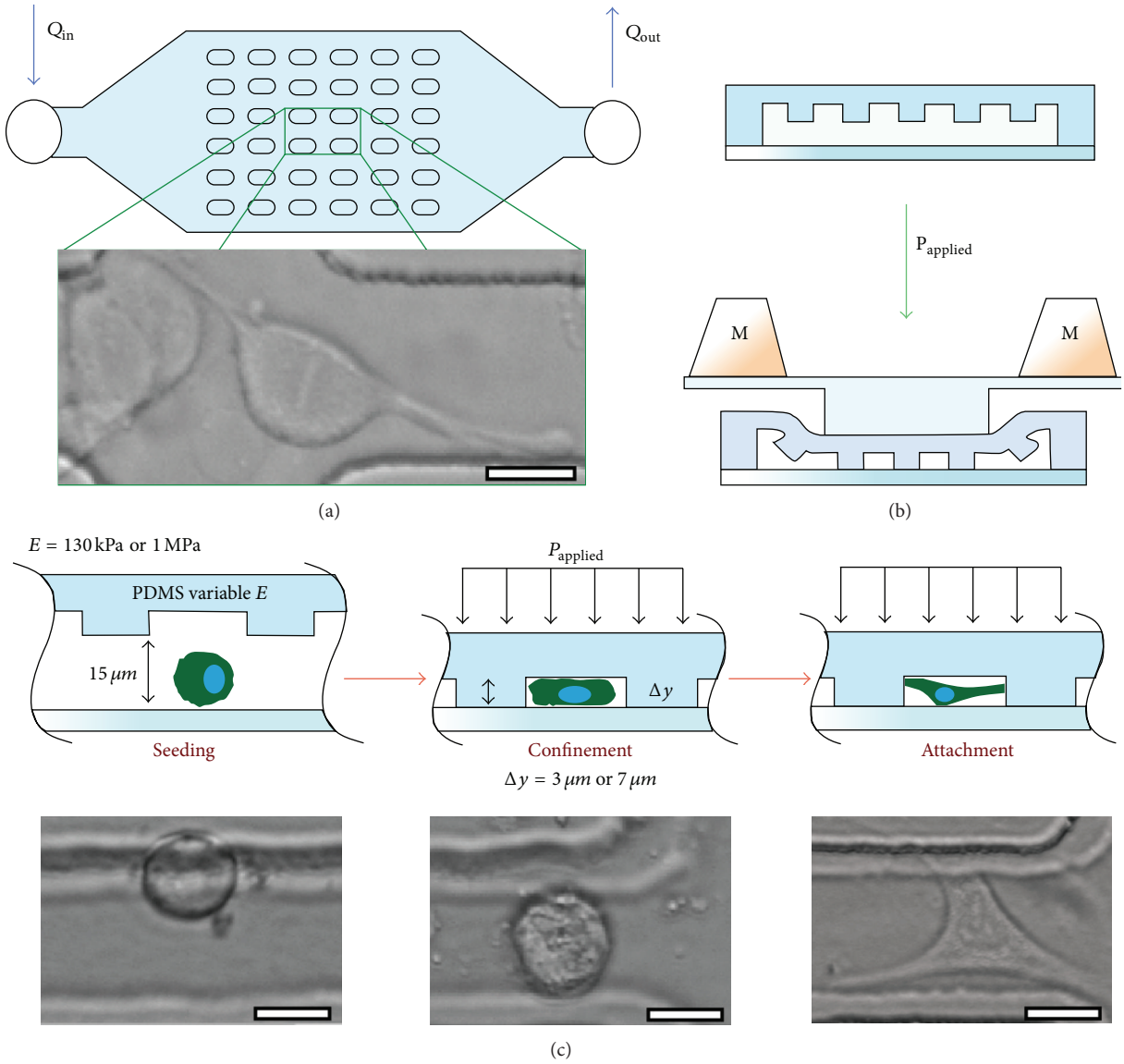

FIGURE 1: The effect of microlevel mechanical confinement on the division of HeLa cells. (a) and (b) show the macroscopic structure of the microfluidic system and the cross-section of PDMS posts. By the application of pressure on the posts, cells can be confined within the area between the posts (the distance between the posts is 40 μm) (c). The confinement caused significant changes in the behavior of the cells during mitosis, such as delays in mitosis, and led to daughter cells of different sizes and multidaughter cells following mitosis. Reproduced from [4].

endocrine, and paracrine secretions, (iv) nano/microscale topography and physical properties of the adjuvant cells and the ECM, and (v) mechanical forces caused by the movement of the organism or the movement of the physiological fluids such as blood. All these have a compound effect on the behavior of the cells, where the relative importance of each component is tissue and cell type dependent, and the next generation of engineered tissues must imitate these effects as much as possible to be functional in their target areas as a long term clinical solution.

Cell microenvironment has many aspects and their control can result in substantial changes in cell behavior. For example, Satyam et al. showed that by macromolecular crowding in the cell microenvironment the secretion of ECM molecules can be significantly improved for corneal fibroblasts [2]. Another recent work shows that nanoscale, micropatterned, and highly flexible membranes can be used to develop retinal pigment epithelium layers for minimally invasive implantation within the eye [3]. By mechanically confining cells in a microfluidic platform, researchers were also able to control the mitotic processes (Figure 1) [4].

Microenvironment of stem cells is a particularly important topic in tissue engineering and regenerative medicine, as they are currently the most technically feasible source which can provide the large amount of cells needed for engineering clinically relevant amounts of tissue. Stem cell reservoirs are available for replenishment of the tissue in tissues in human body. The microenvironmental control over how

these cells can keep their plasticity [5], that is, how they can stay quiescent and be utilized by the body only in case of necessity under healthy conditions, is a benchmark that needs to be met by engineered tissues. Moreover, failure to control the microenvironment of stem cells can also have deleterious effects such as dedifferentiation and subsequent tumor growth.

Another important concept related to the mimicking of tissue microenvironment is multidimensionality as most of the components of tissues have multidimensional order and orientation, which necessitates mimicry to achieve their function [6]. Multidimensionality is also an important aspect of other uses of tissue engineering, namely, model tissues and organs for pharmaceutical testing and also fundamental research. These microorgan structures should match the dimensional properties of the tissue and the organ they represent [7].

In this review, we will focus on different aspects of cell microenvironment and their direct effects on tissue engineering applications with particular focus on osteogenesis and angiogenesis. Each component of the cell microenvironment will be discussed separately and also in conjunction with the other components.

2. Micro/Nanopatterning for Microenvironment Engineering

All the cells in the human body are surrounded by topographical and biochemical signals. The physical structures comprise nanopores, nanofibers, and nanocrystals. Some examples of such structures in physiological settings are nanopores in capillaries, nanofibers in the basement membrane, and nanocrystals in the form of hydroxyapatite in the bone microstructure. Aligned cells are very prevalent in the tissue. For instance, maintenance of cell alignment is essential for muscle, cardiovascular/blood vessel, and corneal and nerve tissue engineering in which the controlling tissue microarchitecture and biological function are tightly connected. Various strategies have been developed to induce cell alignment, including topographical patterning (e.g., micro- and nanogrooves and aligned nanofibers), chemical treatment (patterns with cell-adhesive or repellent chemistries), controlled stress/strain conditions (e.g., stretching, fluid shear stress, and compression), and a combination of these methods.

From topography point of view, recent advances in micro- and nanofabrication enabled development of complex surface features by controlling their pattern, periodicity, shape, and dimensional properties. Today, design and construction of substrates with well-controlled physical and chemical properties and micro- and nanoarchitecture have become an important tool in the construction of tissue engineered replacements. Several top-down and bottom-up techniques such as phase separation, self-assembly, thin film deposition, chemical vapor deposition, chemical etching, nanoimprinting, photolithography, scanning probe lithography, and electron beam lithography [11] can be used in order to tailor micro- and nanoscale structured environments (scaffolds/surfaces) to stimulate cell growth and guide tissue regeneration in much the same way the extracellular matrix (ECM) does.

It is well known that cells can align along micro- and nanosized parallel grooves/ridges patterns [12–19]. Several studies indicate that alignment occurs when the periodicity and dimensions of the patterns are above a critical value. For example, Loesberg et al. [20] have shown that the fibroblasts did not show noticeable alignment with groove depths around 35 nm and ridges narrower than 100 nm. In another study, 100 nm depth was determined as a threshold for alignment of cardiomyocytes [21], osteoblast-like cells [16, 22], and hepatoblastoma cells [23]. On microgrooved surfaces, groove depth is one of the most important parameters in defining cell alignment. The degree of alignment of the cells along the microscale grooves is generally proportional to groove depth and inversely proportional to groove/ridge width if the other parameters are fixed [24]. On the other hand, Glawe et al. [25] studied that effect of high aspect ratio (aspect ratio = groove depth/groove width) microchannels with varying widths (20–60 μm) on the alignment of smooth muscle cells. It was observed that alignment was dependent on the channel width, and narrow microchannels (20 μm and 30 μm) promote alignment of smooth muscle cells. On nanogrooved substrates, cell orientation was also found to be also less sensitive to groove width (90 to 500 nm) with MG-63 cells and C3A cells [16, 22]. When the ridges are smaller than that of focal adhesions (0.25–0.5 μm wide and 2.0–10.0 μm long), cell alignment is inhibited. Nanogrooves were too narrow for the cells to descend into the bottom of grooves. Thus, the focal adhesions and actin filaments are localized on the ridges. However, for vascular smooth muscle cells, channel widths as small as 332.5 nm have been shown to induce alignment and subsequent mechanical property improvement in the direction of alignment [26].

The lack of data on how height and groove width or quantitative interaction of these parameters which determine the degree of cell orientation have forced researchers to establish aspect ratio dependent models. For example, Kemkemer et al. [27] developed a model for predicting the cell orientation for cases where the cell is larger than the grooves. According to this, the square of the product of groove depth and spatial frequency or the aspect ratio for symmetric grooves were found to be the important features for alignment. In another study, Crouch et al. [28] proposed a simple model to explain the relationship between aspect ratio and cell behavior on gratings with varying widths and depths. They observed a direct relationship between the alignment of human dermal fibroblasts and aspect ratios of the channel type patterns. While aspect ratios as small as 0.01 induced significant alignment (60%), 80% alignment was achieved with an aspect ratio of 0.05. The maximum aspect ratio required for 95% alignment was 0.16. This study indicates that within a certain range the aspect ratio can be used for controlling cell response to substrate topography without distinguishing the effects of width and depth. However, it is important to point out that when the grating surface is wider than cell width, the probability of lateral cell spreading is high. Thus, obtaining cell-type-specific contact guidance thresholds by the help of the abovementioned prediction theories can be useful to tailor the cellular microenvironment.

Cell alignment on physically patterned surfaces is a widely used strategy, in some cases together with chemical patterns. The effect of chemical patterns [29, 30] or synergistic effects of physical and chemical patterning [31–34] were also studied intensely. Generally, in order to control cell adhesion and alignment, molecules such as poly(-L-lysine) (PLL), peptides, fibronectin, laminin, collagen, bovine serum albumin, and SAM (self-assembled monolayers) are patterned by soft lithography techniques. In some cases, instead of synergistic effects of chemical and physical patterning, one of the cues can overcome the other one. For example, when Charest et al. [33] used grooves (4 μm depth, 8 μm width) overlaid with an orthogonal chemical pattern (10 μm adhesive lanes with spacing ranged from 10 to 100 μm), physical topography determined the alignment of osteoblast-like cells. Another means to produce patterned surfaces is to use thermoresponsive polymers. These "smart" polymers, based, for example, on a poly(N-isopropylacrylamide) backbone with *n*-butyl methacrylate side chains, are capable of a reversible transition from hydrophilic to hydrophobic state when their temperature is lowered by a few degrees (around its low critical solution temperature of 32°C). Thermoresponsive polymers can be used for cell sheet engineering to treat a wide range of diseases, from corneal dysfunction to oesophageal cancer, tracheal resection, and cardiac failure as growth substrates for cells [35]. By using patterned thermoresponsive surfaces, it is possible to pattern cell sheets when the application requires cellular alignment.

Biological tissues are hierarchically organized from nanometer-to-centimeter scale. For instance, the average roughness of bone tissue is 32 nm and bone tissue has a hierarchical structure composed of collagen and hydroxyapatite [36]. During bone mineralization, the hydroxyapatite crystals form micro- and nanocomposites with collagen fibers. Thus, preparing biomimetic surfaces which present synergistic effects of micro- and nanostructures is expected to provide additional advantages. Two separate studies have examined the behavior of osteoblasts derived from bone marrow stromal cells on micropit and nanonodule hybrid topography of TiO_2 [37, 38]. They created nanonodules with diameters of 100 nm, 300 nm, and 500 nm by self-assembly technique and demonstrated that 300 nm nanonodule containing substrates created the most promising environment for osteoblast differentiation and bone-titanium integration. These results are in agreement with more recent studies [39, 40], which have indicated that the presence of micron and submicron-scale surface roughness on the same surface can accelerate bone differentiation. In another study, surface features which are similar in scale to osteoclast resorption pits were used to study *in vitro* bone formation in basal medium [41] Here, the pit dimensions were as follows: depth: 330 nm, diameters: 20, 30, and 40 μm, and centre-centre spacing: 50, 60, and 90 μm. Osteopontin expression was relatively high in the human osteoblasts grown on the larger diameter (30 and 40 μm) pits. In addition to expression of osteogenic markers, mature calcium depositions were shown by alizarin red staining on these substrates.

In the last decade, several studies reported that micro- and nanopatterned surfaces can be a valuable tool for directed growth [15, 42] and differentiation [19, 32, 43, 44] of neurites. In one of the recent studies, Migliorini et al. [45] analyzed the effect of nanopillars on differentiation of embryonic stem cell derived progenitors in the absence of biochemical factors and observed an increase in the neuronal yield with increasing pillar height from 35 to 400 nm. Pan et al. [46] tested the effects of nanograting substrates with different widths on human induced pluripotent stem cells (hiPSCs). Gene expression profiling by real-time PCR and immunostaining showed significant upregulation of neuronal markers on nanostructured substrates either with solely topographical cues or combined with preneuronal induction. A width of 350 nm, in particular, induced the highest neuronal marker expression. The responsiveness of the cells to nanometer scale cues stems from their specific interactions with extracellular matrix (ECM), which is covered in the following section.

3. Microenvironmental Effects of Extracellular Matrix

The ECM comprises of a wide range of molecules including collagen, elastin, laminin, fibronectin, various glycoproteins, proteoglycans, and polysaccharides [47, 48]. Each ECM component provides different functionalities to this complex network made of structural proteins (e.g., collagen and elastin), adhesive proteins (e.g., fibronectin and vitronectin), and glycosaminoglycans (e.g., hyaluronic acid and heparin sulphate) by presenting different structural and biochemical properties [49]. The microenvironment created by ECM surrounding adherent cells is essential to their survival. ECM is a physical support to physiological cells; the signals for functional orientations such as migration, proliferation, and even survival are transduced from ECM. The absence of cell adhesion to ECM induces cell death by apoptosis [50]. This particular type of apoptosis is named *anoïkis* (Greek word which means "homelessness" or loss of home). This phenomenon was first described in epithelial cells [51] and contributes to maintain tissue homeostasis [52]. In physiological conditions, adherent cells are protected from *anoîkis* by the binding to ECM and the resulting activation of intracellular survival signalling pathways. The loss of *anoikis* induction signal constitutes a hallmark of cancerous cells and contributes to the formation of metastasis [53, 54]. Thus, presentation of an ECM mimic to the cells in tissue engineering applications is important. The three-dimensional organization of the ECM has a regulatory effect on cell cycle as seen in mammary epithelial cells as the ECM suppresses apoptosis, suggesting that ECM signaling is defined by the organization of the cells within a tissue, that is, cell shape, intercellular spacing, and 3D position. These factors determine cellular response to signals.

The microenvironment created by ECM components such as adhesive proteins or glycosaminoglycans maintains tissue stability and cell behavior. Bone matrix, for instance, contains 90% of collagen type I and only 5% of noncollagenous proteins like osteocalcin, osteonectin, fibronectin, or hyaluronan and mineral compounds which are essential to conserve osteoblasts phenotype [55], whereas culturing chondrocytes on type I collagen induces their dedifferentiation [56]. Furthermore ECM components selectively

influence cell adhesion and shape as described by Schlie-Wolter et al. [57]. Hence, cell morphology directed by the interaction with ECM induces modifications of their behaviour and subsequently their fate [58].

One of the main examples of cell signaling is integrin-mediated signaling for cell adhesion where the connection requires structures of focal adhesion that contain complex mixture of proteins. Cell adhesion to ECM is led by transmembrane heterodimeric integrin receptors. During development, integrins facilitate tissue morphogenesis by determining which ECM components the cell would bind to. Integrins are the major mediators of cell-ECM contacts and they are essential to the outside-in transmission of signals from cell microenvironment [59]. Integrin and ligand bindings lead to the formation of focal adhesion complexes which are linked to the intracellular actin cytoskeleton [60, 61]. Another example of this structure-dependent ECM signaling pathway is in tyrosine kinases [62]. For cell binding and migration, integrin signaling modulates the cell signaling pathways of transmembrane protein kinases such as receptor tyrosine kinases (RTK). RTK are high-affinity cell surface receptors for many polypeptide growth factors, cytokines, and hormones. The study of receptor tyrosine kinase (RTK) signaling led to the understanding of how an extracellular signal is transmitted to the nucleus to induce a transcriptional response [63]. Other nonintegrin adhesion receptor families include selectins, cadherins, immunoglobulins, proteoglycans, and some other laminin-binding proteins. In short, this mode of interaction conveys biochemical and positional information by which the cell can know how and when it should undertake a particular activity.

ECM is coupled to cytoskeletal and signalling effector elements which direct crucial downstream functions, such as cell growth, survival, and transcriptional activity [64]. Biochemical and biomechanical modifications of ECM microenvironment are transmitted to cells and induce the resulting changes in their behaviour [65]. Cell mechanosensing is mediated by focal adhesion contacts [66]. Indeed, physical and mechanical forces in cell microenvironment lead to changes in cell morphology and differentiation. Not only the composition of the ECM has direct effects on cell behaviour, but also its physical properties. Stiffness of bone ECM is essential to maintain osteoblast phenotype whereas chondrocytes dedifferentiate where they are cultured on a rigid matrix [67]. Elasticity of ECM determines also the differentiation of progenitor cells [68]. Furthermore, physical modifications of an adhesive protein such as fibronectin are sufficient to influence cell activities. The stretching of fibronectin alters its binding to ligands [69] and more importantly fibronectin conformation regulates integrins attachment which controls downstream cell behaviour [70]. Another type of ECM component variation is biochemical. Glycosylation is one of the most abundant protein modifications having a role in protein stability, secretion, and function. The O-glycosylation in particular is essential in cell adhesion. Zhang and Hagen demonstrated that loss of glycosylation disrupts adhesion of epithelial cells and more generally influences cellular microenvironment [71]. Moreover, glycosylation of adhesive proteins like laminin or fibronectin also stimulates cancerous cell proliferation and dissemination [72].

All differentiated cells have a cell type specific protein expression profile with multifunctional criteria that is responsible for development and protein regulation. This protein expression creates an output signal to be used by cells to control their roles. Changes in the protein expression profile or mutations that result in down- or upregulation of specific proteins can be the causes of cardiac, muscular, or mental illnesses. Hyper- and hyposensitivity responses to the strength of stimuli can also cause sickness in the body. In order to model such illnesses, tissue engineering and biomaterials studies concentrated on producing artificial ECM networks that are made up of synthetic polypeptides or peptide-conjugated synthetic polymers that present bioactive ligands and respond to cell-secreted signals to enable proteolytic remodeling. The production of such biomaterials can be used in differentiating stem cells into neurons [73]. The goal of this approach is to mimic the properties of ECM. The areas of biomimicry are specific cell adhesion, degradation by proteolytic processes involved in cell migration and tissue remodeling, and the ability to control cellular functions such as ECM synthesis. An example of such systems is the use of photopolymerizable polyethylene glycol (PEG) based hydrogels as tissue engineering scaffolds. This material showed, when modified with necessary signals, that it can interact with cells in a manner similar to that of natural ECM, especially in transmitting bioactive signals that control tissue formation and cell phenotype.

ECM microenvironment is not permanent; changes during aging were observed in different organs with variable times of onset. Due to the specific interactions between different tissues, cells, and their surroundings, the cells modify their own environment by reshaping their ECM components into the correct configuration that allows the growth of the functioning tissues which have specific architecture and characteristics. ECM components are essential to stem cell maintenance and subsequently to support tissue regeneration [74].

4. Phenotype Control and Stem Cell Differentiation via Microenvironmental Cues

Tissue homeostasis requires a certain level of phenotypic plasticity from resident cells and also the involvement of circulating cells. The most apparent manifestation of this need is observed upon injury where the inflammatory reaction mediated by immune cells, such as neutrophils and macrophages, decides how an implant, transplant, or an engineered tissue integrates with the body. The phenotypes of the immune cells in the microenvironment have a significant effect on the final outcome. Moreover, many tissues depend on several different cell types with given phenotypes. The quality of bone tissue depends on the interaction between osteoblasts, osteoclasts, and osteocytes. Respiratory epithelium not only has a ciliary epithelium layer but also requires basal cells and glandular cell components.

One of the new paradigms in tissue engineering is the utilization of developmental pathways for engineering tissues [75]. In one of the recent demonstrations of "developmental tissue engineering" [76], Scotti et al. were able to produce a bone organ with functioning bone marrow by putting the human mesenchymal stem cells through an endochondral bone formation route, that is, formation of bone organ via a cartilaginous tissue step [8]. This was achieved via production of hypertrophic cartilage tissue, by application of IL-1β and subsequent subcutaneous implantation. By applying both physical and chemical microenvironmental controls, they were able to push the initial hypertrophic cartilage structure to produce several cell types with their proper phenotypes, which demonstrates the strength of the developmental tissue engineering methods (Figure 2) [8].

The most active literature concerning cell phenotype in tissue engineering is the research on stem cells. Stem cells (SCs), a subset of cells with replenishing ability and the potential of differentiation into various types of mature cells, are categorized into two main groups, namely, embryonic stem cells (ESCs) and adult stem cells (ASCs). It has been shown that the intrinsic genetic programs within these cells and some extracellular regulatory signals control the ability of SCs to proliferate and differentiate into different functional mature cell types [77].

Stem cells reside in a specialized microenvironment called stem cell niche which provides the stem cells with extracellular cues to allow their survival and identity. This niche is a key regulator to the stem cell behavior because it ensures a quiescent and low metabolic environment to prevent exhaustion. It is believed that microenvironmental properties of the niche provide a good balance between the ability of SCs to renew themselves and the ability to differentiate into mature cells so that continuous tissue regeneration occurs. A major part of the cell niche is the ECM (extracellular matrix) which possesses the specific mechanical, biochemical, and biophysical properties for tissues and controls the overall cell behavior [78]. The composition of the ECM provides full support to the niche through its physical and structural properties. The main extrinsic signals that regulate stem cell behavior are those coming from ECM.

Given its three-dimensional organization, the ECM provides an environment that aids in the integration of the signals derived from the cell-ECM interactions in order to allow proper "maintenance of stem cell homeostasis" [78]. The cell-ECM interactions are basically triggered by receptors present on the cell membrane, like integrin as described before. However, studies found that the nonintegrin receptors are the ones that contribute the most to stem cells homing during transplantation. Novel techniques have been developed to observe the interaction between stem cells and ECM proteins and how this interaction influences their fate. Among the factors that influence stem cell fate are ECM adhesion, its stiffness, and its topography [79]. For example, the effect of micro-/nanotopography on stem cells has been recently demonstrated. Oh et al. [80] demonstrated that human MSCs can differentiate into osteoblasts under the influence of only nanotopography of culture substrates. Another example is micropatterned islands, created with specific shapes to observe cell behavior at single-cell level. The degree of spreading of human epidermal stem cells was observed by Connelly et al. [81]. The authors stated that when the shape of the island was changed from elongated to circular, epidermal stem cells showed an increase in their differentiation ability. On the other hand, human MSCs revealed a dependence on the area of the island, that is, while round cells favoured adipogenesis, whereas cell spreading resulted in osteogenesis [82].

In addition to topographical cues, soluble factors like growth factors and cytokines are very important in initiation and control of SC differentiation [83]. Tissue engineering has become an important stem cell application field with the aim of increasing the quality of life. Therefore, researchers have focused more on finding appropriate cues via utilization of biomaterials that could control the cellular environment and monitoring complex cellular levels. Both natural and synthetic materials based biomaterial scaffolds have served to understand the role of chemical cues in controlling stem cell behaviour. It is crucial to direct SCs to differentiate into the right cell type, at the right time and location; therefore, specific cues have been investigated in the *in vivo* microenvironment and have been studied in the *in vitro* systems that mimicked the natural conditions. Controlled microenvironments have been designed to direct stem cell differentiation into the desired mature cell type. Stem cell researchers emphasize the need of a 3D environment instead of 2D since differences have been observed in their self-renewal capacity, differentiation, adhesion, and migration ability. Cellular morphology has been shown to vary depending on the biomaterials structure (2D or 3D) and material type. Human mesenchymal stem cell shape was observed to be round when entrapped in 3D hyaluronic acid hydrogel [84] and elongated when seeded onto fibrous scaffolds or 2D biodegradable elastomer [85]. There are other effects regarding the encapsulation of cells as demonstrated by encapsulation of prostate cancer cells (LNCaP) in polyethylene glycol (PEG) hydrogels, which changed their cell-cell contact formation and response to androgen stimulation where these effects are also relevant to the differentiation of stem cells within confined environments [9] (Figure 3).

5. Cell Microenvironment Control via Delivery of Soluble Bioactive Agents

Another way to control the cell microenvironment is via delivery of bioactive molecules such as drugs, hormones, or growth factors. Variation in the signaling microenvironment might cause perturbations in the signaling processes which are at the root of multiple pathologies, including cancers, diabetes, and many other diseases [63]. Growth factors can regulate activation, growth, proliferation, migration, and differentiation of cells which are crucial for events such as angiogenesis or osteogenesis [86]. Recent studies have focused on inserting signaling molecules such as growth factors and cytokines into biomaterials (Figure 4). Some examples of altering cell behaviour to such molecules are induced vascularisation (new blood vessel formation from fibroblast growth factor 2—FGF-2), regeneration of neurons (from

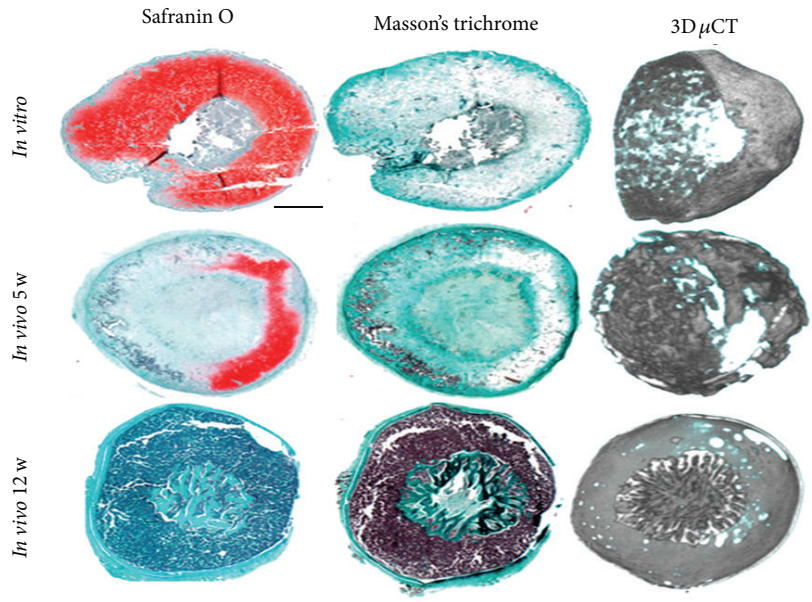

Figure 2: Bone formation via endochondral pathway. An *in vitro* formed artificial cartilage successfully forms a bone containing bone marrow within 12 weeks. The *in vitro* grown tissue is a cartilaginous one as evidenced by the extensive safranin O staining; over time, the cartilaginous tissue has been gradually replaced by bone tissue, as can be seen by the extensive Masson's Trichrome staining. Micro-CT images also showed the development of a bone like structure within 12 weeks. Reproduced from [8].

nerve growth factor, NGF), retention of stem cell phenotype (from immobilization of cytokines to maleic anhydride copolymer thin-film coating), and providing an environment that helps cell survival and proliferation. Epidermal growth factor (EGF), incorporated with the matrix material, increases cell attachment to the implanted matrix and increases the spreading of mesenchymal stem cells [10].

However, these molecules have high instability and very short biological half time and can be enzymatically digested or deactivated while in physiological fluids [87, 88]. Besides, growth factors or drugs need to reach specific location to be effective; thus, their systemic introduction is not a viable way to control their concentration in specific target areas [89]. To overcome these limitations, it was necessary to develop delivery vehicles with growth factors or drugs incorporated within tissue engineering scaffolds. To illustrate this fact, it has been shown that bolus injection of growth factors such as VEGF is less effective than a sustained and localized delivery via biodegradable hydrogels to achieve blood vessel formation [90]. In the case of bolus injection, VEGF was not localized in the target area and stayed only for 72 h, whereas with delivery from biodegradable alginate hydrogel 95% of the growth factor was at the ischemic site (improvement of biodistribution), and it stayed at that location for more than 15 days and its bioactivity was higher (possibly due to the protection from denaturation).

One way to achieve control over local bioactive molecule concentrations is the immobilization of growth or differentiation factors. Mainly, the ECM harbors a lot of growth factor binding proteins. This localization of growth factors by the ECM and their signaling contributes to the establishment of a gradient for the soluble, diffusible morphogens, which play vital roles in shaping the developmental processes [91]. The binding of growth factors to the ECM is regulated by the GAG side chains. One important application of this is the regulation of specific gene expression which is done by using growth factor-ECM interaction, that is, by controlling the growth factor presence via their interaction with ECM [92].

Incorporation of bioactive factors into scaffold can be achieved by two different ways, mainly through covalent and noncovalent immobilization [93–95]. The first approach is based on the covalent binding of the molecule to the scaffold via chemical reaction such as immobilization of VEGF using *N*-(3-dimethylaminopropyl)-*N*′-ethylcarbodiimide hydrochloride chemistry (EDC) [96]. The noncovalent approach is based on interaction of the molecule with the polymer matrix such as electrostatic interaction, hydrogen bonding, or physical entrapment. In the case of incorporation via electrostatic interaction, charged material is required such as polyelectrolytes or gelatin hydrogels. In all these different approaches, the release will be triggered by scaffold degradation, diffusion of the molecule through the material, or cleavage (enzymatic or hydrolysis) of the covalent bond between the molecule and the scaffold material. For example, with the addition of bioactive motifs (from bone morphogenetic protein 2 or osteopontin), it was shown that osteoblast adhesion and the responsiveness to the protein were dependent on the cell adhesive motif from osteopontin. The cell interaction with the protein demonstrated *in vitro* bone formation in a month [97].

These delivery systems were developed with different kind of materials. Two main categories can be identified: (i) natural materials such as collagen, alginate, gelatin, and poly-L-lysine; (ii) synthetic materials such as PLLA, PEG, and PCL

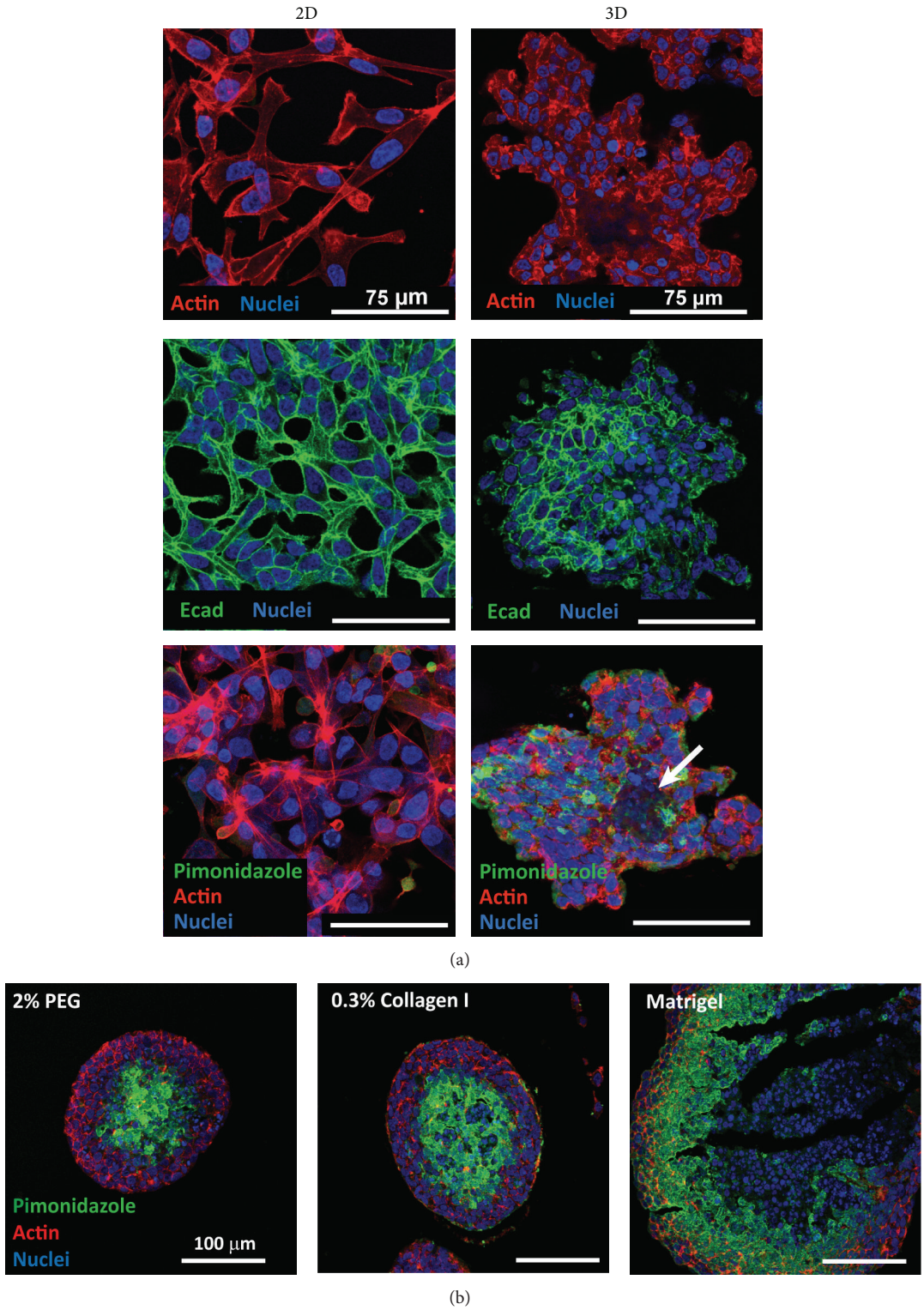

Figure 3: Manipulating the cell microenvironment in 3D via encapsulation within hydrogels. Encapsulation of prostate cancer cells within PEG hydrogels resulted in more pronounced cell-cell contacts as evidenced by E-cadherin staining (a) and also formation of a necrotic core within the cell aggregates as shown by pimonidazole staining (b). All scale bars are 75 μm for (a) and 100 μm for (b). Reproduced from [9].

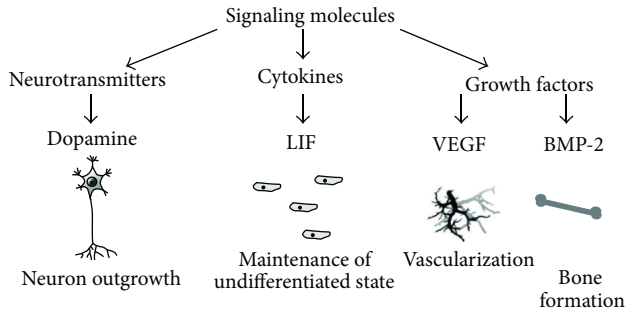

Figure 4: The main types of soluble factors that have distinct effects on the cellular behaviour at both single cell and tissue level. Controlled delivery of such factors and their regulated presence in cell microenvironment is an indispensable tool in tissue engineering research. Reproduced from [10].

[95]. To be an efficient carrier system, these materials must fulfill some requirements: (i) biocompatibility, (ii) biodegradability, and (iii) release of active factors in a controlled spatiotemporal way [98]. Release of growth factors from scaffolds is mainly governed by two mechanisms: (i) diffusion through the material and (ii) degradation rate of the material [86, 99]. Release profile of bioactive molecules is a key parameter to control cell microenvironment. Depending on the application, such as enhancement of angiogenesis, stem cell differentiation, or disease treatment, bioactive factors need to be released for specific time points at specific rates. In the case of degradable scaffolds, the release of molecules can be tuned by varying the degradation profile of the material or the molecule diffusion. The degradation rate of the scaffold can be changed by crosslinking to reinforce the structure and delay the release. Gelatin is a biomaterial obtained by denaturing collagen. It is a good ECM mimicking material for cells [100]. Moreover, gelatin is biodegradable and has been used for a long time in medical field. Gelatin is also a very useful material for drug incorporation because it can be positively (basic gelatin) or negatively charged (acidic gelatin) depending on collagen processing method (acid or alkaline process) so it can complex both positively or negatively charged molecules [101, 102]. This provides a level of versatility which is not available with other commonly used biomaterials. Gelatin hydrogels are systemically cross-linked with different agents such as genipin, transglutaminase, or EDC/NHS because, unless cross-linked, the structure of the physically gelled gelatin hydrogels or films is too weak and the degradation is too fast [103–105]. For other materials, different techniques are available. For example, to control degradation rate of alginate hydrogels, a partial oxidation of the polymer chains rendered the hydrogel degradable by hydrolysis [90]. This strategy has been used to create a delivery vehicle for VEGF. Synthetic hydrogels can also be used to encapsulate and release bioactive molecules. Hyperbranched polyester hydrogels capable of encapsulating hydrophobic molecules such as growth factors or specific drugs (e.g., dexamethasone) have been developed. These hydrogels are photocross-linkable via incorporation of methacrylate group. Normally, it is very difficult to entrap hydrophobic agents in hydrogels. In this case, a sustained release of 8 days was achieved mainly through hydrolysis of ester backbone [106].

Polyelectrolyte multilayer structures (L-b-L, layer by layer) are also used to design delivery systems because L-b-L films are easy to produce; they can act as a reservoir for bioactive molecules [107] and their properties such as permeability, thickness, and charge density can be easily changed and they can be easily coated on implants [108]. The only problem with these films for drug delivery application is the fast release of molecule due to the mobility of polyelectrolyte chains within the film. To solve this problem, recently, a double entrapment system has been developed for VEGF to achieve a long term release [109]. This strategy was based on the twofold control over the release by VEGF containing PCL nanoparticles loaded in polyelectrolyte multilayer film. The mechanism of the release was the following: either PCL nanoparticles containing VEGF were hydrolyzed and then VEGF diffused in the LBL film and then out; or the particle will diffuse out of the film and then hydrolyzed. With this system, a sustained release of 7 days was achieved [109]. To prevent the fast release of drug out of LBL film, another system was developed by adding a mechanosensitive cap as a barrier on top of LBL reservoir films. A bioactive agent was loaded in PLL/HA film and a PAH/PSS barrier was built on top of it. Barrier is cracked under stretch which enables the diffusion of an enzyme (trypsin) within the reservoir and the PLL/HA is enzymatically degraded leading to the release of drug [110]. Layer by layer technique (LBL) with polyelectrolytes can also be used in particle form (i.e., particles formed by polyelectrolyte multilayers) [111]. Using this technique, a stimuli-responsive controlled drug release has been developed in order to release bioactive agents. This system was based on the absorption of the agent on mesoporous silica sphere and then the deposition of a multilayer capping barrier PAH/PSS. The release of the encapsulated molecule was further triggered by change of pH (pH = 1.4) or by change of ionic strength through NaCl concentration of the release media (10 mM NaCl). At higher pH value or lower ionic strength, the PAH/PSS layer acted as a capping barrier since it does not allow bioactive agent diffusion and that explains why this system is appropriate for a controlled and sustained release of bioactive molecules [112].

In some other applications, the delivery of multiple bioactive factors with different release kinetics is required. In tissue engineering, for example, angiogenesis and osteogenesis are regulated by the action of multiple growth factors and all of them need to be released in a specific temporal way. Richardson et al. have investigated the dual delivery of VEGF and PDGF, two growth factors necessary for blood vessels formation. PLG particle with lyophilized VEGF and PLG microspheres containing encapsulated PDGF were used [113]. All these particles were mixed together and a porous PLG scaffold was made using high pressure carbon dioxide fabrication process. These growth factors release profiles were not the same: 1.7 pmol/day for VEGF for the first seven days mainly due to VEGF diffusion out of the scaffold and from 0.10 to 4.7 pmol/day for PDGF depending on degradation of polymer particle using different formulations [113]. In the field of regenerative periodontal therapy, an

interconnected macroporous Dex-GMA (glycidyl methacrylate dextran)/gelatin hydrogel scaffold was developed for the dual delivery of two different growth factors: BMP-2 and IGF-1. These growth factors were encapsulated in Dex-GMA/gelatin microparticles; basic gelatin (negatively charged) was used to encapsulate BMP-2 and acidic gelatin (positively charged) for IGF-1 encapsulation. As Dex-GMA is enzymatically degradable but not hydrolytically degradable, other Dex-GMA microparticles were prepared with neutral gelatin to encapsulate dextranase in order to further trigger the release of growth factors by enzymatic degradation of the Dex-GMA microparticles. All these particles were mixed together and cross-linked via irradiation in order to make the interconnected macroporous scaffold. This mechanism of delivery based on the degradation of microparticle followed by degradation of the scaffold enables the sustained release of growth factors for a period of 20 days [114]. Some disease like periodontitis required the multiple deliveries of antibacterial, anti-inflammatory, antiresorptive, and osteogenic agents. These molecules must be delivered in a very specific order to be effective. To fulfill this requirement, a multilayered device was designed. This laminate structure is made by the association of cellulose acetate phthalate (CAP) and Pluronic F-127(P) and these polymers can be further eroded. The different drugs have been incorporated in a specific order in every stratum by mixing them with the polymer solution and every layer is separated by one or two CAPP blank layers in order to slow the erosion of the structure and delay the release of molecules. This system was able to perform the release of four different drugs in a specific temporal sequence just by unidirectional erosion of the structure for more than 120 hours depending on the condition used [115]. The other important cell microenvironment parameter that needs to be mimicked is the changes induced on cells via dynamic stimuli, such as mechanical stimuli. The spatial and temporal variations of cell microenvironment play vital roles in various paracrine and endocrine cell signaling, 3D tissue remodeling, alteration in stem cell niches cancer progression, and migration of various cells. For these reasons, the dynamic nature of the cell microenvironment is vitally important as discussed below.

6. Dynamic Aspects of Cell Microenvironment

The native ECM microenvironments of cells are highly heterogeneous in three-dimensional space [116] and they go through continuous and dynamic remodeling with time [117]. The interactions of the ECM components with cells are of reciprocal nature, that is, while cells constantly produce, break down, rearrange, and realign components of ECM to change its properties, and any change in ECM in turn regulates the activities and the behavior of the cells [47]. The cell-ECM interactions are highly dynamic and complex; hence, a detailed understanding of the dynamic aspects of cellular microenvironment in terms of spatial and temporal variations of different chemical, mechanical, and biological stimuli is highly important in tissue or organ engineering.

Bioreactors are a crucial part of tissue engineering research as they are the main means to exert mechanical stimuli to the cells in tissue engineering constructs. Bioreactors are systems which enable the continuous replacement of nutrients and gases either by constant agitation (as in the case of spinner flasks) or via perfusion. Most of the bioreactor systems have several entry ports which enables the introduction of different bioactive agents in a controlled manner. Moreover, many bioreactors have the capacity to directly apply physiologically relevant mechanical stress/strain conditions (such as tensile, compressive shear stress according to the target tissue). They mimic the mechanical microenvironment, for functional engineered tissues that undergo mechanical loading (articular cartilage, tendons, heart valves, etc.) under *in vivo* conditions. They are designed to increase the efficiency of exchange of metabolites, oxygen, nutrients, and waste removal within the cell microenvironment and as a result to enhance cellular penetration in 3D scaffolds and to have a better and rapid cellular expansion [118]. For this aim, there exist perfusion bioreactors for culturing encapsulated stem cells and those for cell cultivation on 3D scaffolds.

Mimicking the dynamic mechanical environment is also considered in designing functional bone implants in conjunction with micro-/nanotopographical features. These studies pointed out that osteoblasts change their morphology, gene expression, and matrix mineralization by either introducing surface topography on biomaterials or mechanical stimulation [119, 120]. Prodanov et al. [121] tested the simultaneous effects of nanotextured surface (300 nm wide and 60 nm deep grooves) and mechanical stretching in terms of cell attachment, ECM formation, and osteoblast differentiation. It was shown that by dual stimulation (nanogrooved surface and 8% of strain) the expression of fibronectin and Cfba synergistically increased 2-fold in comparison to nanotextured surface alone. Such combined effects of topography and mechanical stimulation were also observed by other groups [41, 122–124].

Mechanical stimulus by cyclic stretching, fluid flow [121], and hydrostatic compressive pressure has also been used to align cells. In several studies, cardiac, ligament, and tendon derived fibroblasts, myoblasts, vascular smooth muscle cells, and osteoblasts were subjected to mechanical forces under *in vivo* conditions. Regardless of cell types, cells cultured on a 2D substrate that is subjected to uniaxial cyclic stretch tend to align perpendicular to the direction of principal cyclic strain [122, 125, 126]. There are several studies that have used mechanical stimuli together with micro/nanopatterning for cell alignment. It has been shown that when cells grown whether on patterned surfaces with micron sized, or nanosized groove/ridge patterns or on unpatterned [127] substrates subjected to cyclic stretching orient themselves in the direction perpendicular to the applied strain. It should be noted that applied strains in these examples were parallel to the direction of the groove axis. However, there are studies showing that tendon fibroblasts and osteoblasts aligned along the direction of micro grooves regardless of the stretching direction, which suggests that the topographical cues at this scale might be a more important determinant for the cell alignment direction [122, 128]. For instance, mechanical loading, topographical patterning, and surface chemical treatment can also be combined to engineer cell alignment *in vitro*. The combined effects of cyclic strain and substrate

microtopography on the alignment of bovine vascular SMCs have been investigated by Ahmed et al. [124], where they observed that the organisation of actin fibers was dominated by cyclic strain application and the shape of cell nuclei was controlled by the patterns.

6.1. Dynamic Control of Cell Microenvironment Using Microfluidics. Researchers have designed cell-laden matrices in 3D space to mimic functions of human tissues and organs *in vitro*. Many of these structures also change over time (4D biology) [117]. Pioneering work by Petersen et al. revealed that mammary epithelial cells formed a normal acinus structure when encapsulated in a 3D material but aberrantly displayed cancerous phenotypes when cultured on a 2D substrate [129]. Other examples [130, 131] revealed that the materials based presentation and timed removal of the peptide RGDs can enhance differentiation of mesenchymal stem cells into chondrocytes. Thus, the spatial and temporal control of microenvironment has been implemented in various studies. The synergistic effects of chemical factor gradients, cell-cell-interactions, mechanical sensing, and coordinated cell movements in tissue formation can be achieved through various microscale and microfluidic technologies. Microfluidic devices offer novel platforms for precise control and variation of cellular microenvironments in dynamic, automated, and reproducible ways. The use of microfluidic systems in controlling the cellular microenvironment offers numerous advantages, such as the following: (i) they have the potential to simulate real tissue microenvironments including multiple cell types and ECM proteins into a 3D structure, (ii) they use a very small number of cells and small quantities of reagents, typically in the nanoliter to microliter range, (iii) they allow precise control over cell density and cell shape as well as environmental cues such as attachment matrices containing self-assembling proteins and gel based substances, (iv) they provide the ability to precisely control the mechanical properties (e.g., elasticity, rigidity, and strain), chemical properties (e.g., ligand density and orientation), and topographic properties (e.g., patterning of surfaces with substances having different cell-substrate affinity), and (v) they allow high throughput analysis and complete automation of the processes. Due to these advantages, recently microfluidic devices have been widely used in controlling the cell/tissue microenvironment in tissue engineering applications. The variation of the local mechanical properties [132], chemical properties, and topographic features [133, 134] has been achieved using microfluidic platforms. The control over localized ECM [135–138], chemical gradient [139, 140], and fluid flow [141, 142] has also been achieved.

The applications of microfluidic technologies in tissue engineering and biomedical engineering, in general, have become widespread, such as for development of blood vessels and 3D vascularized tissues [143] and use of microfluidic platforms in controlling the cell microenvironment for gene therapies [144].

Gilmore et al. [145] used an affinity capture technique in a microfluidic chamber for capturing and maintaining rotavirus double-layered particles (DLPs) in a liquid environment. In another study, Walker et al. [146] used a laminar flow and diffusion mediated, gradient based microfluidic device to infect the cells at many different concentrations of virus simultaneously within a single microfluidic channel. The laminar flow and diffusion have been used for establishing gradient in many other studies as well [147–150].

Xu et al. [151] used a three-layer microfluidic device for *in situ* monitoring of the infection process of cells by a recombinant virus in real time. They also performed drug screening assays on the microfluidic chip with a tree-like concentration gradient.

Na et al. [152] used soft lithography based technique to create cell adherent and repellent areas on a substrate, thereby depositing cells in desired micropatterns and forming plaques of controlled size, shape, and cells number. Microfluidic platforms have also been used as bioreactors [153] containing separate compartments for production, preservation, and transduction of viruses or compounds on a single microfluidic device. Thus, microfluidic systems and microscale technologies present novel platforms for controlling cell microenvironment for various cell and tissue engineering applications.

7. Microenvironment Monitoring

The level of control over microenvironment is directly related to our level of understanding the mechanisms underlying the dynamic processes. One of the challenges in tissue engineering is continuous monitoring of cellular activities within 3D, generally opaque, thick structures. There are several exciting technologies that have been developed for visualisation of 3D structures that are currently being applied to tissue engineered scaffold.

For screening purposes of biomaterials microenvironment on cells, microelectromechanical systems (MEMS) have been utilized. Features at length scales from 1 μm to 1 cm can be controlled with this technique for stem cell analysis [154]. Response of stem cells toward different microenvironmental signals has been studied by using robotic spotters, which can test cell-matrix interactions with a very high throughput [155, 156]. Another possibility to monitor the cell behaviour at process level is the real-time imaging of cell microenvironment in microfluidic chambers [135].

For direct real-time monitoring of the processes within engineered tissues, one proposed method is the incorporation of biosensors within the artificial tissues. This is a direct extension of implantable biosensors for clinical applications, which can be generalized under continuous monitoring of metabolites such as glucose [157]. Currently, such systems are nearly available and only hindered by the long-term problems of foreign body reaction and biofouling which impede their reliability and precision [158]. In addition to these problems, a remodellable tissue engineering scaffold provides a complex microenvironment which also has degradation byproducts of the scaffold material, host cells, implanted cells, and their secretions. Recently, a three-parameter *in vivo* biosensor system was proposed by Kubon et al. [159] which can simultaneously measure oxygen, pH, and electrical impedance to access the reaction to a given biomaterial. Such a system would provide the necessary information concerning oxygenation

levels, infection, and level of integration for a given volume of the engineered tissue microenvironment. Although this system has not been used *in vivo* yet, it has been validated in an *ex vivo* chorioallantoic membrane assay (CAM assay) system [160].

Noninvasive visualisation techniques are another way to monitor cell microenvironment. Techniques such as optical coherence tomography [161] or nonlinear microscopy techniques [162, 163] can provide relevant information about the scaffold microenvironment and its interaction with the cells. For assessment of the implanted cell activity within the host, modified signal producing cells can be utilised. By using firefly luciferase (ffLuc-MSC) expressing MSCs, Kidd et al. [164] were able to monitor the dispersion of the cells *in vivo* and found out that the MSCs show a preference to accumulate if a tumor or an inflammation site is present in the host mice. This tropism is related to the presence of a cytokine microenvironment which is more permissive and chemoattractive for their incorporation, which provides a guideline to understand how to control the interaction of the host tissue with the implanted engineered tissue. Aside from cellular localization, another crucial information for thick engineered tissues is the level of oxygenation, particularly within the depth of the structure, where the lack of nutrients and oxygen can lead to necrosis. A method to obtain relevant information about the cell microenvironment is to incorporate stimuli-responsive structures that would signal the relevant changes in the microenvironment. Acosta et al. [165] developed a fluorescent microparticle based oxygen sensing system that enables the monitoring of hypoxia and hyperoxia conditions within the 3D tissue engineering scaffolds. A similar method with phosphorescent nanoparticles was used to detect oxygen levels *in vivo* [166].

8. Future Directions

Despite the significant progress made during the last decade, designing materials to control cellular microenvironment remains an important goal. Also, challenges remain in dynamically controlling the cell microenvironments temporally and spatially. Toward modulation of dynamics, the use of stimulus-sensitive linkers, protecting groups, and exposing mechanisms may provide paths forward. It may be possible to exploit biomechanical and biochemical stimuli to expose cryptic biomolecular signals in synthetic biomaterials, as also occurs in some natural ECM molecules [73]. Microarray based material development has received great attention. Materiomics, which allows high throughput testing of complex material surfaces for specific applications, provides the necessary information for producing more complex cell microenvironments [167]. It allows researchers to place a large collection of materials onto two-dimensional substrates in a spatially numbered matrix. This way, the effects of several different properties of materials on cells have been studied simultaneously. The arrays are in the form of combinatorial polymer microarrays [156, 168, 169], peptide microarray [170], combinatorial ECM protein microarrays [171–174], and topographical microarrays [175–178]. These approaches could dramatically increase and accelerate discovery of next generation biomaterials. Moreover, for regenerative medicine and tissue engineering applications, understanding the behaviours of cells in 3D is going to move the field forward. Immunomodulation via modulation of macrophage phenotype or via design of biomaterials, bottom-up techniques for production of multifunctional, multicellular structures, real time biosensing and linked bioactive agent delivery systems within the engineered scaffolds will improve the control of biomedical engineers on artificial tissues further.

Conflict of Interests

The authors declare that there is no conflict of interests regarding the publication of this paper.

Acknowledgments

This work has been supported by EuroTransBio BiMOT Project (ETB-2012-32) and has received funding from the European Union's Seventh Framework Programme for research and technological development and demonstration under Grant Agreement no. 602694 (IMMODGEL).

References

[1] P. Zorlutuna, N. E. Vrana, and A. Khademhosseini, "The expanding world of tissue engineering: The building blocks and new applications of tissue engineered constructs," *IEEE Reviews in Biomedical Engineering*, vol. 6, pp. 47–62, 2013.

[2] A. Satyam, P. Kumar, X. Fan et al., "Macromolecular crowding meets tissue engineering by self-assembly: a paradigm shift in regenerative medicine," *Advanced Materials*, vol. 26, no. 19, pp. 3024–3034, 2014.

[3] T. Fujie, Y. Mori, S. Ito et al., "Micropatterned polymeric nanosheets for local delivery of an engineered epithelial monolayer," *Advanced Materials*, vol. 26, pp. 1699–1705, 2014.

[4] H. T. K. Tse, W. M. Weaver, and D. Carlo, "Increased asymmetric and multi-daughter cell division in mechanically confined microenvironments," *PLoS ONE*, vol. 7, no. 6, Article ID e38986, 2012.

[5] C. M. Metallo, J. C. Mohr, C. J. Detzel, J. J. de Pablo, B. J. van Wie, and S. P. Palecek, "Engineering the stem cell microenvironment," *Biotechnology Progress*, vol. 23, no. 1, pp. 18–23, 2007.

[6] M. M. Stevens and J. H. George, "Exploring and engineering the cell surface interface," *Science*, vol. 310, no. 5751, pp. 1135–1138, 2005.

[7] K. M. Yamada and E. Cukierman, "Modeling tissue morphogenesis and cancer in 3D," *Cell*, vol. 130, no. 4, pp. 601–610, 2007.

[8] C. Scotti, E. Piccinini, H. Takizawa et al., "Engineering of a functional bone organ through endochondral ossification," *Proceedings of the National Academy of Sciences of the United States of America*, vol. 110, no. 10, pp. 3997–4002, 2013.

[9] S. Sieh, A. V. Taubenberger, S. C. Rizzi et al., "Phenotypic characterization of prostate cancer LNCaP cells cultured within a bioengineered microenvironment," *PLoS ONE*, vol. 7, no. 9, Article ID e40217, 2012.

[10] A. J. Mieszawska and D. L. Kaplan, "Smart biomaterials—regulating cell behavior through signaling molecules," *BMC Biology*, vol. 8, article 59, 2010.

[11] V. Hasirci, E. Vrana, P. Zorlutuna et al., "Nanobiomaterials: a review of the existing science and technology, and new

approaches," *Journal of Biomaterials Science, Polymer Edition*, vol. 17, no. 11, pp. 1241–1268, 2006.

[12] A. I. Teixeira, G. A. Abrams, P. J. Bertics, C. J. Murphy, and P. F. Nealey, "Epithelial contact guidance on well-defined micro- and nanostructured substrates," *Journal of Cell Science*, vol. 116, no. 10, pp. 1881–1892, 2003.

[13] A. S. G. Curtis, N. Gadegaard, M. J. Dalby, M. O. Riehle, C. D. W. Wilkinson, and G. Aitchison, "Cells react to nanoscale order and symmetry in their surroundings," *IEEE Transactions on Nanobioscience*, vol. 3, no. 1, pp. 61–65, 2004.

[14] J. B. Recknor, J. C. Recknor, D. S. Sakaguchi, and S. K. Mallapragada, "Oriented astroglial cell growth on micropatterned polystyrene substrates," *Biomaterials*, vol. 25, no. 14, pp. 2753–2767, 2004.

[15] A. Tsuruma, M. Tanaka, S. Yamamoto, N. Fukushima, H. Yabu, and M. Shimomura, "Topographical control of neurite extension on stripe-patterned polymer films," *Colloids and Surfaces A: Physicochemical and Engineering Aspects*, vol. 284-285, pp. 470–474, 2006.

[16] J. Y. Yang, Y. C. Ting, J. Y. Lai, H. L. Liu, H. W. Fang, and W. B. Tsai, "Quantitative analysis of osteoblast-like cells (MG63) morphology on nanogrooved substrata with various groove and ridge dimensions," *Journal of Biomedical Materials Research A*, vol. 90, no. 3, pp. 629–640, 2009.

[17] E. Lamers, X. F. Walboomers, M. Domanski et al., "The influence of nanoscale grooved substrates on osteoblast behavior and extracellular matrix deposition," *Biomaterials*, vol. 31, no. 12, pp. 3307–3316, 2010.

[18] A. Béduer, C. Vieu, F. Arnauduc, J. Sol, I. Loubinoux, and L. Vaysse, "Engineering of adult human neural stem cells differentiation through surface micropatterning," *Biomaterials*, vol. 33, no. 2, pp. 504–514, 2012.

[19] M. Mattotti, Z. Alvarez, J. A. Ortega, J. A. Planell, E. Engel, and S. Alcántara, "Inducing functional radial glia-like progenitors from cortical astrocyte cultures using micropatterned PMMA," *Biomaterials*, vol. 33, no. 6, pp. 1759–1770, 2012.

[20] W. A. Loesberg, J. te Riet, F. C. M. J. M. van Delft et al., "The threshold at which substrate nanogroove dimensions may influence fibroblast alignment and adhesion," *Biomaterials*, vol. 28, no. 27, pp. 3944–3951, 2007.

[21] P. Y. Wang, J. Yu, J. H. Lin, and W. B. Tsai, "Modulation of alignment, elongation and contraction of cardiomyocytes through a combination of nanotopography and rigidity of substrates," *Acta Biomaterialia*, vol. 7, no. 9, pp. 3285–3293, 2011.

[22] W. Tsai, Y. Ting, J. Yang, J. Lai, and H. Liu, "Fibronectin modulates the morphology of osteoblast-like cells (MG-63) on nanogrooved substrates," *Journal of Materials Science: Materials in Medicine*, vol. 20, no. 6, pp. 1367–1378, 2009.

[23] W.-B. Tsai and J.-H. Lin, "Modulation of morphology and functions of human hepatoblastoma cells by nano-grooved substrata," *Acta Biomaterialia*, vol. 5, no. 5, pp. 1442–1454, 2009.

[24] M. G. Holthaus, J. Stolle, L. Treccani, and K. Rezwan, "Orientation of human osteoblasts on hydroxyapatite-based microchannels," *Acta Biomaterialia*, vol. 8, no. 1, pp. 394–403, 2012.

[25] J. D. Glawe, J. B. Hill, D. K. Mills, and M. J. McShane, "Influence of channel width on alignment of smooth muscle cells by high-aspect-ratio microfabricated elastomeric cell culture scaffolds," *Journal of Biomedical Materials Research A*, vol. 75, no. 1, pp. 106–114, 2005.

[26] P. Zorlutuna, A. Elsheikh, and V. Hasirci, "Nanopatterning of collagen scaffolds improve the mechanical properties of tissue engineered vascular grafts," *Biomacromolecules*, vol. 10, no. 4, pp. 814–821, 2009.

[27] R. Kemkemer, S. Jungbauer, D. Kaufmann, and H. Gruler, "Cell orientation by a microgrooved substrate can be predicted by automatic control theory," *Biophysical Journal*, vol. 90, no. 12, pp. 4701–4711, 2006.

[28] A. S. Crouch, D. Miller, K. J. Luebke, and W. Hu, "Correlation of anisotropic cell behaviors with topographic aspect ratio," *Biomaterials*, vol. 30, no. 8, pp. 1560–1567, 2009.

[29] B. C. Wheeler, J. M. Corey, G. J. Brewer, and D. W. Branch, "Microcontact printing for precise control of nerve cell growth in culture," *Journal of Biomechanical Engineering*, vol. 121, no. 1, pp. 73–78, 1999.

[30] C. D. James, R. Davis, M. Meyer et al., "Aligned microcontact printing of micrometer-scale poly-L-lysine structures for controlled growth of cultured neurons on planar microelectrode arrays," *IEEE Transactions on Biomedical Engineering*, vol. 47, no. 1, pp. 17–21, 2000.

[31] A. Magnani, A. Priamo, D. Pasqui, and R. Barbucci, "Cell behaviour on chemically microstructured surfaces," *Materials Science and Engineering C*, vol. 23, no. 3, pp. 315–328, 2003.

[32] J. B. Recknor, D. S. Sakaguchi, and S. K. Mallapragada, "Directed growth and selective differentiation of neural progenitor cells on micropatterned polymer substrates," *Biomaterials*, vol. 27, no. 22, pp. 4098–4108, 2006.

[33] J. L. Charest, M. T. Eliason, A. J. García, and W. P. King, "Combined microscale mechanical topography and chemical patterns on polymer cell culture substrates," *Biomaterials*, vol. 27, no. 11, pp. 2487–2494, 2006.

[34] J. Zhang, S. Venkataramani, H. Xu et al., "Combined topographical and chemical micropatterns for templating neuronal networks," *Biomaterials*, vol. 27, no. 33, pp. 5734–5739, 2006.

[35] J. Yang, M. Yamato, T. Shimizu et al., "Reconstruction of functional tissues with cell sheet engineering," *Biomaterials*, vol. 28, no. 34, pp. 5033–5043, 2007.

[36] E. Palin, H. Liu, and T. J. Webster, "Mimicking the nanofeatures of bone increases bone-forming cell adhesion and proliferation," *Nanotechnology*, vol. 16, no. 9, pp. 1828–1835, 2005.

[37] K. Kubo, N. Tsukimura, F. Iwasa et al., "Cellular behavior on TiO_2 nanonodular structures in a micro-to-nanoscale hierarchy model," *Biomaterials*, vol. 30, no. 29, pp. 5319–5329, 2009.

[38] T. Ogawa, L. Saruwatari, K. Takeuchi, H. Aita, and N. Ohno, "Ti nano-nodular structuring for bone integration and regeneration," *Journal of Dental Research*, vol. 87, no. 8, pp. 751–756, 2008.

[39] G. Mendonça, D. B. S. Mendonça, F. J. L. Aragão, and L. F. Cooper, "The combination of micron and nanotopography by H_2SO_4/H_2O_2 treatment and its effects on osteoblast-specific gene expression of hMSCs," *Journal of Biomedical Materials Research A*, vol. 94, no. 1, pp. 169–179, 2010.

[40] R. A. Gittens, T. McLachlan, R. Olivares-Navarrete et al., "The effects of combined micron-/submicron-scale surface roughness and nanoscale features on cell proliferation and differentiation," *Biomaterials*, vol. 32, no. 13, pp. 3395–3403, 2011.

[41] A. Wilkinson, R. N. Hewitt, L. E. McNamara, D. McCloy, R. M. Dominic Meek, and M. J. Dalby, "Biomimetic microtopography to enhance osteogenesis in vitro," *Acta Biomaterialia*, vol. 7, no. 7, pp. 2919–2925, 2011.

[42] M. J. Mahoney, R. R. Chen, J. Tan, and W. Mark Saltzman, "The influence of microchannels on neurite growth and architecture," *Biomaterials*, vol. 26, no. 7, pp. 771–778, 2005.

[43] E. K. F. Yim, S. W. Pang, and K. W. Leong, "Synthetic nanostructures inducing differentiation of human mesenchymal stem cells into neuronal lineage," *Experimental Cell Research*, vol. 313, no. 9, pp. 1820–1829, 2007.

[44] A. Sørensen, T. Alekseeva, K. Katechia, M. Robertson, M. O. Riehle, and S. C. Barnett, "Long-term neurite orientation on astrocyte monolayers aligned by microtopography," *Biomaterials*, vol. 28, no. 36, pp. 5498–5508, 2007.

[45] E. Migliorini, G. Grenci, J. Ban et al., "Acceleration of neuronal precursors differentiation induced by substrate nanotopography," *Biotechnology and Bioengineering*, vol. 108, no. 11, pp. 2736–2746, 2011.

[46] F. Pan, M. Zhang, G. Wu et al., "Topographic effect on human induced pluripotent stem cells differentiation towards neuronal lineage," *Biomaterials*, vol. 34, no. 33, pp. 8131–8139, 2013.

[47] P. Lu, V. M. Weaver, and Z. Werb, "The extracellular matrix: a dynamic niche in cancer progression," *The Journal of Cell Biology*, vol. 196, no. 4, pp. 395–406, 2012.

[48] H. Shin, S. Jo, and A. G. Mikos, "Biomimetic materials for tissue engineering," *Biomaterials*, vol. 24, no. 24, pp. 4353–4364, 2003.

[49] P. Lu, V. M. Weaver, and Z. Werb, "The extracellular matrix: a dynamic niche in cancer progression," *Journal of Cell Biology*, vol. 196, no. 4, pp. 395–406, 2012.

[50] J. Gekas, M. Hindié, N. Faucheux et al., "The inhibition of cell spreading on a cellulose substrate (cuprophan) induces an apoptotic process via a mitochondria-dependent pathway," *FEBS Letters*, vol. 563, no. 1–3, pp. 103–107, 2004.

[51] S. M. Frisch and H. Francis, "Disruption of epithelial cell-matrix interactions induces apoptosis," *Journal of Cell Biology*, vol. 124, no. 4, pp. 619–626, 1994.

[52] J. Grossmann, "Molecular mechanisms of 'detachment-induced apoptosis—Anoikis'," *Apoptosis*, vol. 7, no. 3, pp. 247–260, 2002.

[53] P. Paoli, E. Giannoni, and P. Chiarugi, "Anoikis molecular pathways and its role in cancer progression," *Biochimica et Biophysica Acta*, 2013.

[54] A. Usui, S. Y. Ko, N. Barengo, and H. Naora, "P-cadherin promotes ovarian cancer dissemination through tumor cell aggregation and tumor-peritoneum interactions," *Molecular Cancer Research*, vol. 12, no. 4, pp. 504–513, 2014.

[55] K. Anselme, "Osteoblast adhesion on biomaterials," *Biomaterials*, vol. 21, no. 7, pp. 667–681, 2000.

[56] S. Nehrer, H. A. Breinan, A. Ramappa et al., "Matrix collagen type and pore size influence behaviour of seeded canine chondrocytes," *Biomaterials*, vol. 18, no. 11, pp. 769–776, 1997.

[57] S. Schlie-Wolter, A. Ngezahayo, and B. N. Chichkov, "The selective role of ECM components on cell adhesion, morphology, proliferation and communication in vitro," *Experimental Cell Research*, vol. 319, no. 10, pp. 1553–1561, 2013.

[58] C. S. Chen, M. Mrksich, S. Huang, G. M. Whitesides, and D. E. Ingber, "Geometric control of cell life and death," *Science*, vol. 276, no. 5317, pp. 1425–1428, 1997.

[59] S. H. Kim, J. Turnbull, and S. Guimond, "Extracellular matrix and cell signalling: the dynamic cooperation of integrin, proteoglycan and growth factor receptor," *Journal of Endocrinology*, vol. 209, no. 2, pp. 139–151, 2011.

[60] K. Burridge, K. Fath, T. Kelly, G. Nuckolls, and C. Turner, "Focal adhesions: transmembrane junctions between the extracellular matrix and the cytoskeleton," *Annual Review of Cell Biology*, vol. 4, pp. 487–525, 1988.

[61] R. Zaidel-Bar, S. Itzkovitz, A. Ma'ayan, R. Iyengar, and B. Geiger, "Functional atlas of the integrin adhesome," *Nature Cell Biology*, vol. 9, no. 8, pp. 858–867, 2007.

[62] M. E. Lukashev and Z. Werb, "ECM signalling: orchestrating cell behaviour and misbehaviour," *Trends in Cell Biology*, vol. 8, no. 11, pp. 437–441, 1998.

[63] D. Ashton-Beaucage and M. Therrien, "The greater RTK/RAS/ERK signalling pathway: How genetics has helped piece together a signalling network," *Medecine/Sciences*, vol. 26, no. 12, pp. 1067–1073, 2010.

[64] R. O. Hynes, "Integrins: bidirectional, allosteric signaling machines," *Cell*, vol. 110, no. 6, pp. 673–687, 2002.

[65] G. F. Weber, M. A. Bjerke, and D. W. DeSimone, "Integrins and cadherins join forces to form adhesive networks," *Journal of Cell Science*, vol. 124, no. 8, pp. 1183–1193, 2011.

[66] D.-H. Kim, S. B. Khatau, Y. Feng et al., "Actin cap associated focal adhesions and their distinct role in cellular mechanosensing," *Scientific Reports*, vol. 2, article 555, 2012.

[67] D. H. Rosenzweig, S. Solar-Cafaggi, and T. M. Quinn, "Functionalization of dynamic culture surfaces with a cartilage extracellular matrix extract enhances chondrocyte phenotype against dedifferentiation," *Acta Biomaterialia*, vol. 8, no. 9, pp. 3333–3341, 2012.

[68] A. J. Engler, S. Sen, H. L. Sweeney, and D. E. Discher, "Matrix elasticity directs stem cell lineage specification," *Cell*, vol. 126, no. 4, pp. 677–689, 2006.

[69] M. J. Bradshaw and M. L. Smith, "Multiscale relationships between fibronectin structure and functional properties," *Acta Biomaterialia*, vol. 10, no. 4, pp. 1524–1531, 2014.

[70] S. N. Stephansson, B. A. Byers, and A. J. García, "Enhanced expression of the osteoblastic phenotype on substrates that modulate fibronectin conformation and integrin receptor binding," *Biomaterials*, vol. 23, no. 12, pp. 2527–2534, 2002.

[71] L. Zhang and K. G. T. Hagen, "The cellular microenvironment and cell adhesion: a role for O-glycosylation," *Biochemical Society Transactions*, vol. 39, no. 1, pp. 378–382, 2011.

[72] A. Akhavan, O. L. Griffith, L. Soroceanu et al., "Loss of cell-surface laminin anchoring promotes tumor growth and is associated with poor clinical outcomes," *Cancer Research*, vol. 72, no. 10, pp. 2578–2588, 2012.

[73] M. P. Lutolf and J. A. Hubbell, "Synthetic biomaterials as instructive extracellular microenvironments for morphogenesis in tissue engineering," *Nature Biotechnology*, vol. 23, no. 1, pp. 47–55, 2005.

[74] A. Kurtz and S. J. Oh, "Age related changes of the extracellular matrix and stem cell maintenance," *Preventive Medicine*, vol. 54, supplement, pp. S50–S56, 2012.

[75] P. Lenas, M. Moos Jr., and F. P. Luyten, "Developmental engineering: a new paradigm for the design and manufacturing of cell-based products. Part I: from three-dimensional cell growth to biomimetics of *in vivo* development," *Tissue Engineering B: Reviews*, vol. 15, no. 4, pp. 381–394, 2009.

[76] D. E. Ingber, V. C. Mow, D. Butler et al., "Tissue engineering and developmental biology: going biomimetic," *Tissue Engineering*, vol. 12, no. 12, pp. 3265–3283, 2006.

[77] L. Li and T. Xie, "Stem cell niche: Structure and function," *Annual Review of Cell and Developmental Biology*, vol. 21, pp. 605–631, 2005.

[78] F. Gattazzo, A. Urciuolo, and P. Bonaldo, "Extracellular matrix: a dynamic microenvironment for stem cell niche," *Biochimica et Biophysica Acta*, vol. 1840, no. 8, pp. 2506–2519, 2014.

[79] F. M. Watt and W. T. S. Huck, "Role of the extracellular matrix in regulating stem cell fate," *Nature Reviews Molecular Cell Biology*, vol. 14, no. 8, pp. 467–473, 2013.

[80] S. Oh, K. S. Brammer, Y. S. J. Li et al., "Stem cell fate dictated solely by altered nanotube dimension," *Proceedings of the National Academy of Sciences of the United States of America*, vol. 106, no. 7, pp. 2130–2135, 2009.

[81] J. T. Connelly, J. E. Gautrot, B. Trappmann et al., "Actin and serum response factor transduce physical cues from the microenvironment to regulate epidermal stem cell fate decisions," *Nature Cell Biology*, vol. 12, no. 7, pp. 711–718, 2010.

[82] R. McBeath, D. M. Pirone, C. M. Nelson, K. Bhadriraju, and C. S. Chen, "Cell shape, cytoskeletal tension, and RhoA regulate stem cell lineage commitment," *Developmental Cell*, vol. 6, no. 4, pp. 483–495, 2004.

[83] J. A. Burdick and G. Vunjak-Novakovic, "Engineered microenvironments for controlled stem cell differentiation," *Tissue Engineering A*, vol. 15, no. 2, pp. 205–219, 2009.

[84] I. E. Erickson, A. H. Huang, S. Sengupta, S. Kestle, J. A. Burdick, and R. L. Mauck, "Macromer density influences mesenchymal stem cell chondrogenesis and maturation in photocrosslinked hyaluronic acid hydrogels," *Osteoarthritis and Cartilage*, vol. 17, no. 12, pp. 1639–1648, 2009.

[85] H. Tian, S. Bharadwaj, Y. Liu et al., "Myogenic differentiation of human bone marrow mesenchymal stem cells on a 3D nano fibrous scaffold for bladder tissue engineering," *Biomaterials*, vol. 31, no. 5, pp. 870–877, 2010.

[86] K. Lee, E. A. Silva, and D. J. Mooney, "Growth factor delivery-based tissue engineering: general approaches and a review of recent developments," *Journal of the Royal Society Interface*, vol. 8, no. 55, pp. 153–170, 2011.

[87] S. J. Konturek, W. Pawlik, W. Mysh et al., "Comparison of organ uptake and disappearance half-time of human epidermal growth factor and insulin," *Regulatory Peptides*, vol. 30, no. 2, pp. 137–148, 1990.

[88] F. M. Chen, R. M. Shelton, Y. Jin, and I. L. C. Chapple, "Localized delivery of growth factors for periodontal tissue regeneration: role, strategies, and perspectives," *Medicinal Research Reviews*, vol. 29, no. 3, pp. 472–513, 2009.

[89] Y. Bai, G. Yin, Z. Huang et al., "Localized delivery of growth factors for angiogenesis and bone formation in tissue engineering," *International Immunopharmacology*, vol. 16, no. 2, pp. 214–223, 2013.

[90] E. A. Silva and D. J. Mooney, "Spatiotemporal control of vascular endothelial growth factor delivery from injectable hydrogels enhances angiogenesis," *Journal of Thrombosis and Haemostasis*, vol. 5, no. 3, pp. 590–598, 2007.

[91] S. Kim, J. Turnbull, and S. Guimond, "Extracellular matrix and cell signalling: the dynamic cooperation of integrin, proteoglycan and growth factor receptor," *Journal of Endocrinology*, vol. 209, no. 2, pp. 139–151, 2011.

[92] F. Rosso, A. Giordano, M. Barbarisi, and A. Barbarisi, "From cell-ECM interactions to tissue engineering," *Journal of Cellular Physiology*, vol. 199, no. 2, pp. 174–180, 2004.

[93] S. Mitragotri and J. Lahann, "Physical approaches to biomaterial design," *Nature Materials*, vol. 8, no. 1, pp. 15–23, 2009.

[94] R. Langer, "New methods of drug delivery," *Science*, vol. 249, no. 4976, pp. 1527–1533, 1990.

[95] F. M. Chen, M. Zhang, and Z. F. Wu, "Toward delivery of multiple growth factors in tissue engineering," *Biomaterials*, vol. 31, no. 24, pp. 6279–6308, 2010.

[96] Y. H. Shen, M. S. Shoichet, and M. Radisic, "Vascular endothelial growth factor immobilized in collagen scaffold promotes penetration and proliferation of endothelial cells," *Acta Biomaterialia*, vol. 4, no. 3, pp. 477–489, 2008.

[97] E. A. Mitchell, B. T. Chaffey, A. W. McCaskie, J. H. Lakey, and M. A. Birch, "Controlled spatial and conformational display of immobilised bone morphogenetic protein-2 and osteopontin signalling motifs regulates osteoblast adhesion and differentiation *in vitro*," *BMC Biology*, vol. 8, article 57, 2010.

[98] G. Zhang and L. J. Suggs, "Matrices and scaffolds for drug delivery in vascular tissue engineering," *Advanced Drug Delivery Reviews*, vol. 59, no. 4-5, pp. 360–373, 2007.

[99] K. Y. P. Lee, M. C. Anderson, K. W. Mooney, and J. David, "Controlled growth factor release from synthetic extracellular matrices," *Nature*, vol. 408, no. 6815, pp. 998–1000, 2000.

[100] N. E. Vrana, P. A. Cahill, and G. B. McGuinness, "Endothelialization of PVA/gelatin cryogels for vascular tissue engineering: effect of disturbed shear stress conditions," *Journal of Biomedical Materials Research A*, vol. 94, no. 4, pp. 1080–1090, 2010.

[101] M. Yamamoto, Y. Ikada, and Y. Tabata, "Controlled release of growth factors based on biodegradation of gelatin hydrogel," *Journal of Biomaterials Science*, vol. 12, no. 1, pp. 77–88, 2001.

[102] Y. Tabata and Y. Ikada, "Protein release from gelatin matrices," *Advanced Drug Delivery Reviews*, vol. 31, no. 3, pp. 287–301, 1998.

[103] M. K. McDermott, T. Chen, C. Williams, K. M. Markley, and G. F. Payne, "Mechanical properties of biomimetic tissue adhesive based on the microbial transglutaminase-catalyzed crosslinking of gelatin," *Biomacromolecules*, vol. 5, no. 4, pp. 1270–1279, 2004.

[104] J. Chang, J. Lin, C. Yao, J. Chen, T. Lai, and Y. Chen, "In vivo evaluation of a biodegradable EDC/NHS-cross-linked gelatin peripheral nerve guide conduit material," *Macromolecular Bioscience*, vol. 7, no. 4, pp. 500–507, 2007.

[105] A. Bigi, G. Cojazzi, S. Panzavolta, N. Roveri, and K. Rubini, "Stabilization of gelatin films by crosslinking with genipin," *Biomaterials*, vol. 23, no. 24, pp. 4827–4832, 2002.

[106] H. Zhang, A. Patel, A. K. Gaharwar et al., "Hyperbranched polyester hydrogels with controlled drug release and cell adhesion properties," *Biomacromolecules*, vol. 14, no. 5, pp. 1299–1310, 2013.

[107] C. Vodouhê, E. L. Guen, J. M. Garza et al., "Control of drug accessibility on functional polyelectrolyte multilayer films," *Biomaterials*, vol. 27, no. 22, pp. 4149–4156, 2006.

[108] M. L. Macdonald, R. E. Samuel, N. J. Shah, R. F. Padera, Y. M. Beben, and P. T. Hammond, "Tissue integration of growth factor-eluting layer-by-layer polyelectrolyte multilayer coated implants," *Biomaterials*, vol. 32, no. 5, pp. 1446–1453, 2011.

[109] N. E. Vrana, O. Erdemli, G. Francius et al., "Double entrapment of growth factors by nanoparticles loaded into polyelectrolyte multilayer films," *Journal of Materials Chemistry B*, vol. 2, pp. 999–1008, 2014.

[110] J. Barthes, D. Mertz, C. Bach et al., "Stretch-induced biodegradation of polyelectrolyte multilayer films for drug release," *Langmuir*, vol. 28, no. 38, pp. 13550–13554, 2012.

[111] A. P. R. Johnston, C. Cortez, A. S. Angelatos, and F. Caruso, "Layer-by-layer engineered capsules and their applications," *Current Opinion in Colloid & Interface Science*, vol. 11, no. 4, pp. 203–209, 2006.

[112] Y. Zhu, J. Shi, W. Shen et al., "Stimuli-responsive controlled drug release from a hollow mesoporous silica sphere/polyelectrolyte multilayer core-shell structure," *Angewandte Chemie*, vol. 117, pp. 5213–5217, 2005.

[113] T. P. Richardson, M. C. Peters, A. B. Ennett, and D. J. Mooney, "Polymeric system for dual growth factor delivery," *Nature Biotechnology*, vol. 19, no. 11, pp. 1029–1034, 2001.

[114] F.-M. Chen, R. Chen, X.-J. Wang, H.-H. Sun, and Z.-F. Wu, "In vitro cellular responses to scaffolds containing two microencapulated growth factors," *Biomaterials*, vol. 30, no. 28, pp. 5215–5224, 2009.

[115] S. C. Sundararaj, M. V. Thomas, R. Peyyala, T. D. Dziubla, and D. A. Puleo, "Design of a multiple drug delivery system directed at periodontitis," *Biomaterials*, vol. 34, no. 34, pp. 8835–8842, 2013.

[116] M. A. Hasan, K. Ragaert, and W. Swieszkowski, "Biomechanical properties of native and tissue engineered heart valve constructs," *Journal of Biomechanics*, vol. 47, no. 9, pp. 1949–1963, 2014.

[117] M. W. Tibbitt and K. S. Anseth, "Dynamic microenvironments: the fourth dimension," *Science Translational Medicine*, vol. 4, no. 160, 2012.

[118] J. A. King and W. M. Miller, "Bioreactor development for stem cell expansion and controlled differentiation," *Current Opinion in Chemical Biology*, vol. 11, no. 4, pp. 394–398, 2007.

[119] G. Song, Y. Ju, X. Shen, Q. Luo, Y. Shi, and J. Qin, "Mechanical stretch promotes proliferation of rat bone marrow mesenchymal stem cells," *Colloids and Surfaces B: Biointerfaces*, vol. 58, no. 2, pp. 271–277, 2007.

[120] V. Dumas, A. Perrier, L. Malaval et al., "The effect of dual frequency cyclic compression on matrix deposition by osteoblast-like cells grown in 3D scaffolds and on modulation of VEGF variant expression," *Biomaterials*, vol. 30, no. 19, pp. 3279–3288, 2009.

[121] L. Prodanov, J. te Riet, E. Lamers et al., "The interaction between nanoscale surface features and mechanical loading and its effect on osteoblast-like cells behavior," *Biomaterials*, vol. 31, no. 30, pp. 7758–7765, 2010.

[122] J. Wang, G. Yang, Z. Li, and W. Shen, "Fibroblast responses to cyclic mechanical stretching depend on cell orientation to the stretching direction," *Journal of Biomechanics*, vol. 37, no. 4, pp. 573–576, 2004.

[123] W. A. Loesberg, X. F. Walboomers, J. J. W. A. van Loon, and J. A. Jansen, "The effect of combined cyclic mechanical stretching and microgrooved surface topography on the behavior of fibroblasts," *Journal of Biomedical Materials Research A*, vol. 75, no. 3, pp. 723–732, 2005.

[124] W. W. Ahmed, T. Wolfram, A. M. Goldyn et al., "Myoblast morphology and organization on biochemically micro-patterned hydrogel coatings under cyclic mechanical strain," *Biomaterials*, vol. 31, no. 2, pp. 250–258, 2010.

[125] R. Kaunas, P. Nguyen, S. Usami, and S. Chien, "Cooperative effects of Rho and mechanical stretch on stress fiber organization," *Proceedings of the National Academy of Sciences of the United States of America*, vol. 102, no. 44, pp. 15895–15900, 2005.

[126] C. Neidlinger-Wilke, E. S. Grood, J. H. Wang, R. A. Brand, and L. Claes, "Cell alignment is induced by cyclic changes in cell length: studies of cells grown in cyclically stretched substrates," *Journal of Orthopaedic Research*, vol. 19, no. 2, pp. 286–293, 2001.

[127] G. Houtchens, M. Foster, T. Desai, E. Morgan, and J. Wong, "Combined effects of microtopography and cyclic strain on vascular smooth muscle cell orientation," *Journal of Biomechanics*, vol. 41, no. 4, pp. 762–769, 2008.

[128] J. H. Wang, E. S. Grood, J. Florer, and R. Wenstrup, "Alignment and proliferation of MC3T3-E1 osteoblasts in microgrooved silicone substrata subjected to cyclic stretching," *Journal of Biomechanics*, vol. 33, no. 6, pp. 729–735, 2000.

[129] O. W. Petersen, L. Ronnov-Jessen, A. R. Howlett, and M. J. Bissell, "Interaction with basement membrane serves to rapidly distinguish growth and differentiation pattern of normal and malignant human breast epithelial cells," *Proceedings of the National Academy of Sciences of the United States of America*, vol. 89, no. 19, pp. 9064–9068, 1992.

[130] A. M. Kloxin, A. M. Kasko, C. N. Salinas, and K. S. Anseth, "Photodegradable hydrogels for dynamic tuning of physical and chemical properties," *Science*, vol. 324, no. 5923, pp. 59–63, 2009.

[131] C. N. Salinas and K. S. Anseth, "The enhancement of chondrogenic differentiation of human mesenchymal stem cells by enzymatically regulated RGD functionalities," *Biomaterials*, vol. 29, no. 15, pp. 2370–2377, 2008.

[132] B. Jiang, T. M. Waller, J. C. Larson, A. A. Appel, and E. M. Brey, "Fibrin-loaded porous poly(Ethylene Glycol) hydrogels as scaffold materials for vascularized tissue formation," *Tissue Engineering A*, vol. 19, no. 1-2, pp. 224–234, 2013.

[133] M. Nikkhah, F. Edalat, S. Manoucheri, and A. Khademhosseini, "Engineering microscale topographies to control the cell-substrate interface," *Biomaterials*, vol. 33, no. 21, pp. 5230–5246, 2012.

[134] J. J. Moon, M. S. Hahn, I. Kim, B. A. Nsiah, and J. L. West, "Micropatterning of poly(ethylene glycol) diacrylate hydrogels with biomolecules to regulate and guide endothelial morphogenesis," *Tissue Engineering A*, vol. 15, no. 3, pp. 579–585, 2009.

[135] V. Vickerman, J. Blundo, S. Chung, and R. Kamm, "Design, fabrication and implementation of a novel multi-parameter control microfluidic platform for three-dimensional cell culture and real-time imaging," *Lab on a Chip: Miniaturisation for Chemistry and Biology*, vol. 8, no. 9, pp. 1468–1477, 2008.

[136] J. W. Song, D. Bazou, and L. L. Munn, "Anastomosis of endothelial sprouts forms new vessels in a tissue analogue of angiogenesis," *Integrative Biology*, vol. 4, no. 8, pp. 857–862, 2012.

[137] C. P. Huang, J. Lu, H. Seon et al., "Engineering microscale cellular niches for three-dimensional multicellular co-cultures," *Lab on a Chip: Miniaturisation for Chemistry and Biology*, vol. 9, no. 12, pp. 1740–1748, 2009.

[138] K. C. Chaw, M. Manimaran, F. E. H. Tay, and S. Swaminathan, "Matrigel coated polydimethylsiloxane based microfluidic devices for studying metastatic and non-metastatic cancer cell invasion and migration," *Biomedical Microdevices*, vol. 9, no. 4, pp. 597–602, 2007.

[139] A. Shamloo and S. C. Heilshorn, "Matrix density mediates polarization and lumen formation of endothelial sprouts in VEGF gradients," *Lab on a Chip: Miniaturisation for Chemistry and Biology*, vol. 10, no. 22, pp. 3061–3068, 2010.

[140] B. Mosadegh, C. Huango, J. W. Park et al., "Generation of stable complex gradients across two-dimensional surfaces and three-dimensional gels," *Langmuir*, vol. 23, no. 22, pp. 10910–10912, 2007.

[141] M. A. Unger, H. Chou, T. Thorsen, A. Scherer, and S. R. Quake, "Monolithic microfabricated valves and pumps by multilayer soft lithography," *Science*, vol. 288, no. 5463, pp. 113–116, 2000.

[142] W. Gu, X. Zhu, N. Futai, B. S. Cho, and S. Takayama, "Computerized microfluidic cell culture using elastomeric channels and Braille displays," *Proceedings of the National Academy of Sciences of the United States of America*, vol. 101, no. 45, pp. 15861–15866, 2004.

[143] A. Hasan, A. Paul, N. E. Vrana et al., "Microfluidic techniques for development of 3D vascularized tissue," *Biomaterials*, vol. 35, no. 26, pp. 7308–7325, 2014.

[144] A. Paul, A. Hasan, L. Rodes, M. Sangaralingam, and S. Prakash, "Bioengineered baculoviruses as new class of therapeutics

using micro and nanotechnologies: principles, prospects and challenges," *Advanced Drug Delivery Reviews*, vol. 71, pp. 115–130, 2014.

[145] B. L. Gilmore, S. P. Showalter, M. J. Dukes et al., "Visualizing viral assemblies in a nanoscale biosphere," *Lab on a Chip: Miniaturisation for Chemistry and Biology*, vol. 13, no. 2, pp. 216–219, 2013.

[146] G. M. Walker, M. S. Ozers, and D. J. Beebe, "Cell infection within a microfluidic device using virus gradients," *Sensors and Actuators B: Chemical*, vol. 98, no. 2-3, pp. 347–355, 2004.

[147] S. K. W. Dertinger, D. T. Chiu, and G. M. Whitesides, "Generation of gradients having complex shapes using microfluidic networks," *Analytical Chemistry*, vol. 73, no. 6, pp. 1240–1246, 2001.

[148] S. K. W. Dertinger, X. Jiang, Z. Li, V. N. Murthy, and G. M. Whitesides, "Gradients of substrate-bound laminin orient axonal specification of neurons," *Proceedings of the National Academy of Sciences of the United States of America*, vol. 99, no. 20, pp. 12542–12547, 2002.

[149] N. L. Jeon, S. K. W. Dertinger, D. T. Chiu, I. S. Choi, A. D. Stroock, and G. M. Whitesides, "Generation of solution and surface gradients using microfluidic systems," *Langmuir*, vol. 16, no. 22, pp. 8311–8316, 2000.

[150] N. Li Jeon, H. Baskaran, S. K. W. Dertinger, G. M. Whitesides, L. V. de Water, and M. Toner, "Neutrophil chemotaxis in linear and complex gradients of interleukin-8 formed in a microfabricated device," *Nature Biotechnology*, vol. 20, no. 8, pp. 826–830, 2002.

[151] N. Xu, Z. F. Zhang, L. Wang, B. Gao, D. W. Pang, and H. Z. Wang, "A microfluidic platform for real-time and in situ monitoring of virus infection process," *Biomicrofluidics*, vol. 6, Article ID 034122, 2012.

[152] K. Na, M. Lee, B. Shin, Y. Je, and J. Hyun, "Polymer-templated microarrays for highly reliable plaque purification," *Biotechnology Progress*, vol. 22, no. 1, pp. 285–287, 2006.

[153] H. N. Vu, Y. Li, M. Casali, D. Irimia, Z. Megeed, and M. L. Yarmush, "A microfluidic bioreactor for increased active retrovirus output," *Lab on a Chip*, vol. 8, no. 1, pp. 75–80, 2007.

[154] R. S. Kane, S. Takayama, E. Ostuni, D. E. Ingber, and G. M. Whitesides, "Patterning proteins and cells using soft lithography," *Biomaterials*, vol. 20, no. 23-24, pp. 2363–2376, 1999.

[155] D. G. Anderson, S. Levenberg, and R. Langer, "Nanoliter-scale synthesis of arrayed biomaterials and application to human embryonic stem cells," *Nature Biotechnology*, vol. 22, no. 7, pp. 863–866, 2004.

[156] D. G. Anderson, D. Putnam, E. B. Lavik, T. A. Mahmood, and R. Langer, "Biomaterial microarrays: rapid, microscale screening of polymer-cell interaction," *Biomaterials*, vol. 26, no. 23, pp. 4892–4897, 2005.

[157] S. Vaddiraju, I. Tomazos, D. J. Burgess, F. C. Jain, and F. Papadimitrakopoulos, "Emerging synergy between nanotechnology and implantable biosensors: a review," *Biosensors and Bioelectronics*, vol. 25, no. 7, pp. 1553–1565, 2010.

[158] P. Vadgama, "Sensor biocompatibility: final frontier in bioanalytical measurement," *Analyst*, vol. 132, no. 6, pp. 495–499, 2007.

[159] M. Kubon, M. Moschallski, G. Link et al., "A microsensor system to probe physiological environments and tissue response," in *Proceedings of the IEEE Sensors*, pp. 2607–2611, Kona, Hawaii, USA, November 2010.

[160] M. Kubon, M. Moschallski, T. Ensslen et al., "Towards quantification of biocompatibility: monitoring ingrowth behavior of biomaterials in tissue with a microsensor implant," in *Proceedings of the 16th International Solid-State Sensors, Actuators and Microsystems Conference (TRANSDUCERS '11)*, pp. 1935–1937, June 2011.

[161] Y. Yang, A. Dubois, X.-P. Qin, J. Li, A. E. Haj, and R. K. Wang, "Investigation of optical coherence tomography as an imaging modality in tissue engineering," *Physics in Medicine and Biology*, vol. 51, no. 7, pp. 1649–1659, 2006.

[162] P. P. Provenzano, K. W. Eliceiri, and P. J. Keely, "Multiphoton microscopy and fluorescence lifetime imaging microscopy (FLIM) to monitor metastasis and the tumor microenvironment," *Clinical and Experimental Metastasis*, vol. 26, no. 4, pp. 357–370, 2009.

[163] M. Vielreicher, S. Schürmann, R. Detsch et al., "Taking a deep look: modern microscopy technologies to optimize the design and functionality of biocompatible scaffolds for tissue engineering in regenerative medicine," *Journal of the Royal Society Interface*, vol. 10, no. 86, article 0263, 2013.

[164] S. Kidd, E. Spaeth, J. L. Dembinski et al., "Direct evidence of mesenchymal stem cell tropism for tumor and wounding microenvironments using in vivo bioluminescent imaging," *Stem Cells*, vol. 27, no. 10, pp. 2614–2623, 2009.

[165] M. A. Acosta, P. Ymele-Leki, Y. V. Kostov, and J. B. Leach, "Fluorescent microparticles for sensing cell microenvironment oxygen levels within 3D scaffolds," *Biomaterials*, vol. 30, no. 17, pp. 3068–3074, 2009.

[166] N. W. Choi, S. S. Verbridge, R. M. Williams et al., "Phosphorescent nanoparticles for quantitative measurements of oxygen profiles invitro and invivo," *Biomaterials*, vol. 33, no. 9, pp. 2710–2722, 2012.

[167] G. A. A. Saracino, D. Cigognini, D. Silva, A. Caprini, and F. Gelain, "Nanomaterials design and tests for neural tissue engineering," *Chemical Society Reviews*, vol. 42, no. 1, pp. 225–262, 2013.

[168] K. Saha, Y. Mei, C. M. Reisterer et al., "Surface-engineered substrates for improved human pluripotent stem cell culture under fully defined conditions," *Proceedings of the National Academy of Sciences of the United States of America*, vol. 108, no. 46, pp. 18714–18719, 2011.

[169] D. C. Hay, S. Pernagallo, J. J. Diaz-Mochon et al., "Unbiased screening of polymer libraries to define novel substrates for functional hepatocytes with inducible drug metabolism," *Stem Cell Research*, vol. 6, no. 2, pp. 92–102, 2011.

[170] R. Derda, S. Musah, B. P. Orner, J. R. Klim, N. Li, and L. L. Kiessling, "High-throughput discovery of synthetic surfaces that support proliferation of pluripotent cells," *Journal of the American Chemical Society*, vol. 132, no. 4, pp. 1289–1295, 2010.

[171] C. J. Flaim, D. Teng, S. Chien, and S. N. Bhatia, "Combinatorial signaling microenvironments for studying stem cell fate," *Stem Cells and Development*, vol. 17, no. 1, pp. 29–39, 2008.

[172] Y. Soen, A. Mori, T. D. Palmer, and P. O. Brown, "Exploring the regulation of human neural precursor cell differentiation using arrays of signaling microenvironments," *Molecular Systems Biology*, vol. 2, 2006.

[173] D. A. Brafman, S. Chien, and K. Willert, "Arrayed cellular microenvironments for identifying culture and differentiation conditions for stem, primary and rare cell populations," *Nature Protocols*, vol. 7, no. 4, pp. 703–717, 2012.

[174] Y. Mei, C. Cannizzaro, H. Park et al., "Cell-compatible, multicomponent protein arrays with subcellular feature resolution," *Small*, vol. 4, no. 10, pp. 1600–1604, 2008.

[175] H. V. Unadkat, M. Hulsman, K. Cornelissen et al., "An algorithm-based topographical biomaterials library to instruct cell

fate," *Proceedings of the National Academy of Sciences of the United States of America*, vol. 108, no. 40, pp. 16565–16570, 2011.

[176] H. N. Kim, Y. Hong, M. S. Kim, S. M. Kim, and K. Suh, "Effect of orientation and density of nanotopography in dermal wound healing," *Biomaterials*, vol. 33, no. 34, pp. 8782–8792, 2012.

[177] D. Rajput, S. W. Crowder, L. Hofmeister, L. Costa, H. Sung, and W. Hofmeister, "Cell interaction study method using novel 3D silica nanoneedle gradient arrays," *Colloids and Surfaces B: Biointerfaces*, vol. 102, pp. 111–116, 2013.

[178] P. M. Reynolds, R. H. Pedersen, J. Stormonth-Darling, M. J. Dalby, M. O. Riehle, and N. Gadegaard, "Label-free segmentation of co-cultured cells on a nanotopographical gradient," *Nano Letters*, vol. 13, no. 2, pp. 570–576, 2013.

Hindawi Publishing Corporation
BioMed Research International
Volume 2014, Article ID 648459, 8 pages
http://dx.doi.org/10.1155/2014/648459

Review Article

The ECM-Cell Interaction of Cartilage Extracellular Matrix on Chondrocytes

Yue Gao, Shuyun Liu, Jingxiang Huang, Weimin Guo, Jifeng Chen, Li Zhang, Bin Zhao, Jiang Peng, Aiyuan Wang, Yu Wang, Wenjing Xu, Shibi Lu, Mei Yuan, and Quanyi Guo

Institute of Orthopedics, Chinese PLA General Hospital, Beijing 100853, China

Correspondence should be addressed to Quanyi Guo; guoquanyi301@gmail.com

Received 14 February 2014; Accepted 24 April 2014; Published 18 May 2014

Academic Editor: Albana Ndreu-Halili

Cartilage extracellular matrix (ECM) is composed primarily of the network type II collagen (COLII) and an interlocking mesh of fibrous proteins and proteoglycans (PGs), hyaluronic acid (HA), and chondroitin sulfate (CS). Articular cartilage ECM plays a crucial role in regulating chondrocyte metabolism and functions, such as organized cytoskeleton through integrin-mediated signaling via cell-matrix interaction. Cell signaling through integrins regulates several chondrocyte functions, including differentiation, metabolism, matrix remodeling, responses to mechanical stimulation, and cell survival. The major signaling pathways that regulate chondrogenesis have been identified as wnt signal, nitric oxide (NO) signal, protein kinase C (PKC), and retinoic acid (RA) signal. Integrins are a large family of molecules that are central regulators in multicellular biology. They orchestrate cell-cell and cell-matrix adhesive interactions from embryonic development to mature tissue function. In this review, we emphasize the signaling molecule effect and the biomechanics effect of cartilage ECM on chondrogenesis.

1. What Is ECM?

In biology, the extracellular matrix (ECM) is the extracellular part of multicellular structure (e.g., organisms, tissues, and biofilms) that typically provides structural and biochemical support to the surrounding cells [1]. Because multicellularity evolved independently in different multicellular lineages, the composition of ECM varies between multicellular structures; however, cell adhesion, cell-to-cell communication, and differentiation are common functions of the ECM [2].

Cartilage ECM is composed primarily of COLII and large networks of PGs that contain GAG such as HA and CS. Because cartilage shows little tendency for self-repair, injuries remain unhealed for years and can lead to further degeneration [3]. Cartilaginous ECM is remodeled continuously by a combination of production, degradation by matrix metalloproteinases (MMPs), and inhibition of MMPs activity by tissue inhibitors of MMPs [4]. The ECM of articular cartilage is a unique environment. ECM components through their action on integrin clustering are involved in cell adhesion, cortical actin cytoskeleton organization, and cell spreading [5].

The ECM is composed of large proteoglycans (PGs) that contain glycosaminoglycan (GAG), hyaluronic acid (HA), fibers, and other molecular components about fibronectin and laminin. Fibers contain elastin and collagen that include fibrillar (types I, II, III, V, and XI), FACIT (types IX, XII, and XIV), short chain (types VIII and X), basement membrane (type IV), and others (types VI, VII, and XIII) [6] (Figure 1). In the ECM, especially the basement membrane, the multidomain proteins perlecan, agrin, and COLXVIII are the main proteins to which heparan sulfate attaches [7]. At last, there are important molecular components called integrins. Integrins are transmembrane receptors that mediate the attachment between a cell and its surroundings, such as other cells or the extracellular matrix (ECM). In signal transduction, integrins pass information about the chemical composition and mechanical status of the ECM into the cell. Therefore, in addition to transmitting mechanical forces across otherwise vulnerable membranes, they are involved in cell signaling and the regulation of cell cycle, shape, and motility.

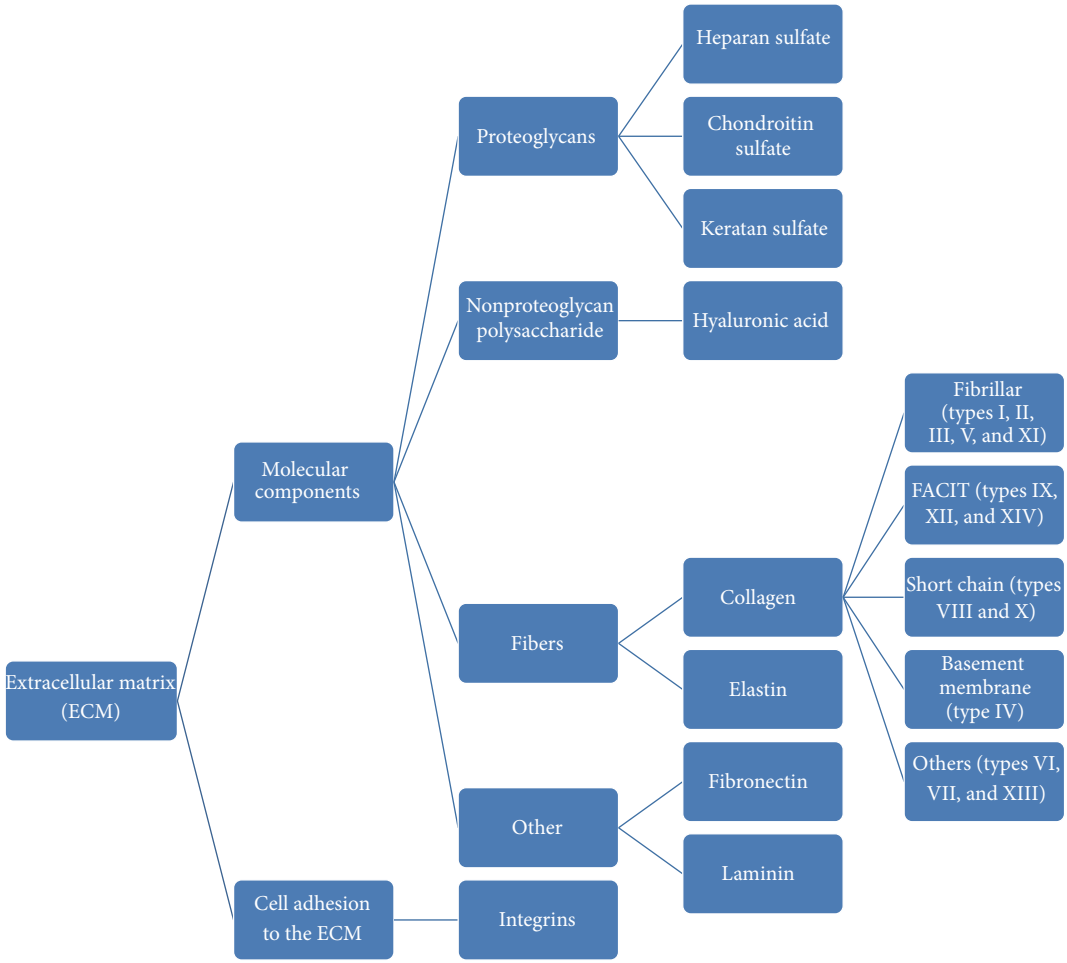

Figure 1

2. What Is the Function of ECM?

Because of its diverse nature and composition, the ECM can have many functions, such as providing support, segregating tissues, and regulating intercellular communication. The ECM regulates a cell's dynamic behavior. In addition, it stores a wide range of cellular growth factors and acts as a local depot for them. Changes in physiological conditions can trigger protease activities that cause the local release of such depots. This situation allows for the rapid and local growth-factor-mediated activation of cellular functions. The formation of the ECM is essential for processes such as growth, wound healing, and fibrosis. PGs have a net negative charge that attracts positively charged sodium ions which attracts water molecules via osmosis. PGs can keep the ECM and resident cells hydrated. PGs may also help trap and store growth factors within the ECM. Once secreted, the molecules aggregate with the existing matrix. Resident cells intracellularly produce the components of the ECM via exocytosis [6].

Articular cartilage ECM plays a crucial role in regulating chondrocyte functions via cell-matrix interaction, organized cytoskeleton, and integrin-mediated signaling. The ECM has a significant effect on the swelling behavior and osmotic environment of chondrocytes [8]. Factors produced by chondrocytes can affect the synthesis of the ECM. These factors are ILs, basic fibroblast growth factor (BFGF), bone morphogenic proteins (BMPs), and insulin-like growth factor (IGF). Cell signaling mediated by integrin regulates several chondrocyte functions, including differentiation, matrix remodeling, responses to mechanical stimulation, and cell survival [9–11]. CS and HA influence the proliferation and differentiation of chondrocytes. Scaffolds composed of COLII, CS, and HA may create an environment that can preserve the normal phenotype of cells to promote regeneration of cartilage-like constructs [12]. CS contributes to the tensile strength of cartilage, tendons, ligaments, and walls of the aorta. Low-molecular-weight isoforms of the aggrecanases are responsible for the cytokine-induced proteolysis of aggrecan in a porcine chondrocyte culture system [13, 14]. Abnormal contact between chondrocytes and the ECM has serious consequences. Chondrocytes isolated from Rac1-deficient growth plates show reduced adhesion to COLII and fibronectin [15]. To provide a larger space to allow for cell proliferation and generation of new ECM, we found that a COLII scaffold composed of collagen with genipin is similar to natural ECM; the application of CS can increase mRNA and DNA biosynthesis and promote cell metabolism the

same as with the acid mucopolysaccharide HA, with strong bonding and hydrophilic properties, to retain moisture, so that it better resembles the natural ECM and promotes cell proliferation [12].

Interactions between chondrocytes and the ECM regulate many biological processes important to homeostasis and repair of articular cartilage, including cell attachment, growth, differentiation, and survival. Integrins have two main functions: (1) attachment of the cell to the ECM and (2) signal transduction from the ECM to the cell.

However, they are also involved in a wide range of other biological activities, including immune patrolling, cell migration, and binding to cells by certain viruses, such as adenovirus, echovirus, hantavirus, and foot and mouth disease viruses.

A prominent function of the integrins is seen in the molecule GPIIbIIIa, an integrin on the surface of blood platelets (thrombocytes) responsible for attachment to fibrin within a developing blood clot. This molecule dramatically increases its binding affinity for fibrin/fibrinogen through association of platelets with exposed collagens in the wound site. Upon association of platelets with collagen, GPIIbIIIa changes shape, allowing it to bind to fibrin and other blood components to form the clot matrix and stop blood loss. Integrins are adhesion receptor heterodimers that transmit information from the ECM to the cell through activation of cell signaling pathways. The integrins are a large family of heterodimeric cell adhesion receptors involved in cell-cell and cell-matrix interactions [16, 17].

3. ECM and Cell Interaction

The general concept of chondrogenesis is as follows. In embryogenesis, the skeletal system is derived from the mesoderm germ layer. Chondrogenesis is the process by which cartilage is formed from condensed mesenchyme tissue, which differentiates into chondrocytes and begins secreting the molecules that form the ECM.

The relationship between ECM and chondrogenesis should be discussed here. The 3D environment of the ECM guides the morphogenesis of tissue types with anisotropic structures [18]. Chondrocyte differentiation is a multistep process characterized by successive changes in cell morphologic features and gene expression. Early in fetal development, the greater part of the skeleton is cartilaginous. This temporary cartilage is gradually replaced by bone (endochondral ossification), a process that ends at puberty. In contrast, the cartilage in the joints remains unossified during the whole life and is, therefore, permanent. During the early phase of the chondrocyte life cycle, cell-cell adhesion occurs via molecules such as N-cadherin. At later stages, such as in growth-plate chondrocytes, adhesion signaling occurs from ECM proteins via integrin and other ECM receptors. Cell-matrix interactions are also important for chondrogenesis.

3.1. Signals and Integrins. The major signaling pathways that regulate chondrogenesis must play an important role through the cell-matrix interaction. These molecules are bound to plasma membrane or intracellular receptors and are interpreted by complex molecular pathways that use specific combinations of a cell or tissue-specific signaling toolkit, and, by eventually converging on transcription factors, they induce changes in gene expression. These signals are required to adjust the cellular metabolism to the needs of the tissue and/or organism or to affect the fate of cells: proliferation, differentiation, or apotosis [19] through wnt signal, nitric oxide signal, retinoic acid (RA) signal, and protein kinase C (PKC).

Wnt9a was shown to be required for chondrocyte proliferation and mediolateral intercalation, cellular mechanisms that mediate extension during zebrafish palate morphogenesis [20]. *Frzb* and *fzd7a* are dispensable for directed migration of the bilateral trabeculae, but necessary for the convergence and extension of the palatal elements, where the extension process is mediated by chondrocyte proliferation, morphologic change, and intercalation. *Bapx1* was specifically downregulated in the *wnt9a/frzb/fzd7a* morphants. Overexpression of *bapx1* can partially rescue the lower jaw elements in *wnt9a*, *frzb*, and *fzd7a* morphants [21].

Nitric oxide (NO) was recognized as an important second messenger signaling molecule generated from metabolism of L-arginine by the nitric oxide synthase (NOS) family of enzymes [22]. Nitric oxide synthase inhibitor 1-(2-[trifluoromethyl] phenyl) imidazole (TRIM) can disrupt chondrogenic differentiation. So TRIM-treated embryo only formed scattered chondrocyte clusters. TRIM treatment could be reasoned by several developmental events, such as failure in identity specification within changes in cell proliferation and survival, and/or defects in chondrogenic differentiation. NO might function upstream of histone acetylation and/or through nonacetylation pathways (e.g., through S-nitrosylation; or NO may directly target the expression of chondrogenic genes). TRIM inhibited chondrogenic differentiation, which were mediated through impaired nitric oxide (NO) production without appreciable effect on global protein S-nitrosylation. TRIM perturbed Hox gene patterning and caused histone hypoacetylation [23]. NO regulates cartilage degradation by causing dedifferentiation and apoptosis of chondrocytes via activation of ERK1/2 and p38 [24].

RA is responsible for most of the activity of vitamin A and saves visual pigment effects that require retinal (retinaldehyde) and cell metabolism effects that may require retinol itself. Also, some biochemical functions necessary for fertility in vitamin A deficient male and female mammals originally appeared to require retinol for rescue, but this is due to a requirement for local conversion of retinol to RA, as administered RA does not reach some critical tissues unless given in high amounts. RA significantly increased the motility of neural crest cells, as shown by the wound-healing assay, and inhibited their proliferation. Cartilage elements originate from midbrain neural crest cells. RA can cause abnormal craniofacial cartilage development in other vertebrates, resulting in dose- and stage-dependent losses of *dlx* homeobox gene expression in several regions of the embryo [25, 26].

During chondrogenesis, reversible phosphorylation of key target proteins is of particular importance during this process. Among protein kinases known to be involved in these pathways, PKC subtypes play pivotal roles. PKC is a quintessential regulator of chondrogenesis. PKCs regulate the chondrocyte phenotype via the actin cytoskeleton. PKC exerts its chondrogenesis-promoting effect via the ERK-MAPK pathway. PKC mediates chondrogenesis via the ERK1/2 pathway. Chondrocyte de- and redifferentiation are regulated by PKC and MAPK signaling. PKC mediates the effects of IGF-1 and EGF during chondrogenesis. PKC-dependent regulation of chondrogenesis is via cell adhesion molecules [19].

In all, 24 unique integrin dimers are formed *in vivo* from the 18α and 8β subunits found in mammalian cells. The composition of the ECM is expressed in a given cell type. Integrins and cell signals can regulate cell shape and affinity. Chondrocytes express a subset of integrin subunits including fibronectin receptors, a laminin receptor, and collagen receptors [10, 27–32]. The β1 chain is a component of most chondrocyte integrins. Cartilage-specific deactivation of the β1-integrin gene results in severe changes in the cartilage phenotype [33]. Chondrocytes from knock-out mice show abnormal cell shape, reduced proliferation, and deregulated expression of cell-cycle proteins, including D-type cyclins and cyclin-dependent kinase inhibitors. *In vitro* experiments also suggest that the loss of β1 and αnβ5 integrin promotes apoptosis in growth-plate chondrocytes and that antibodies against β1, α2, or α3 integrin [33–35] repress hypertrophic differentiation and decrease chondrocyte survival.

Integrin-mediated activation of members of the mitogen-activated protein kinase family plays a key role in transmitting signals regulating chondrocyte gene expression. Some research has verified with isotope-labeled monoclonal antibodies that chondrocyte phenotype remains may be due to the attachment mediated via integrin, including members of both the β1 and β3 subunit families. Then, chondrocytes showed significant attachment to fibronectin matrix Gla protein, osteopontin, bone sialoprotein II, vitronectin, and COLII and VI [36, 37], which suggests a link between matrix synthesis and integrin expression in chondrocytes. Chondrocytes express several members of the integrin family, including α5β1, the primary chondrocyte receptor for fibronectin. The α5β1 integrin provides matrix survival signals for normal and osteoarthritic human articular chondrocytes, to prevent apoptosis. Therefore, β-integrin-mediated chondrocyte-ECM interactions are decreased in osteoarthritic cartilage, which suggests that perturbations of chondrocyte-matrix signaling occurs during OA [10, 38, 39]. β1 integrin, the protein encoded by the ITGB1 gene (also known as CD29 and VLAB) [17], is a multifunctional protein involved in cell-matrix adhesion, cell signaling, cell adhesion, protein binding, and receptor-mediated activity. The β1-integrin family of cell-surface receptors appears to play a major role in mediating cell-matrix interactions that are important in regulating these fundamental processes.

Degradation of HA results in chondrocyte aggregation and then reduces chondrocyte apoptosis. As well, β1-integrin-collagen interaction reduces chondrocyte apoptosis [40], to achieve their goals by antagonizing hyaluronidase. So, like integrin-deficient chondrocytes, adhesion to the ECM decreased in Flnb (−/−) chondrocytes, and inhibition of β1 integrin in these cells further impaired cell spreading [41]. TGF-β1 and integrin stimuli interact before *Smad2* and *-3* phosphorylation in the cytoplasm of chondrocytes, which regulates the expression of ECM components in chondrocytes. Under culture and seeding conditions, β1, α5β1, and αvβ5 integrins [42] mediate human chondrocyte adhesion to cartilage. These chondrocyte integrins have a potential role in the initial adhesion and retention of chondrocytes at a cartilage defect site. The fibronectin receptor (α5β1 integrin), in conjunction with its ligand fibronectin, the GPIIb/IIIa receptor and the integrin-linked kinase, integrin cytoplasmic-domain-associated protein 1, and CD47 pathway play a pivotal role in dedifferentiation of chondrocytes [16]. TGF-β3, MMP9, MMP13 [43–46], and vascular endothelial growth factor are key regulators for remodeling cartilage tissues. They coordinate matrix degradation and the recruitment and differentiation of osteoprogenitors. IL-1 receptor antagonist upregulates major components of the cartilage ECM genes, so we can use it to protect the ECM for anti-inflammatory and chondroprotective therapy.

3.2. Factors and Enzymes. After disruption of cell-matrix interactions and lack of growth factors, certain cells are selected and channelled through proliferation into the new stable phenotype. Chondrocyte mechanoreceptors may incorporate β1-integrins and mechanosensitive ion channels linked with key ECM, cytoskeletal, and signaling proteins to maintain the chondrocyte phenotype, prevent chondrocyte apoptosis, and regulate chondrocyte-specific gene expression [17, 47]. Tumor necrosis factor α (TNF-α) and interleukins-1β (IL-1β) cause the release of the stress-injury-related protein to relieve mechanical damage. TNF and IL-1 or anti-Fas antibody growth-regulated oncogene α in ECM can induce chondrocyte apoptosis. Chondrocyte apoptosis and caspase-3 activity are associated [9, 48]. IGF-1 is known to inhibit the catabolic effects of IL-1 on PG synthesis in cartilage explants and suppresses the degradation of ECM components by reducing matrix metalloproteinase-1 (MMP-1) and MMP-8 expression and activity [49].

Apoptosis is programmed cell death. Apoptotic cells take the initiative of cell death (necrosis). A disease such as OA can lead to apoptosis. OA results from the aberrant production of inflammatory mediators (cytokines and chemokines) and effectors (MMPs and reactive oxygen and nitrogen species) by chondrocytes [48]. Cartilage oligomeric matrix protein (COMP) plays an important role in cartilage cell-matrix interactions. COMPs induce the survival of the inhibitor of apoptosis family of proteins to lead to the strong inhibition of chondrocyte apoptosis by blocking the activation of caspase-3. The synthesis of COMP is regulated by transforming growth factor (TGF) in these 2 regions of the human articular cartilage [50–52]. COMP mutation has a great impact. Although it is a small molecule in the ECM, its mutation is the major reason for pseudoachondroplasia. COMP specifically locates in some cells of the rough endoplasmic reticulum and

has toxic effects on chondrocyte precursors, thus hindering the formation of cartilage and bone [53–59]. A certain amount of strontium and COMP can maintain the structural integrity of the cartilage collagen and fibronectin [52, 60].

3.3. Biomechanics. In terms of biomechanics, cartilage tissue can remodel its ECM in response to alterations in functional demand. The pericellular matrix (PCM) is a narrow tissue region surrounding chondrocytes in articular cartilage, which together with the enclosed cell(s) has been termed the "chondron" [8]. The PCM is rich in fibronectin, PGs (e.g., aggrecan, HA, and decorin), and collagen (types II, VI, and IX) but, as compared with the ECM, is defined primarily by the presence of COLVI. The mechanical properties of PCM relative to those of the ECM can significantly affect the micromechanical environment of the chondrocyte. Changes in the properties of the PCM with osteoarthritis (OA) may alter the stress-strain and fluid-flow environment of chondrocytes [8, 61, 62].

OA leads to the degradation of the PCM and then alters the cellular environment of cartilage in terms of macroscopic loading features and material properties of the ECM and the chondron. At the microscale, estimates of Young's modulus of the PCM range from about 24 to 59 kPa by the axisymmetric boundary element method. Therefore, the PCM may have an important role in modulating the mechanical environment of the chondrocyte [63, 64]. Compressed damage by overloading the integrity of the cartilage ECM may cause cell membrane damage and eventually cell death. TNF and IL-1 cause the release of the stress-injury-related protein to relieve mechanical damage [65, 66].

4. Conclusions

The survey of the considerable domain of definition, components, and ECM-cell interaction of ECM can indicate the amount of knowledge accumulated and the directions of research and applications. It is evident that we are only at the beginning of understanding the precise role of cell-matrix interaction during chondrogenesis and how they are regulated. There are a lot of unexplored fields in this area; exploiting these novel approaches and applying them to not only healthy but also inflammatory chondrocytes may enable us to halt or even reverse disease progression. Shedding more light on exactly how the ECM and cell interact with each other PCM-mediated control mechanisms would open new perspectives for a better understanding of healthy as well as pathological differentiation processes of chondrocytes and may also lead to the development of new therapeutic approaches.

5. Perspective

Regulation of cell shape and signaling from cell-cell and cell-ECM interactions are vital to the maturation of chondrocytes. Determining signaling pathways and targets downstream of these events will aid in the development of novel strategies for cartilage replacement and new approaches for regenerating cartilage and preventing and treating cartilage disorders. Still, illustrating the mechanisms integrating signals from adhesion receptors with those from growth factor and hormone receptors will contribute to a better understanding of physiologic and pathologic endochondral ossification. Complex approaches to gene mutagenesis in mice combined with advanced genomic, proteomic, and imaging tools will provide a powerful stage for rapid progress in these areas.

Abbreviations

BFGF: Basic fibroblast growth factor
BMP: Bone morphogenic proteins
COLII: Type II collagen
COMP: Cartilage oligomeric matrix protein
CS: Chondroitin sulfate
ECM: Extracellular matrix
GAG: Glycosaminoglycan
HA: Hyaluronic acid
IGF: Insulin-like growth factor
ILs: Interleukins
ITGB1: Integrin 1
MMPs: Matrix metalloproteinases
Na^+: Sodium ions
NO: Nitric oxide
PCM: Pericellular matrix
PGs: Proteoglycans
PKC: Protein kinase C
RA: Retinoic acid
TNF: Tumor necrosis factor
TGF: Transforming growth factor.

Conflict of Interests

The authors declare that there is no conflict of interests regarding the publication of this paper.

Acknowledgments

This work was funded by the Beijing Metropolis Beijing Nova Program (2011115), the National Natural Science Foundation of China (General Program) (31170946), the National Natural Science Foundation of China (Youth Program) (31100696), the National High Technology Research and Development Program of China (2012AA020502), the People's Liberation Army 12th Five-Year Plan Period (Key Program) (BWS11J025), the National Basic Research Program of China (973 Program) (2012CB518106), the National Natural Science Foundation of China (Key Program) (21134004), and the New Drug Creation of the Special Ministry of Science and Technology.

References

[1] G. Michel, T. Tonon, D. Scornet, J. M. Cock, and B. Kloareg, "The cell wall polysaccharide metabolism of the brown alga Ectocarpus siliculosus. Insights into the evolution of extracellular matrix polysaccharides in Eukaryotes," *New Phytologist*, vol. 188, no. 1, pp. 82–97, 2010.

[2] M. Abedin and N. King, "Diverse evolutionary paths to cell adhesion," *Trends in Cell Biology*, vol. 20, no. 12, pp. 734–742, 2010.

[3] C.-H. Wu, C.-S. Ko, J.-W. Huang, H.-J. Huang, and I.-M. Chu, "Effects of exogenous glycosaminoglycans on human chondrocytes cultivated on type II collagen scaffolds," *Journal of Materials Science: Materials in Medicine*, vol. 21, no. 2, pp. 725–729, 2010.

[4] I. Takahashi, K. Onodera, J.-W. Bae, H. Mitani, Y. Sasano, and H. Mitani, "Age-related changes in the expression of gelatinase and tissue inhibitor of metalloproteinase genes in mandibular condylar, growth plate, and articular cartilage in rats," *Journal of Molecular Histology*, vol. 36, no. 5, pp. 355–366, 2005.

[5] S. Honoré, V. Pichard, C. Penel et al., "Outside-in regulation of integrin clustering processes by ECM components per se and their involvement in actin cytoskeleton organization in a colon adenocarcinoma cell line," *Histochemistry and Cell Biology*, vol. 114, no. 4, pp. 323–335, 2000.

[6] P. G, "The extracellular matrix and cell adhesion," in *Cells*, B. Lewin, L. Cassimeris, V. Lingappa, and G. Plopper, Eds., 2007.

[7] E. Sweeney, D. Roberts, and O. Jacenko, "Altered matrix at the chondro-osseous junction leads to defects in lymphopoiesis," *Annals of the New York Academy of Sciences*, vol. 1237, no. 1, pp. 79–87, 2011.

[8] F. Guilak, L. G. Alexopoulos, M. L. Upton et al., "The pericellular matrix as a transducer of biomechanical and biochemical signals in articular cartilage," *Annals of the New York Academy of Sciences*, vol. 1068, no. 1, pp. 498–512, 2006.

[9] B. A. Fischer, S. Mundle, and A. A. Cole, "Tumor necrosis factor-alpha induced DNA cleavage in human articular chondrocytes may involve multiple endonucleolytic activities during apoptosis," *Microscopy Research and Technique*, vol. 50, no. 3, pp. 236–242, 2000.

[10] R. F. Loeser, "Integrins and cell signaling in chondrocytes," *Biorheology*, vol. 39, no. 1-2, pp. 119–124, 2002.

[11] S. Ab-Rahim, L. Selvaratnam, and T. Kamarul, "The effect of TGF-β1 and β-estradiol on glycosaminoglycan and type II collagen distribution in articular chondrocyte cultures," *Cell Biology International*, vol. 32, no. 7, pp. 841–847, 2008.

[12] C.-S. Ko, J.-P. Huang, C.-W. Huang, and I.-M. Chu, "Type II collagen-chondroitin sulfate-hyaluronan scaffold cross-linked by genipin for cartilage tissue engineering," *Journal of Bioscience and Bioengineering*, vol. 107, no. 2, pp. 177–182, 2009.

[13] T. K. Hensch, "Critical Period Mechanisms in Developing Visual Cortex," *Current Topics in Developmental Biology*, vol. 69, pp. 215–237, 2005.

[14] A. J. Powell, C. B. Little, and C. E. Hughes, "Low molecular weight isoforms of the aggrecanases are responsible for the cytokine-induced proteolysis of aggrecan in a porcine chondrocyte culture system," *Arthritis and Rheumatism*, vol. 56, no. 9, pp. 3010–3019, 2007.

[15] A. Woods, G. Wang, and F. Beier, "Regulation of chondrocyte differentiation by the act in cytoskeleton and adhesive interactions," *Journal of Cellular Physiology*, vol. 213, no. 1, pp. 1–8, 2007.

[16] U. R. Goessler, P. Bugert, K. Bieback et al., "Differential modulation of integrin expression in chondrocytes during expansion for tissue engineering," *In Vivo*, vol. 19, no. 3, pp. 501–508, 2005.

[17] M. Shakibaei, C. Csaki, and A. Mobasheri, "Diverse roles of integrin receptors in articular cartilage," *Advances in Anatomy, Embryology, and Cell Biology*, vol. 197, pp. 1–60, 2008.

[18] B. Lanfer, F. P. Seib, U. Freudenberg et al., "The growth and differentiation of mesenchymal stem and progenitor cells cultured on aligned collagen matrices," *Biomaterials*, vol. 30, no. 30, pp. 5950–5958, 2009.

[19] C. Matta and A. Mobasheri, "Regulation of chondrogenesis by protein kinase C: emerging new roles in calcium signalling," *Cellular Signalling*, vol. 26, no. 5, pp. 979–1000, 2014.

[20] M. Dougherty, G. Kamel, M. Grimaldi et al., "Distinct requirements for wnt9a and irf6 in extension and integration mechanisms during zebrafish palate morphogenesis," *Development*, vol. 140, no. 1, pp. 76–81, 2013.

[21] G. Kamel, T. Hoyos, L. Rochard et al., "Requirement for frzb and fzd7a in cranial neural crest convergence and extension mechanisms during zebrafish palate and jaw morphogenesis," *Developmental Biology*, vol. 381, no. 2, pp. 423–433, 2013.

[22] S. Moncada and A. Higgs, "The L-arginine-nitric oxide pathway," *The New England Journal of Medicine*, vol. 329, no. 27, pp. 2002–2012, 1993.

[23] Y. Kong, M. Grimaldi, E. Curtin et al., "Neural crest development and craniofacial morphogenesis is coordinated by nitric oxide and histone acetylation," *Chemistry & Biology*, no. 21, pp. 1–14, 2014.

[24] S.-J. Kim, N.-W. Ju, C.-D. Oh et al., "ERK-1/2 and p38 kinase oppositely regulate nitric oxide-induced apoptosis of chondrocytes in association with p53, caspase-3, and differentiation status," *Journal of Biological Chemistry*, vol. 277, no. 2, pp. 1332–1339, 2002.

[25] D. L. Ellies, R. M. Langille, C. C. Martin, M.-A. Akimenko, and M. Ekker, "Specific craniofacial cartilage dysmorphogenesis coincides with a loss of dlx gene expression in retinoic acid-treated zebrafish embryos," *Mechanisms of Development*, vol. 61, no. 1, pp. 23–36, 1997.

[26] B. Kinikoglu, Y. Kong, and E. C. Liao, "Characterization of cultured multipotent zebrafish neural crest cells," *Experimental Biology and Medicine*, vol. 239, no. 2, pp. 159–168, 2013.

[27] M. Shakibaei, B. Zimmermann, and H.-J. Merker, "Changes in integrin expression during chondrogenesis in vitro: an immunomorphological study," *Journal of Histochemistry and Cytochemistry*, vol. 43, no. 10, pp. 1061–1069, 1995.

[28] R. F. Loeser, "Chondrocyte integrin expression and function," *Biorheology*, vol. 37, no. 1-2, pp. 109–116, 2000.

[29] A. Van der Flier and A. Sonnenberg, "Function and interactions of integrins," *Cell and Tissue Research*, vol. 305, no. 3, pp. 285–298, 2001.

[30] R. O. Hynes, "Integrins: bidirectional, allosteric signaling machines," *Cell*, vol. 110, no. 6, pp. 673–687, 2002.

[31] D. G. Stupack and D. A. Cheresh, "Get a ligand, get a life: integrins, signaling and cell survival," *Journal of Cell Science*, vol. 115, no. 19, pp. 3729–3738, 2002.

[32] M. A. Arnaout, B. Mahalingam, and J.-P. Xiong, "Integrin structure, allostery, and bidirectional signaling," *Annual Review of Cell and Developmental Biology*, vol. 21, pp. 381–410, 2005.

[33] A. Aszodi, E. B. Hunziker, C. Brakebusch, and R. Fässler, "β1 integrins regulate chondrocyte rotation, G1 progression, and cytokinesis," *Genes and Development*, vol. 17, no. 19, pp. 2465–2479, 2003.

[34] M. S. Hirsch, L. E. Lunsford, V. Trinkaus-Randall, and K. K. Svoboda, "Chondrocyte survival and differentiation in situ are integrin mediated," *Developmental Dynamics*, vol. 210, no. 3, pp. 249–263, 1997.

[35] W. Wang and T. Kirsch, "Annexin V/β5 integrin interactions regulate apoptosis of growth plate chondrocytes," *Journal of Biological Chemistry*, vol. 281, no. 41, pp. 30848–30856, 2006.

[36] R. F. Loeser, "Integrin-mediated attachment of articular chondrocytes to extracellular matrix proteins," *Arthritis and Rheumatism*, vol. 36, no. 8, pp. 1103–1110, 1993.

[37] R. F. Loeser, "Modulation of integrin-mediated attachment of chondrocytes to extracellular matrix proteins by cations, retinoic acid, and transforming growth factor β," *Experimental Cell Research*, vol. 211, no. 1, pp. 17–23, 1994.

[38] G. Lapadula, F. Iannone, C. Zuccaro et al., "Chondrocyte phenotyping in human osteoarthritis," *Clinical Rheumatology*, vol. 17, no. 2, pp. 99–104, 1998.

[39] J. I. Pulai, M. Del Carlo Jr., and R. F. Loeser, "The α5β1 integrin provides matrix survival signals for normal and osteoarthritic human articular chondrocytes in vitro," *Arthritis and Rheumatism*, vol. 46, no. 6, pp. 1528–1535, 2002.

[40] L. Cao, V. Lee, M. E. Adams et al., "β1-Integrin-collagen interaction reduces chondrocyte apoptosis," *Matrix Biology*, vol. 18, no. 4, pp. 343–355, 1999.

[41] J. Lu, G. Lian, R. Lenkinski et al., "Filamin B mutations cause chondrocyte defects in skeletal development," *Human Molecular Genetics*, vol. 16, no. 14, pp. 1661–1675, 2007.

[42] M. S. Kurtis, T. A. Schmidt, W. D. Bugbee, R. F. Loeser, and R. L. Sah, "Integrin-mediated adhesion of human articular chondrocytes to cartilage," *Arthritis and Rheumatism*, vol. 48, no. 1, pp. 110–118, 2003.

[43] N. Ortega, D. Behonick, D. Stickens, and Z. Werb, "How proteases regulate bone morphogenesis," *Annals of the New York Academy of Sciences*, vol. 995, pp. 109–116, 2003.

[44] K. H. Park and K. Na, "Effect of growth factors on chondrogenic differentiation of rabbit mesenchymal cells embedded in injectable hydrogels," *Journal of Bioscience and Bioengineering*, vol. 106, no. 1, pp. 74–79, 2008.

[45] C. T. Jayasuriya, M. B. Goldring, R. Terek, and Q. Chen, "Matrilin-3 Induction of IL-1 receptor antagonist Is required for up-regulating collagen II and aggrecan and down-regulating ADAMTS-5 gene expression," *Arthritis Research & Therapy*, vol. 14, no. 5, article R197, 2012.

[46] J. B. Vincourt, S. Etienne, L. Grossin et al., "Matrilin-3 switches from anti- to pro-anabolic upon integration to the extracellular matrix," *Matrix Biology*, vol. 31, no. 5, pp. 290–298, 2012.

[47] J. Erenpreisa and H. I. Roach, "Epigenetic selection as a possible component of transdifferentiation. Further study of the commitment of hypertrophic chondrocytes to become osteocytes," *Mechanisms of Ageing and Development*, vol. 87, no. 3, pp. 165–182, 1996.

[48] R. M. Borzi, I. Mazzetti, G. Magagnoli et al., "Growth-related oncogene α induction of apoptosis in osteoarthritis chondrocytes," *Arthritis and Rheumatism*, vol. 46, no. 12, pp. 3201–3211, 2002.

[49] C. Tavera, T. Abribat, P. Reboul et al., "IGF and IGF-binding protein system in the synovial fluid of osteoarthritic and rheumatoid arthritic patients," *Osteoarthritis and Cartilage*, vol. 4, no. 4, pp. 263–274, 1996.

[50] Y. Du, Y. Wang, L. Wang et al., "Cartilage oligomeric matrix protein inhibits vascular smooth muscle calcification by interacting with bone morphogenetic protein-2," *Circulation Research*, vol. 108, no. 8, pp. 917–928, 2011.

[51] S. C. K. M. Motaung, P. E. Di Cesare, and A. Hari Reddi, "Differential response of cartilage oligomeric matrix protein (COMP) to morphogens of bone morphogenetic protein/transforming growth factor-β family in the surface, middle and deep zones of articular cartilage," *Journal of Tissue Engineering and Regenerative Medicine*, vol. 5, no. 6, pp. e87–e96, 2011.

[52] C. M. Thomas, R. Murray, and M. Sharif, "Chondrocyte apoptosis determined by caspase-3 expression varies with fibronectin distribution in equine articular cartilage," *International Journal of Rheumatic Diseases*, vol. 14, no. 3, pp. 290–297, 2011.

[53] J. Hecht, E. Hayes, M. Snuggs et al., "Calreticulin, PDI, Grp94 and BiP chaperone proteins are associated with retained COMP in pseudoachondroplasia chondrocytes," *Matrix Biology*, vol. 20, no. 4, pp. 251–262, 2001.

[54] J. Vranka, A. Mokashi, D. R. Keene et al., "Selective intracellular retention of extracellular matrix proteins and chaperones associated with pseudoachondroplasia," *Matrix Biology*, vol. 20, no. 7, pp. 439–450, 2001.

[55] R. Dinser, F. Zaucke, F. Kreppe et al., "Pseudoachondroplasia is caused through both intra- and extracellular pathogenic pathways," *Journal of Clinical Investigation*, vol. 110, no. 4, pp. 505–513, 2002.

[56] T.-L. L. Chen, J. W. Stevens, W. G. Cole, J. T. Hecht, and B. M. Vertel, "Cell-type specific trafficking of expressed mutant COMP in a cell culture model for PSACH," *Matrix Biology*, vol. 23, no. 7, pp. 433–444, 2004.

[57] J. T. Hecht and E. H. Sage, "Retention of the matricellular protein SPARC in the endoplasmic reticulum of chondrocytes from patients with pseudoachondroplasia," *Journal of Histochemistry and Cytochemistry*, vol. 54, no. 3, pp. 269–274, 2006.

[58] K. L. Posey and J. T. Hecht, "The role of cartilage oligomeric matrix protein (COMP) in skeletal disease," *Current Drug Targets*, vol. 9, no. 10, pp. 869–877, 2008.

[59] K. L. Posey, A. C. Veerisetty, P. Liu et al., "An inducible cartilage oligomeric matrix protein mouse model recapitulates human pseudoachondroplasia phenotype," *American Journal of Pathology*, vol. 175, no. 4, pp. 1555–1563, 2009.

[60] S. A. Abbah, W. W. Lu, S. L. Peng et al., "Extracellular matrix stability of primary mammalian chondrocytes and intervertebral disc cells cultured in alginate-based microbead hydrogels," *Cell Transplantation*, vol. 17, no. 10-11, pp. 1181–1192, 2008.

[61] L. G. Alexopoulos, L. A. Setton, and F. Guilak, "The biomechanical role of the chondrocyte pericellular matrix in articular cartilage," *Acta Biomaterialia*, vol. 1, no. 3, pp. 317–325, 2005.

[62] L. G. Alexopoulos, G. M. Williams, M. L. Upton, L. A. Setton, and F. Guilak, "Osteoarthritic changes in the biphasic mechanical properties of the chondrocyte pericellular matrix in articular cartilage," *Journal of Biomechanics*, vol. 38, no. 3, pp. 509–517, 2005.

[63] E. Kim, F. Guilak, and M. A. Haider, "The dynamic mechanical environment of the chondrocyte: a biphasic finite element model of cell-matrix interactions under cyclic compressive loading," *Journal of Biomechanical Engineering*, vol. 130, no. 6, Article ID 061009, 2008.

[64] E. Kim, F. Guilak, and M. A. Haider, "An axisymmetric boundary element model for determination of articular cartilage pericellular matrix properties in situ via inverse analysis of chondron deformation," *Journal of Biomechanical Engineering*, vol. 132, no. 3, Article ID 031011, 2010.

[65] M. Wong, M. Siegrist, and X. Cao, "Cyclic compression of articular cartilage explants is associated with progressive consolidation and altered expression pattern of extracellular matrix proteins," *Matrix Biology*, vol. 18, no. 4, pp. 391–399, 1999.

[66] A. L. Stevens, J. S. Wishnok, D. H. Chai, A. J. Grodzinsky, and S. R. Tannenbaum, "A sodium dodecyl sulfate-polyacrylamide gel electrophoresis-liquid chromatography tandem mass spectrometry analysis of bovine cartilage tissue response to mechanical compression injury and the inflammatory cytokines tumor necrosis factor α and interleukin-1β," *Arthritis and Rheumatism*, vol. 58, no. 2, pp. 489–500, 2008.

Hindawi Publishing Corporation
BioMed Research International
Volume 2014, Article ID 760709, 9 pages
http://dx.doi.org/10.1155/2014/760709

Clinical Study

The Effect of Autologous Activated Platelet Rich Plasma (AA-PRP) Injection on Pattern Hair Loss: Clinical and Histomorphometric Evaluation

V. Cervelli,[1] S. Garcovich,[2] A. Bielli,[3] G. Cervelli,[4] B. C. Curcio,[1] M. G. Scioli,[3] A. Orlandi,[3] and P. Gentile[1,5]

[1] *Plastic and Reconstructive Surgery Department, University of Rome Tor Vergata, Via Montpellier, No. 1, 00173 Rome, Italy*
[2] *Institute of Dermatology, Catholic University of the Sacred Heart, Rome, Italy*
[3] *Institute of Anatomic Pathology, University of Rome Tor Vergata, Via Montpellier, No. 1, 00173 Rome, Italy*
[4] *Science Education Department, University of Rome Tor Vergata, Via Montpellier, No. 1, 00173 Rome, Italy*
[5] *San Salvatore in Lauro Place, No. 15, 00186 Rome, Italy*

Correspondence should be addressed to P. Gentile; pietrogentile2004@libero.it

Received 28 November 2013; Revised 23 January 2014; Accepted 5 March 2014; Published 6 May 2014

Academic Editor: Garrett McGuinness

To investigate the safety and clinical efficacy of AA-PRP injections for pattern hair loss. AA-PRP, prepared from a small volume of blood, was injected on half of the selected patients' scalps with pattern hair loss. The other half was treated with placebo. Three treatments were given for each patient, with intervals of 1 month. The endpoints were hair re-growth, hair dystrophy as measured by dermoscopy, burning or itching sensation, and cell proliferation as measured by Ki-67 evaluation. At the end of the 3 cycles of treatment, the patients presented clinical improvement in the mean number of hairs, with a mean increase of 18.0 hairs in the target area, and a mean increase in total hair density of 27.7 (number of hairs/cm^2) compared with baseline values. Microscopic evaluation showed the increase of epidermis thickness and of the number of hair follicles two weeks after the last AA-PRP treatment compared to baseline value ($P < 0.05$). We also observed an increase of Ki67$^+$ keratinocytes of epidermis and of hair follicular bulge cells and a slight increase of small blood vessels around hair follicles in the treated skin compared to baseline ($P < 0.05$).

1. Introduction

Proponents of platelet-rich plasma (PRP) technology suggest that its benefits include an increase in hard- and soft-tissue wound healing. In addition, the role of PRP for the treatment of pattern hair loss has been demonstrated in recent reports [1–4]. In particular, Rinaldi described the use of PRP in alopecia areata (AA). This pilot study suggests that PRP may serve as a safe and effective treatment option in AA and calls for more extensive controlled studies with this method [4]. Uebel et al. showed that pretreatment of follicular units with PRP before transplantation resulted in improved hair growth and density [3]. Activated autologous PRP has been reported to induce the proliferation of dermal papilla cells by upregulating fibroblast growth factor 7 (FGF-7) and b-catenin as well as extracellular signal-related kinase (ERK) and Akt signalling [2]. Anagen-associated angiogenesis has been suggested as one of the important factors in active hair growth [5], due to the secretion of vascular endothelial growth factor (VEGF) by the keratinocytes of the outer root sheath and fibroblasts of the dermal papilla [5–7]. Increased secretion of VEGF influences growth of normal and pathological dermal structures [8]. Tobin et al. reported that the hair follicle mesenchyme exhibits significant hair cycle-associated plasticity. Modulation of these cell interchanges is likely to be important during clinically important hair follicle transformations, for example, vellus-to-terminal and terminal-to-vellus transformations during androgenetic alopecia [9]. Injection of PRP has been demonstrated to improve cutaneous ischemic conditions and to increase vascular structures around hair follicles [1, 10]. Many of the current treatment modalities for pattern hair loss have been

Table 1: Summary of patients' characteristics.

Case	Age	The Norwood-Hamilton classification stage	Injection site
1	20	IIa	Frontal
2	32	IIa	Frontal
3	42	III	Parietal
4	40	III vertex	Parietal
5	41	IIa	Frontal
6	52	IV	Parietal and vertex
7	25	III vertex	Parietal
8	26	III	Parietal
9	28	III	Frontal
10	21	IIa	Frontal

shown to modulate angiogenesis and enhance blood flow [11]. The aim is to evaluate the effects of AA-PRP obtained from a small volume of blood on active hair growth. The data we reported proves the clinical efficacy of the treatment with AA-PRP; moreover, patients' satisfaction further confirms the quality of the results. After studying this paper, the reader should be able to (1) prepare AA-PRP, (2) apply PRP intraoperatively, (3) evaluate the clinical effect of AA-PRP on hair growth, and (4) evaluate the histomorphometric effect of AA-PRP on the proliferation of dermal papilla cells.

2. Material and Methods

2.1. Patients. A total of 10 male patients (age range: 22–60) with male pattern hair loss (MPHL) were treated. The patient characteristics are summarized in Table 1. Patients, who had received topical (such as minoxidil, prostaglandin, analogues, retinoids, and corticosteroid) or systemic treatments for MPHL (such as finasteride, dutasteride, and antiandrogens) in the previous 12 months were excluded. Patients with a propensity for keloids and patients who were immunosuppressed were also excluded. In addition, the numbers of platelets in PRP obtained from all participants were microscopically counted. This was a randomized, TrichoScan evaluator blinded, placebo half-head group study.

The diagnosis of MPHL was established on the basis of clinical and trichoscopic features (more than 20% variability in hair diameter between affected and uninvolved areas), while the extent and stage of MPHL were assessed according to the Norwood-Hamilton classification (as shown in Table 1).

All patients provided written informed consent before participating in the study, which was performed according to the Declaration of Helsinki.

2.2. Treatment Protocol. AA-PRP was prepared from a small volume of blood (18 cc) according to the method of Cascade-Selphyl-Esforax system, with modifications [12–14]. Briefly, to prepare PRP, blood was taken from a peripheral vein using sodium citrate as an anticoagulant. The current systems for preparing platelet concentrations use various centrifuges (however in this case we used 1100 g for 10 min). AA-PRP was prepared in all cases with approval of the Transfusional Service. Although the method of preparation was not selective and may include leukocytes, the final aim is to obtain a platelet pellet. Growth factors are only secreted once platelet activation begins, which in turn is stimulated by Ca^{2+}. To optimize the secretion process, the optimum concentration of Ca^{2+} was previously determined [12, 13]. Then, autologous-PRP not activated (A-PRP) obtained after centrifugation (9 mL) was switched into 10-mL tubes containing Ca^{2+} extracted by Cascade-Selphyl-Esforax Kit. The patients' scalp affected by hair loss was divided in four halves (Figure 8(a)) and cleansed with 70% alcohol, but local anaesthesia was not injected on the treated areas. The AA-PRP was injected on selected areas of the scalp at the amount of 0.1 mL/cm^2 (Figure 3(d)). AA-PRP injections were injected with the AAPRP only on the frontal areas (Figures 1(b), 9(b), and 10(b)); the parietal area was treated with placebo (Figure 8(b)). The scalps of patients affected by hair loss were divided, respectively, into four parts: frontal, parietal, vertex, and occipital parts. Patients with hair loss localized to the frontal and parietal areas (Figures 1(a), 2(a), 9(a), and 10(a)) were injected with the AA-PRP only on the frontal areas (Figure 1(b)); the parietal area was treated with placebo based on the injection of physiological solution. Patients with hair loss in the parietal and vertex parts (Figures 3(a) and 4(a)) were injected with the AA-PRP only in the parietal part of the scalp (Figure 4(b)); the vertex area was treated with placebo based on the injection of physiological solution. In detail the authors repeat the same numbers of injections in the half treated with PRP and in the half treated with placebo. The analysis of the areas of the scalp treated with PRP and placebo was reported in Figures 8(a), 8(b), and 8(c).

2.3. Assessment Criteria. All patients were evaluated in four stages: T0, beginning of study; T1 in 14 weeks; T2, 6 months; and T3, 12 months. The effects of the treatment on hair growth were assessed in all patients with the help of global photography, physician's and patient's global assessment scale, and standardized phototrichograms.

Phototrichograms were performed in all patients by a trained evaluator by means of FotoFinder-video-epiluminescence microscopy in combination with the TrichoScan digital image analysis (Figure 7). TrichoScan is a digital software-supported epiluminescence technique for measuring hair count (number of hairs/0.65 cm^2), hair density (number of hairs/cm^2), hair diameter, anagen/telogen ratio, and vellus hair/terminal hair ratio. To determine the quality of hair leading to an increased hair density, it is important to differentiate the number of terminal and vellus hairs. In TrichoScan all hairs with a diameter > 40 μm are categorized as terminal hair, and all hairs with lesser diameter are categorized as vellus hair. In all patients, in both the treatment and control half heads, two transitional areas of hair loss were defined and marked with a semipermanent tattoo for the subsequent trichogram. In the target area hairs were clipped and dyed with hair brown color for ten

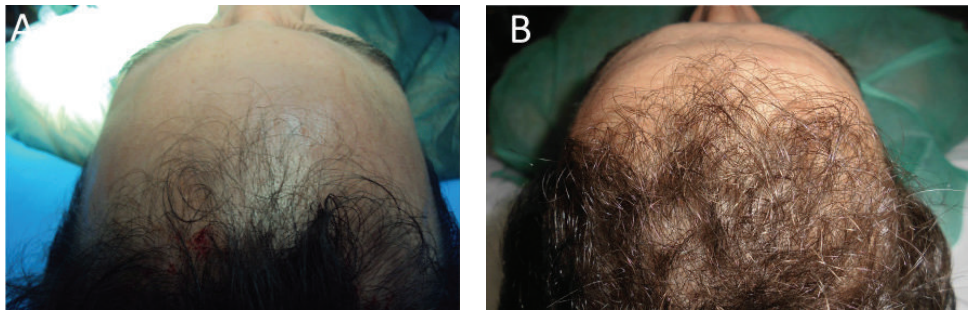

(a) (b)

Figure 1: A smoker 34-year-old male patient affected by hair loss. (a): preoperative situation of the frontal line. (b): postoperative situation of the frontal line after two weeks from the last treatment with increase of the hair count and hair density.

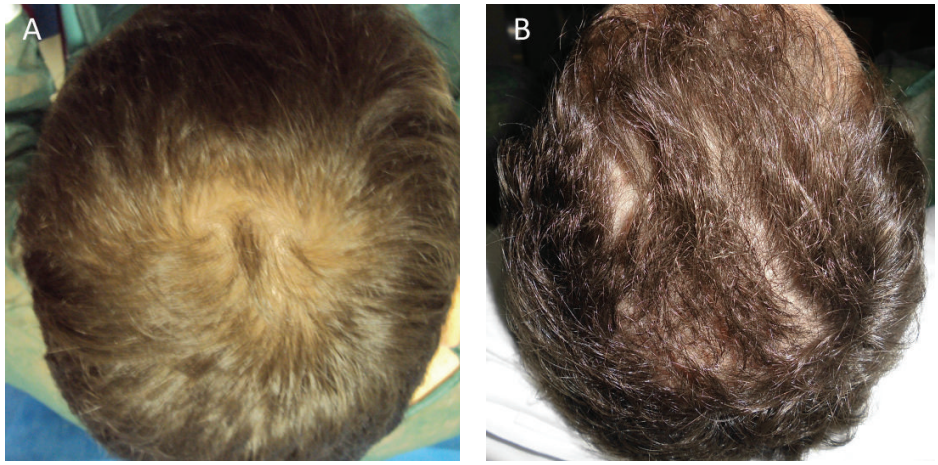

(a) (b)

Figure 2: (a): preoperative situation of the scalp. (b): postoperative situation of the scalp two weeks from the last treatment. The picture shows a postoperative situation with increase of the hair count and hair density.

minutes in order to improve the hair contrast for the analytic software. TrichoScan analysis. The evaluator of TrichoScan analysis was blinded regarding the treatment and control areas of the scalp and not involved in administration of treatment.

2.4. Histological Evaluation. Incisional punch biopsies (3 mm in diameter) of the hair skin were obtained (Figure 3(c)) at baseline and after two months from the last AA-PRP treatment and fixed in buffered formalin. Morphometric analysis [15] was performed on Haematoxylin-Eosin-stained paraffin serial sections (Figures 5 and 6) by evaluating the thickness of epidermis and the number of follicles per mm^2, according to the method [1]. About the orientation of skin biopsies, all samples were cut perpendicularly at the surface and embedded making attention to the correct orientation.

2.5. Immunohistochemistry. Immunohistochemistry was performed using mouse monoclonal anti-Ki67 (DakoCytomation, Denmark) and anti-CD31 (DakoCytomation, Denmark), with positive and negative controls [16, 17]. The percentage of $Ki67^+$ cells in basal layer of epidermis, in outer root sheath of hair follicles, and the number of vessels per mm^2 were calculated according to morphometric criteria [17].

3. Results

3.1. Clinical Evaluation of AA-PRP Injection on Pattern Hair Loss. The various hair growth parameters measured after 3 months of the first treatment were compared with the baseline study before treatment (Figures 1(a), 2(a), 3(a), and 4(a)) and between both treatment and control areas. Mean total hair counts, hair density, and terminal and vellus hair densities for the treatment and control areas are listed in Table 2. At baseline, there were no statistical differences in hair count, hair density, and terminal and anagen hair densities between the treatment and control area of the scalp. The results of this study showed a significant increase in the mean hair count for the treatment area after three months (3 months versus 0 month), with a mean increase of 18.0

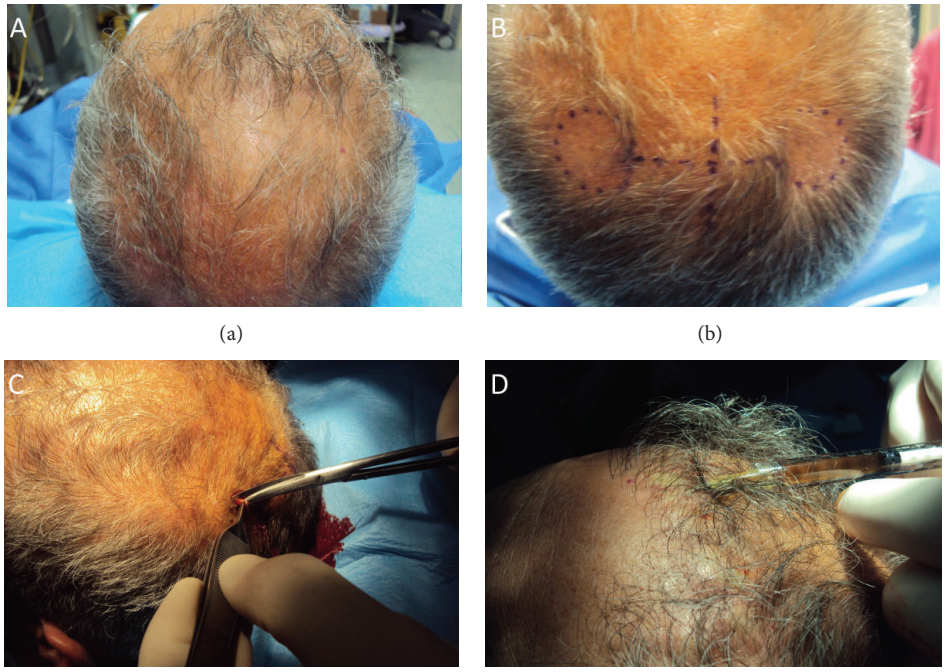

(a) (b)

(c) (d)

Figure 3: A nonsmoker 52-year-old male patient affected by hair loss. (a): preoperative situation of the scalp with hair loss localized to the temporal and nuchal areas. (b): intraoperative injection with the AA-PRP at 0.1 mL/cm2. (c): intraoperative incisional punch biopsies (3 mm in diameter) of the hair skin fixed in buffered formalin. (d): intraoperative study design.

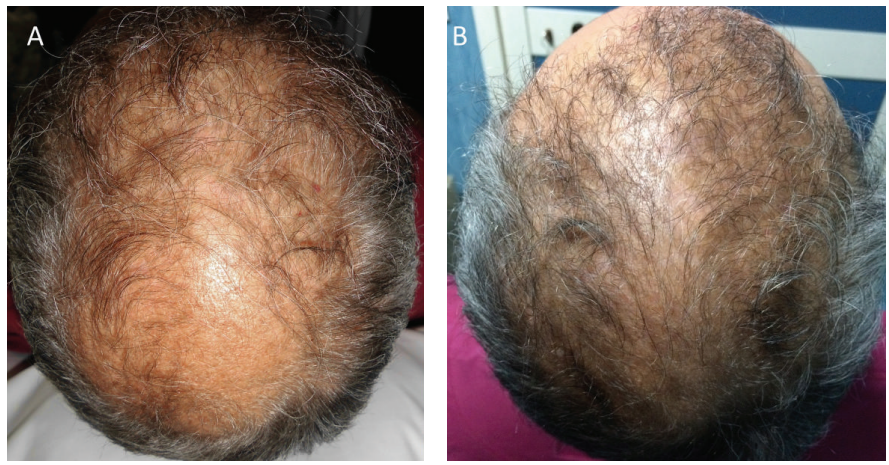

(a) (b)

Figure 4: A nonsmoker 52-year-old male patient affected by hair loss. (a): preoperative situation of the scalp with hair loss localized to the parietal and vertex areas. (b): postoperative situation of the scalp two weeks from the last treatment with increase of the hair count and hair density.

hairs in the target area compared to baseline, while the control area showed a mean decrease of 2,0 hairs (control versus treatment; $P < 0.0001$). Accordingly, in the treatment area, a mean increase in total hair density of 27.7 (number of hairs/cm^2) compared to baseline was observed after 3 months and the control area displayed a mean decrease of 3.0 (number of hairs/cm^2) in hair density at the same time (control versus treatment; $P < 0.0001$). In addition, terminal hair density improved significantly by 27.0 ± 15.3 (number of hairs/cm^2) in the treatment area (Figures 1(b), 2(b), and 4(b)) compared to baseline, while decreasing by 2.1 ± 12.4 (number of hairs/cm^2) in the control area of the scalp (control versus treatment; $P = 0.0003$). There were no statistically significant differences in vellus hair density between the study and the control area after three months.

3.2. Histomorphometric Evaluation of AA-PRP Injection on Pattern Hair Loss. Microscopic evaluation showed the

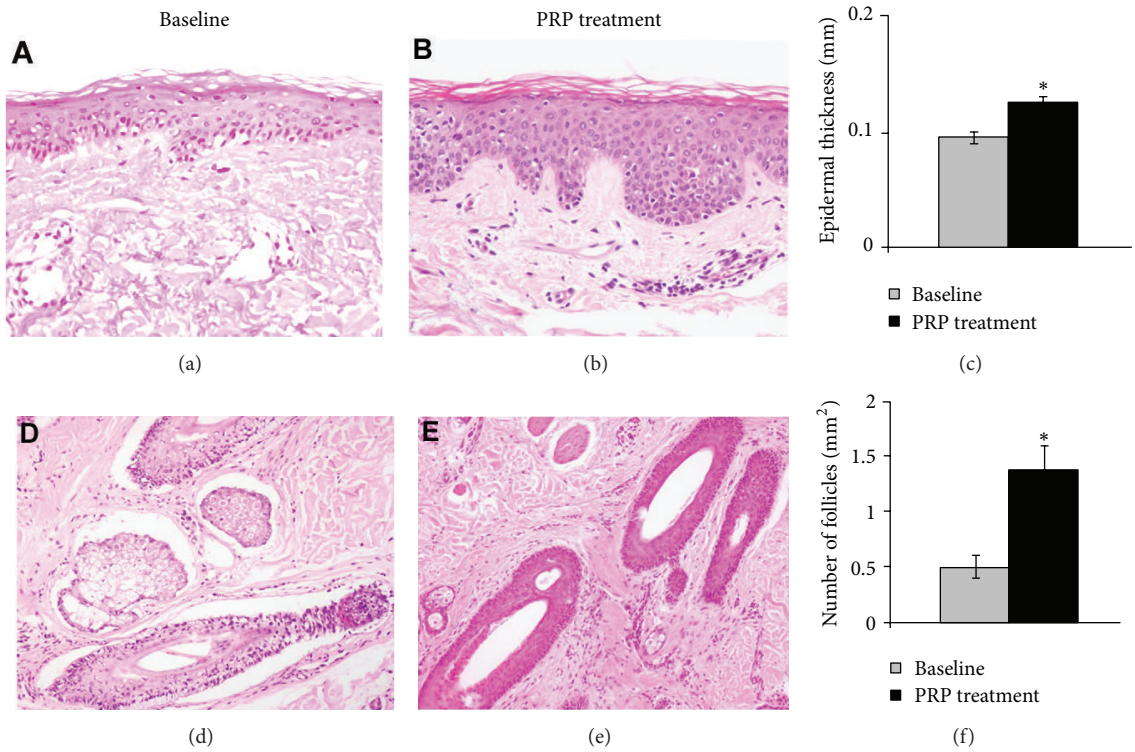

Figure 5: PRP treatment increases the thickness of epidermis and the number of follicles of hair skin. (a) and (b): representative microphotographs of hair skin epidermis at baseline (a) and after PRP treatment (b). (c): bar graph of epidermis thickness. (d) and (e): representative microphotographs of dermal hair follicles at baseline (d) and after PRP treatment (e). (f): bar graph of the number of hair follicles/mm^2 at baseline and after PRP treatment; $*$ indicates $P < 0.05$. Original magnification: (a) and (b): 200x and (d) and (e): 100x.

Table 2: Relevant hair growth parameters assessed by TrichoScan analysis for the treatment and control half-head areas at baseline and after 14 weeks (T1).

	Treatment area	Control area
Hair count (mean ± SD)		
Baseline	103.6 ± 30.9	111.3 ± 28.9
T1	121.6 ± 34.1	109.3 ± 28.2
Hair density [1/cm^2] (mean ± SD)		
Baseline	159.4 ± 47.6	171.2 ± 44.4
T1	187.1 ± 52.5	168.1 ± 43.3
Terminal hair density [1/cm^2] (mean ± SD)		
Baseline	142.7 ± 41.8	152.7 ± 39.7
T1	169.8 ± 47.0	150.6 ± 41.7
Vellus hair density [1/cm^2] (mean ± SD)		
Baseline	14.8 ± 9.7	16.9 ± 10.4
T1	15.8 ± 8.5	17.4 ± 13.9

increase of epidermis thickness (Figure 5(c); $P < 0.05$) in PRP-treated hair skin (Figure 5(b); $P < 0.05$) after three months from the AA-PRP treatment compared to baseline value (Figure 5(a)). Two-week PRP treatment (Figure 5(e); $P < 0.05$) was also accompanied by an increase of the number of follicles (Figure 5(f); $P < 0.05$) compared to baseline value (Figure 5(d)). To better report the effects of PRP, we investigated the proliferation of epidermal and hair follicular bulge cells (Figures 6(b) and 6(e); $P < 0.05$). After two weeks from the last treatment, we observed an increase of Ki67$^+$ basal keratinocytes of epidermis and of hair follicular bulge cells (Figures 6(c) and 6(f); $P < 0.05$) compared to baseline (Figures 6(a) and 6(d)). PRP treatment (Figure 6(h); $P < 0.05$) also associated with a slight increase of small blood vessels around hair follicles in the skin treated (Figure 6(i); $P < 0.05$) compared to baseline (Figure 6(g)).

4. Discussion

Current strategies for the treatment of pattern hair loss are mainly focused on promoting cellular proliferation and differentiation during the hair growth cycle. It has been postulated that minoxidil prolongs anagen and increases hair follicle size through stimulation of potassium channels and prostaglandin endoperoxide synthase-1, which increase level of prostaglandin E2 (PGE2) [11]. Minoxidil promotes the survival of dermal papilla cells by increasing Bcl-2/Bax ratio and by activating ERK and Akt [18]. Oral finasteride also induces the prolongation of anagen hairs, which results in gradual thickening and elongation of the hairs [19]. In addition, finasteride has been shown to reduce the pattern

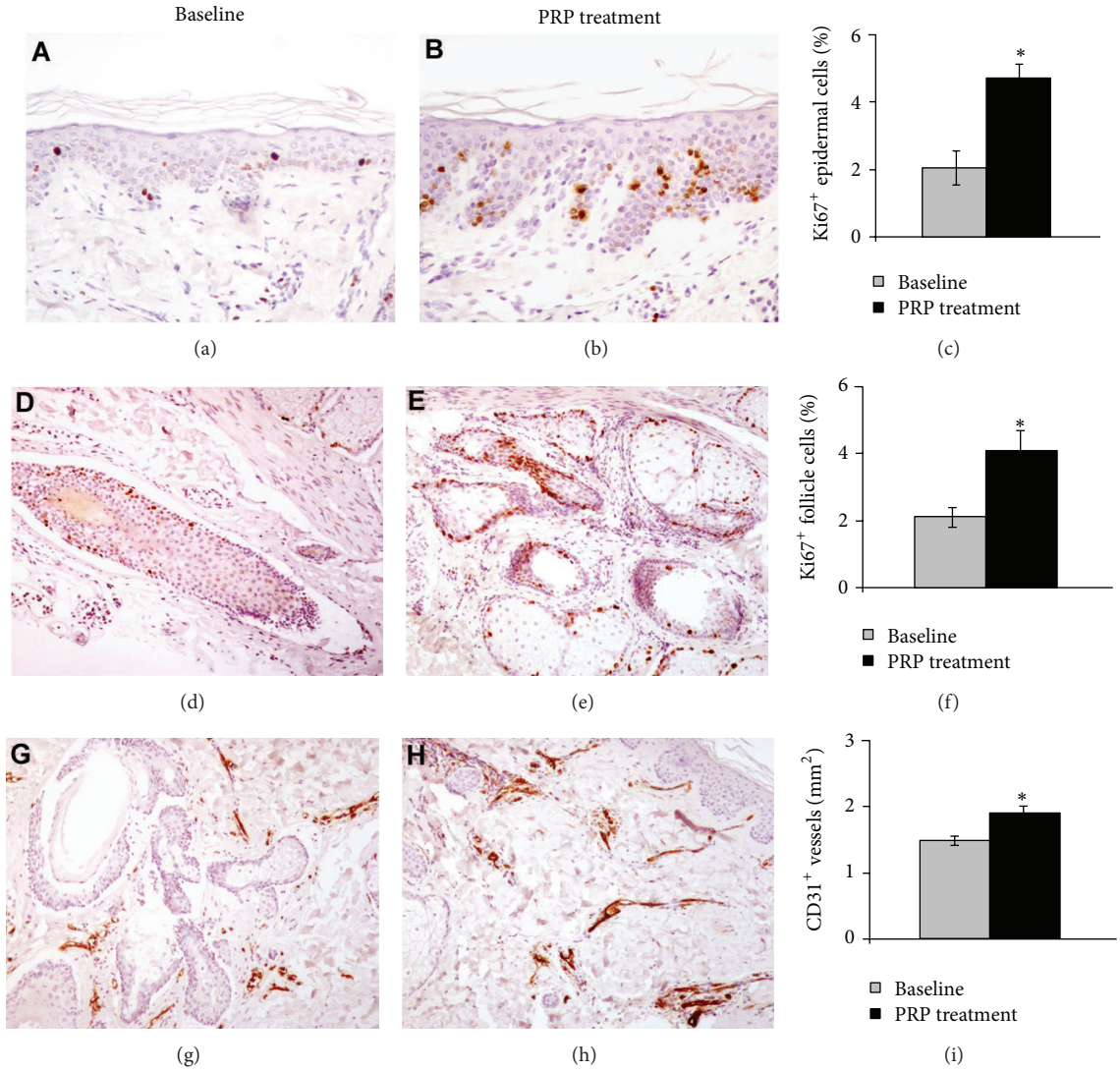

Figure 6: PRP treatment increases proliferation of epidermis basal cells and hair follicular bulge cells. (a) and (b): representative microphotographs of Ki67+ proliferating cells by immunohistochemistry of hair skin epidermis at baseline (a) and after PRP treatment (b). (c): morphometric analysis of $Ki67^+$ cells of hair skin epidermis at baseline and after PRP treatment. (d) and (e): representative microphotographs of $Ki67^+$ proliferating cells by immunohistochemistry of hair follicles at baseline (d) and after PRP treatment (e). (f): morphometric analysis of the percentage of $Ki67^+$ nuclei in hair follicles at baseline and after PRP treatment. (g) and (h): representative microphotographs of $CD31^+$ small dermal vessels of hair skin at baseline (g) and after PRP treatment (h). (i): morphometric analysis of CD31+ small dermal vessels of hair skin at baseline and after PRP treatment; $*$ indicates $P < 0.05$. Original magnification: (a) and (b): 200x and (d), (e), (g), and (h): 100x.

hair loss associated with increased expression of caspases and apoptosis inhibitors and therefore it is ultimately suggested to activate anagen hair growth [20, 21]. Antiapoptotic effects of activated PRP have been suggested as one of the major contributing factors stimulating hair growth [2, 22]. PRP-induced activation of antiapoptotic regulators, such as the Bcl-2 protein and Akt signalling, prolongs the survival of dermal papilla cells during the hair cycle [2, 23]. In addition, the upregulation of FGF-7/b-catenin signalling pathways with PRP treatment is suggested to stimulate hair growth by inducing follicular stem cell differentiation as well as prolonging the anagen phase of the hair growth cycle [2, 24].

Kang et al. [25] reported the clinical efficacy of injection of $CD34^+$ cell-containing PRP preparation for pattern hair loss. In this study, at three months after the first treatment, the patients presented clinical improvement in the mean number of hairs, 20.5 ± 17.0%, mean hair thickness, 31.3 ± 30.1%, and mean two-point score, 84.4 ± 51.7%, compared with baseline values. At 6 months, the patients presented clinical improvement in mean hair count, 29.2 ± 17.8%, mean hair thickness, 46.4 ± 37.5%, and mean two-point score, 121.3 ± 66.8%, compared with baseline.

In our study, AA-PRP was prepared from a small volume of blood (18 cc) according to the method of Cascade-Selphyl-Esforax system [12, 13]. The authors suggested that a sufficient number of platelets could be obtained in all patients by using an automated PRP preparation system. Giusti et al. demonstrated that the optimal platelet concentration for the

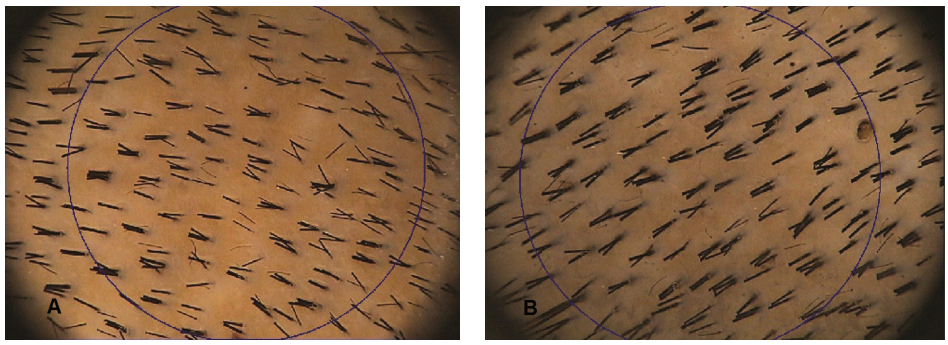

(a) (b)

Figure 7: TrichoScan digital image analysis. (a) shows a preoperative hair count 154.5 hairs per cm^2 and density 237.3 per cm^2. (b) shows a postoperative hair count 169,0 hairs per cm^2, and density 259.6 per cm^2.

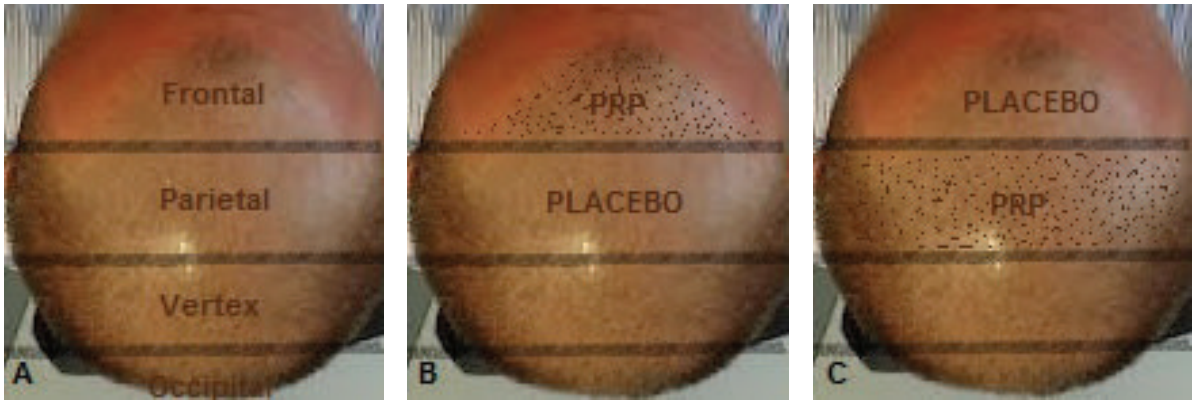

(a) (b) (c)

Figure 8: Photos demonstrating the division of the scalp in four halves: frontal, parietal, vertex, and occipital (a). Patients with hair loss localized to the frontal and parietal areas were injected with the AA-PRP only on the frontal areas (b); the parietal area was treated with placebo based on the injection of physiological solution. Patients with hair loss in the parietal and vertex parts were injected with the AA-PRP only in the parietal part of the scalp (c); the vertex area was treated with placebo based on the injection of physiological solution.

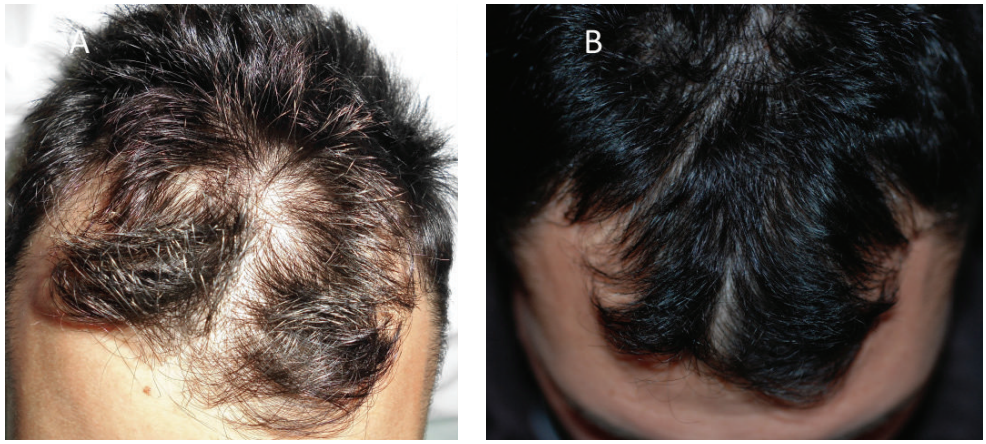

(a) (b)

Figure 9: A nonsmoker 52-year-old male patient affected by hair loss. (a) Preoperative situation of the scalp with hair loss localized to the parietal and frontal areas. (b) Postoperative situation of the scalp two weeks from the last treatment with increase of the hair count and hair density.

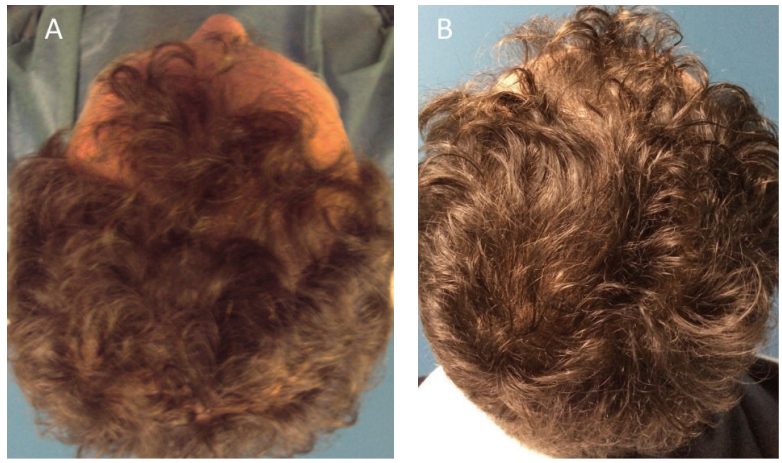

(a) (b)

Figure 10: A smoker 42-year-old male patient affected by hair loss. (a) Preoperative situation of the scalp with hair loss localized to the parietal and frontal areas. (b) Postoperative situation of the scalp two weeks from the last treatment with increase of the hair count and hair density.

induction of angiogenesis in human endothelial cells was 1,500,000 platelets/μL, whereas excessively high concentrations of platelets were suggested to decrease the angiogenic potential [26]. In this study, a mean 1,484,555.6 platelets/μL in the PRP preparation could effectively stimulate follicular and perifollicular angiogenesis, which is suggested to be one of the major factors in active hair growth [5, 11]. Our data suggest that the injection of AA-PRP preparations has a positive therapeutic effect on male and pattern hair loss without major side effects.

Conflict of Interests

The authors declare that there is no conflict of interests regarding the publication of this paper.

Authors' Contribution

Pietro Gentile and Valerio Cervelli contributed to the following: conception and design, paper writing, and final approval of the paper; Augusto Orlandi, Alessandra Bielli, and Maria Giovanna Scioli contributed to the following: histomorphometric evaluation of AA-PRP injection on pattern hair loss and immunohistochemistry analysis; Simone Garcovich contributed to the following: assessment criteria analysis and TrichoScan evaluation; Beniamino Cristiano Curcio and Giulio Cervelli contributed to the following: English editing, collection and assembly of data, and data analysis.

References

[1] M. Takikawa, S. Nakamura, S. Nakamura et al., "Enhanced effect of platelet-rich plasma containing a new carrier on hair growth," *Dermatologic Surgery*, vol. 37, no. 12, pp. 1721–1729, 2011.

[2] Z. J. Li, H.-I. Choi, D.-K. Choi et al., "Autologous platelet-rich plasma: a potential therapeutic tool for promoting hair growth," *Dermatologic Surgery*, vol. 38, no. 7, part 11, pp. 1040–1046, 2012.

[3] C. O. Uebel, J. B. da Silva, D. Cantarelli, and P. Martins, "The role of platelet plasma growth factors in male pattern baldness surgery," *Plastic and Reconstructive Surgery*, vol. 118, no. 6, pp. 1458–1466, 2006.

[4] A. Trink, E. Sorbellini, P. Bezzola et al., "A randomized, double-blind, placebo- and active-controlled, half-head study to evaluate the effects of platelet-rich plasma on alopecia areata," *British Journal of Dermatology*, vol. 169, no. 3, pp. 690–694, 2013.

[5] L. Mecklenburg, D. J. Tobin, S. Müller-Röver et al., "Active hair growth (anagen) is associated with angiogenesis," *Journal of Investigative Dermatology*, vol. 114, no. 5, pp. 909–916, 2000.

[6] S. Lachgar, H. Moukadiri, F. Jonca et al., "Vascular endothelial growth factor is an autocrine growth factor for hair dermal papilla cells," *Journal of Investigative Dermatology*, vol. 106, no. 1, pp. 17–23, 1996.

[7] U. Kozlowska, U. Blume-Peytavi, V. Kodelja et al., "Expression of vascular endothelial growth factor (VEGF) in various compartments of the human hair follicle," *Archives of Dermatological Research*, vol. 290, no. 12, pp. 661–668, 1998.

[8] V. Tarallo, L. Vesci, O. Capasso et al., "A placental growth factor variant unable to recognize Vascular Endothelial Growth Factor (VEGF) receptor-1 inhibits VEGF-dependent tumor angiogenesis via heterodimerization," *Cancer Research*, vol. 70, no. 5, pp. 1804–1813, 2010.

[9] D. J. Tobin, A. Gunin, M. Magerl, B. Handijski, and R. Paus, "Plasticity and cytokinetic dynamics of the hair follicle mesenchyme: implications for hair growth control," *Journal of Investigative Dermatology*, vol. 120, no. 6, pp. 895–904, 2003.

[10] W. Li, M. Enomoto, M. Ukegawa et al., "Subcutaneous injections of platelet-rich plasma into skin flaps modulate proangiogenic gene expression and improve survival rates," *Plastic and Reconstructive Surgery*, vol. 129, no. 4, pp. 858–866, 2012.

[11] M. Semalty, A. Semalty, G. P. Joshi, and M. S. M. Rawat, "Hair growth and rejuvenation: an overview," *Journal of Dermatological Treatment*, vol. 22, no. 3, pp. 123–132, 2011.

[12] V. Cervelli, M. G. Scioli, P. Gentile et al., "Platelet-rich plasma greatly potentiates insulin-induced adipogenic differentiation of human adipose-derived stem cells through a

serine/threonine kinase Akt-dependent mechanism and promotes clinical fat graft maintenance," *Stem Cells Translational Medicine*, vol. 1, no. 3, pp. 206–220, 2012.

[13] V. Cervelli, P. Gentile, M. G. Scioli et al., "Application of platelet-rich plasma in plastic surgery: clinical and in vitro evaluation," *Tissue Engineering C: Methods*, vol. 15, no. 4, pp. 625–634, 2009.

[14] V. Cervelli, P. Gentile, B. de Angelis et al., "Application of enhanced stromal vascular fraction and fat grafting mixed with PRP in post-traumatic lower extremity ulcers," *Stem Cell Research*, vol. 6, no. 2, pp. 103–111, 2011.

[15] L. Campagnolo, G. Costanza, A. Francesconi, G. Arcuri, I. Moscatelli, and A. Orlandi, "Sortilin expression is essential for pro-nerve growth factor-induced apoptosis of rat vascular smooth muscle cells," *PLoS ONE*, vol. 9, no. 1, Article ID e84969, 2014.

[16] A. Francesconi, G. Arcuri, E. Doldo et al., "Age-related increase of stem marker expression influences vascular smooth muscle cell properties," *Atherosclerosis*, vol. 224, no. 1, pp. 51–57, 2012.

[17] M. A. Stasi, M. G. Scioli, G. Arcuri et al., "Propionyl-L-carnitine improves postischemic blood flow recovery and arteriogenetic revascularization and reduces endothelial NADPH-oxidase 4-mediated superoxide production," *Arteriosclerosis, Thrombosis, and Vascular Biology*, vol. 30, no. 3, pp. 426–435, 2010.

[18] J. H. Han, O. S. Kwon, J. H. Chung, K. H. Cho, H. C. Eun, and K. H. Kim, "Effect of minoxidil on proliferation and apoptosis in dermal papilla cells of human hair follicle," *Journal of Dermatological Science*, vol. 34, no. 2, pp. 91–98, 2004.

[19] A. Tosti and B. M. Piraccini, "Finasteride and the hair cycle," *Journal of the American Academy of Dermatology*, vol. 42, no. 5, pp. 848–849, 2000.

[20] M. E. Sawaya, U. Blume-Peytavi, D. L. Mullins et al., "Effects of finasteride on apoptosis and regulation of the human hair cycle," *Journal of Cutaneous Medicine and Surgery*, vol. 6, no. 1, pp. 1–9, 2002.

[21] J. P. D. R. Vaccari, M. E. Sawaya, F. Brand III et al., "Caspase-1 level is higher in the scalp in androgenetic alopecia," *Dermatologic Surgery*, vol. 38, no. 7, part 11, pp. 1033–1039, 2012.

[22] C. Ferraris, M. Cooklis, R. R. Polakowska, and A. R. Haake, "Induction of apoptosis through the PKC pathway in cultured dermal papilla fibroblasts," *Experimental Cell Research*, vol. 234, no. 1, pp. 37–46, 1997.

[23] O. S. Kwon, H. K. Pyo, Y. J. Oh et al., "Promotive effect of minoxidil combined with all-*trans* retinoic acid (tretinoin) on human hair growth in vitro," *Journal of Korean Medical Science*, vol. 22, no. 2, pp. 283–289, 2007.

[24] K.-C. Sohn, G. Shi, S. Jang et al., "Pitx2, a β-catenin-regulated transcription factor, regulates the differentiation of outer root sheath cells cultured in vitro," *Journal of Dermatological Science*, vol. 54, no. 1, pp. 6–11, 2009.

[25] J.-S. Kang, Z. Zheng, M. J. Choi, S.-H. Lee, D.-Y. Kim, and S. B. Cho, "The effect of CD34+ cell-containing autologous platelet-rich plasma injection on pattern hair loss: a preliminary study," *Journal of the European Academy of Dermatology and Venereology*, vol. 28, no. 1, pp. 72–79, 2014.

[26] I. Giusti, A. Rughetti, S. D'Ascenzo et al., "Identification of an optimal concentration of platelet gel for promoting angiogenesis in human endothelial cells," *Transfusion*, vol. 49, no. 4, pp. 771–778, 2009.

Hindawi Publishing Corporation
BioMed Research International
Volume 2014, Article ID 762570, 11 pages
http://dx.doi.org/10.1155/2014/762570

Research Article

The Study of the Frequency Effect of Dynamic Compressive Loading on Primary Articular Chondrocyte Functions Using a Microcell Culture System

Wan-Ying Lin,[1] Yu-Han Chang,[2] Hsin-Yao Wang,[1] Tzu-Chi Yang,[3] Tzu-Keng Chiu,[4] Song-Bin Huang,[3] and Min-Hsien Wu[3]

[1] *School of Medicine, Chang Gung University, 259 Wen-Hwa 1st Road, Gueishan Township, Taoyuan County 333, Taiwan*
[2] *Department of Orthopaedic Surgery, Chang Gung Memorial Hospital, Linko, 5 Fusing St., Gueishan Township, Taoyuan County 333, Taiwan*
[3] *Graduate Institute of Biochemical and Biomedical Engineering, Chang Gung University, 259 Wen-Hwa 1st Road, Gueishan Township, Taoyuan County 333, Taiwan*
[4] *Graduate Institute of Chemical and Materials Engineering, Chang Gung University, 259 Wen-Hwa 1st Road, Gueishan Township, Taoyuan County 333, Taiwan*

Correspondence should be addressed to Min-Hsien Wu; mhwu@mail.cgu.edu.tw

Received 3 December 2013; Revised 12 March 2014; Accepted 17 March 2014; Published 16 April 2014

Academic Editor: Nihal Engin Vrana

Compressive stimulation can modulate articular chondrocyte functions. Nevertheless, the relevant studies are not comprehensive. This is primarily due to the lack of cell culture apparatuses capable of conducting the experiments in a high throughput, precise, and cost-effective manner. To address the issue, we demonstrated the use of a perfusion microcell culture system to investigate the stimulating frequency (0.5, 1.0, and 2.0 Hz) effect of compressive loading (20% and 40% strain) on the functions of articular chondrocytes. The system mainly integrates the functions of continuous culture medium perfusion and the generation of pneumatically-driven compressive stimulation in a high-throughput micro cell culture system. Results showed that the compressive stimulations explored did not have a significant impact on chondrocyte viability and proliferation. However, the metabolic activity of chondrocytes was significantly affected by the stimulating frequency at the higher compressive strain of 40% (2 Hz, 40% strain). Under the two compressive strains studied, the glycosaminoglycans (GAGs) synthesis was upregulated when the stimulating frequency was set at 1 Hz and 2 Hz. However, the stimulating frequencies explored had no influence on the collagen production. The results of this study provide useful fundamental insights that will be helpful for cartilage tissue engineering and cartilage rehabilitation.

1. Introduction

Articular cartilage is a tough and resilient connective tissue lying at the end surface of long bones near joints. The biological function of cartilage to provide resistance to mechanical loading is primarily attributed to its abundant extracellular matrix (ECM), mainly consisting of glycosaminoglycans (GAGs) and collagen [1]. The homeostasis of the ECM is maintained by the articular chondrocytes, the only cell species existing in articular cartilage. Upon damage, adult cartilage has a limited ability of self-repairing. To treat cartilage defects, cartilage tissue engineering is generally regarded as a promising method. The common approach to cartilage tissue engineering involves the *in vitro* cultivation of tissue constructs by using (1) chondrogenic cells, (2) scaffolds capable of providing a three-dimensional (3D) structure for tissue development, and (3) bioreactors capable of providing the suitable extracellular conditions necessary for the cells to regenerate functional cartilaginous tissues [2]. Although proof of principle has been demonstrated [1], few *in vitro*

cartilage tissue engineering investigations have generated an appropriate tissue that meets the functional demands placed upon this tissue *in vivo*.

One of the key technical hurdles to functional cartilage tissue engineering is the lack of fundamental understanding of the link between extracellular conditions and chondrocyte functions. Though several studies have been carried out to find out the relationship between articular chondrocyte and environment, the majority of them have focused on exploring the effect of biochemical factors on cellular functions [3]. Physical factors like mechanical stimulation have been reported to play an important role in modulating chondrocyte physiology and, in turn, cartilage homeostasis [4]. Although some fundamental investigations have been carried out to probe the effect of mechanical stimulation on articular chondrocyte physiology [1, 5–11], the relevant studies are, to some extent, not comprehensive. The possible cause behind this is a lack of appropriate experimental tools, by which the effect of mechanical stimulation on chondrocyte function can be quantitatively determined in an efficient, precise, physiologically meaningful, and cost-effective manner.

The effects of mechanical loading on articular chondrocytes are complex. Under physiological mechanical stimulation, the articular chondrocytes in cartilage are subjected to complicated physical events including hydrostatic pressure, tensile stress, shear stress, and compressive stress [11]. Among these events, compressive stimulation plays an important role in modulating the articular chondrocyte functions [1]. Several devices or bioreactors have been developed for investigating the effect of compressive stimulation on articular chondrocyte physiology. These cell or tissue culture apparatuses commonly make use of the direct compression on the chondrocytes-embedded constructs or on cartilage explants due to its similarity to *in vivo* loading by intra-articular contact [1]. According to the working regimen, the cell or tissue culture devices capable of providing compressive loading to cells can be divided into two categories, namely, static [5] and dynamic systems [1, 6–11]. Dynamic compressive stimulation is predominantly adopted because dynamic loading is physiologically meaningful [1, 12]. Numerous cell or tissue culture devices, capable of generating dynamic compressive stimulation, have been demonstrated to be feasible for providing compressive loading to the cartilage explants, or chondrocytes-embedded scaffold [1, 5–10]. Nevertheless, these devices are normally technically demanding, complicated, large, and costly, which could limit the experimental throughput. Moreover, most of these devices adopt static cell culture format [1, 5–7, 9, 10, 13], where the culture medium is literally supplied in a manual and batch-wise manner. This could lead to high contamination risk and fluctuating culture condition [14]. The latter could hamper the precise quantification of the link between the mechanical stimulation and articular chondrocyte functions since reports in literature have demonstrated that the articular chondrocytes are fairly sensitive to extracellular environments [15].

While tissue engineering scientists are making progress [16], they might need an appropriate device to aid their research. To address the issue, a microcell culture system capable of providing dynamic compressive loading to 3D cell culture constructs was proposed in our previous study (Figure 1(a)) [11]. One of its distinctive features is the function of tunable compressive loading generation. The mechanism is based on the pneumatically driven deformation of an elastic polydimethylsiloxane (PDMS) membrane, which in turn exerts compressive loading onto a 3D cell culture construct through a micropillar (Figure 1(a)) [11]. By modulating the frequency and pressure of the input pneumatic conditions, the compressive loading can be generated in a controllable manner. Other technical features of the microcell culture system are (1) low cost, (2) high throughput, (3) low consumption of research resources due to its small scale, (4) maintaining a stable and well-defined culture condition due to the perfusion culture format and miniaturized culture scale [14, 17], (5) efficient and precise sample (e.g., cells) loading, and (6) easy operation. Borrowing from our previous experience on the micro cellculture system, the frequency (0.5, 1.0, and 2.0 Hz) effect of dynamic compressive loading (strain: 20 and 40%) on the cell viability and proliferation as well as the metabolic and biosynthetic activities of primary articular chondrocytes were investigated.

2. Materials and Methods

2.1. The Microcell Culture System and Experimental Setup. The microcell culture system is composed of 12 individual microbioreactors (D: 7.5 mm; H: 6.5 mm). At the bottom of each microbioreactor, there is a cylindrical cavity (D: 1 mm; H: 2.3 mm; volume: 1.8 μL), which is not only used to accommodate a cell/biomaterial scaffold for 3D cell culture but also to quantitatively define the volume of such sample loading. The overall sample-loading process was described previously [11].

For high throughput perfusion cell culture purpose, each microbioreactor was designed to perfuse with its own separate medium supply through silicon tubing driven by a multichannel syringe pump (KDS 220, KD Scientific Ltd., USA). In addition, the microcell culture platform was placed on the surface of a transparent indium-tin-oxide- (ITO-) based microheater chip to provide a stable thermal condition of $37 \pm 0.2^{\circ}$C for cell culture [18]. To pneumatically drive and control the compressive loading mechanism, 4 via holes were connected with 4 air tubes from a custom-made pneumatic controller. Within the hand-held controller, an air compressor (MDR2-1A/11, Jun-Air Inc., Japan), 4 electromagnetic valves (EMV) (S070M-5BG-32, SMC Inc., Taiwan), and a programmable control circuit were integrated to activate and to control the generation of compressive loading. The overall experimental setup is illustrated in Figure 1(b).

2.2. The Exertions of Dynamic Compressive Loading: Operating Conditions and Long-Term Stability. In this study, the operating stimulating frequencies (0.5, 1.0, and 2.0 Hz) were manipulated through the programmable control circuit and EMVs. For the magnitude of compressive loading, it was modulated by tuning the magnitude of the pneumatic pressure exerted in the pneumatic chamber (Figure 1(a)) through an air pressure regulator (Figure 1(b)). It was expressed as

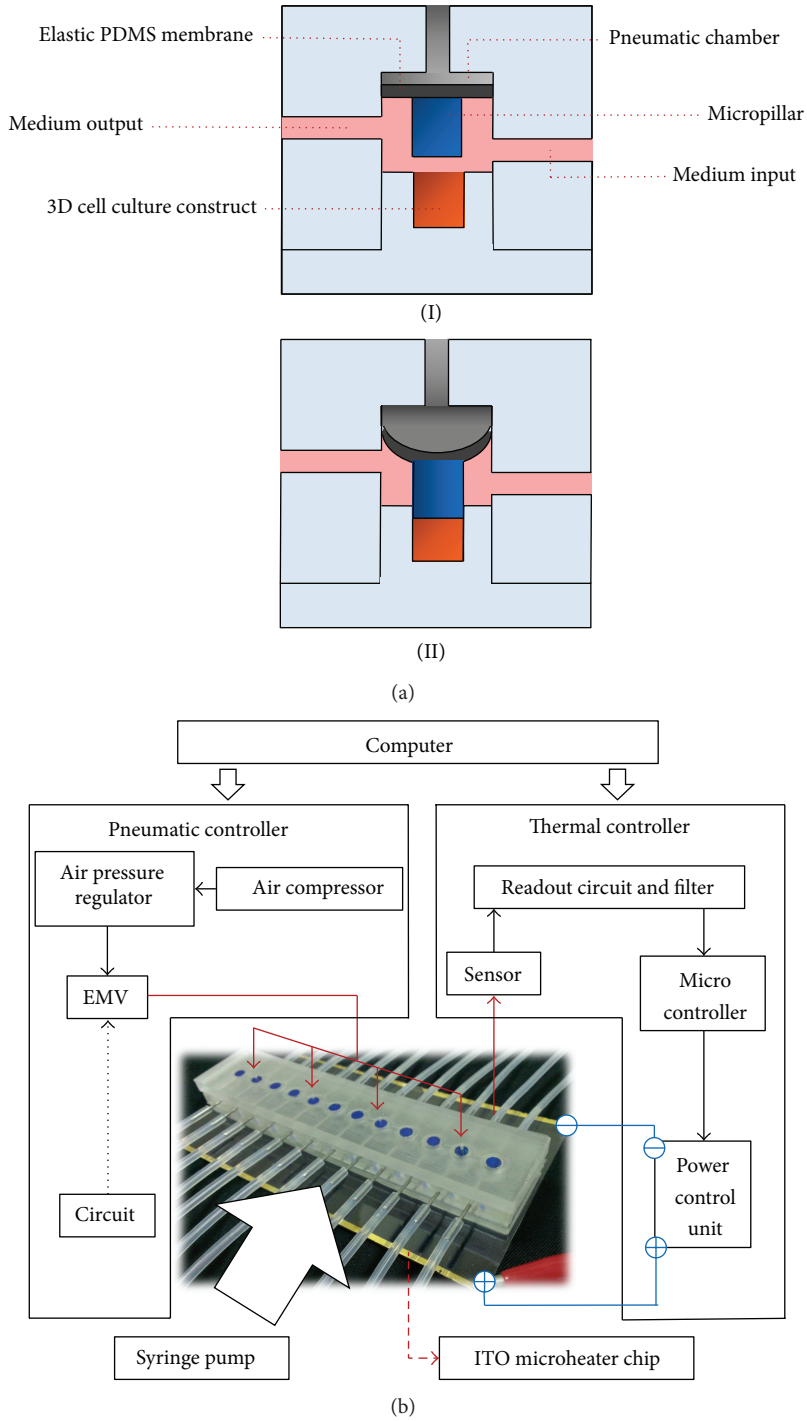

Figure 1: (a) Schematic illustration of the pneumatically-driven compressive loading mechanism: (I) the rest state and (II) the pneumatically-driven deformation of an elastic PDMS membrane leading to the vertical movement of the connected micropillar that in turn generates compressive loading onto the 3D cell culture construct below (cross-sectional view) (a video clip is provided as a Supplementary Material available online at http://dx.doi.org/10.1155/2014/762570), and (b) the photograph of the microcell culture system, and the schematic illustration of overall experimental setup (EMV: electromagnetic valves; ITO: indium tin oxide).

compressive strain (the ratio of compressive deformation per unit length along the compressive axis) and quantified by the method reported previously [11]. Briefly, the dynamic deformation of a 3D cell culture construct was experimentally observed with the aid of a high-speed charge-coupled device (CCD) camera (MC1311, Mikrotron, Germany). In the measurements, the sequential action images of the dynamic deformation of a 3D cell culture construct were captured at the resolution speed of 100 frames sec^{-1}. The compressive strain (%) was then measured by the equation:

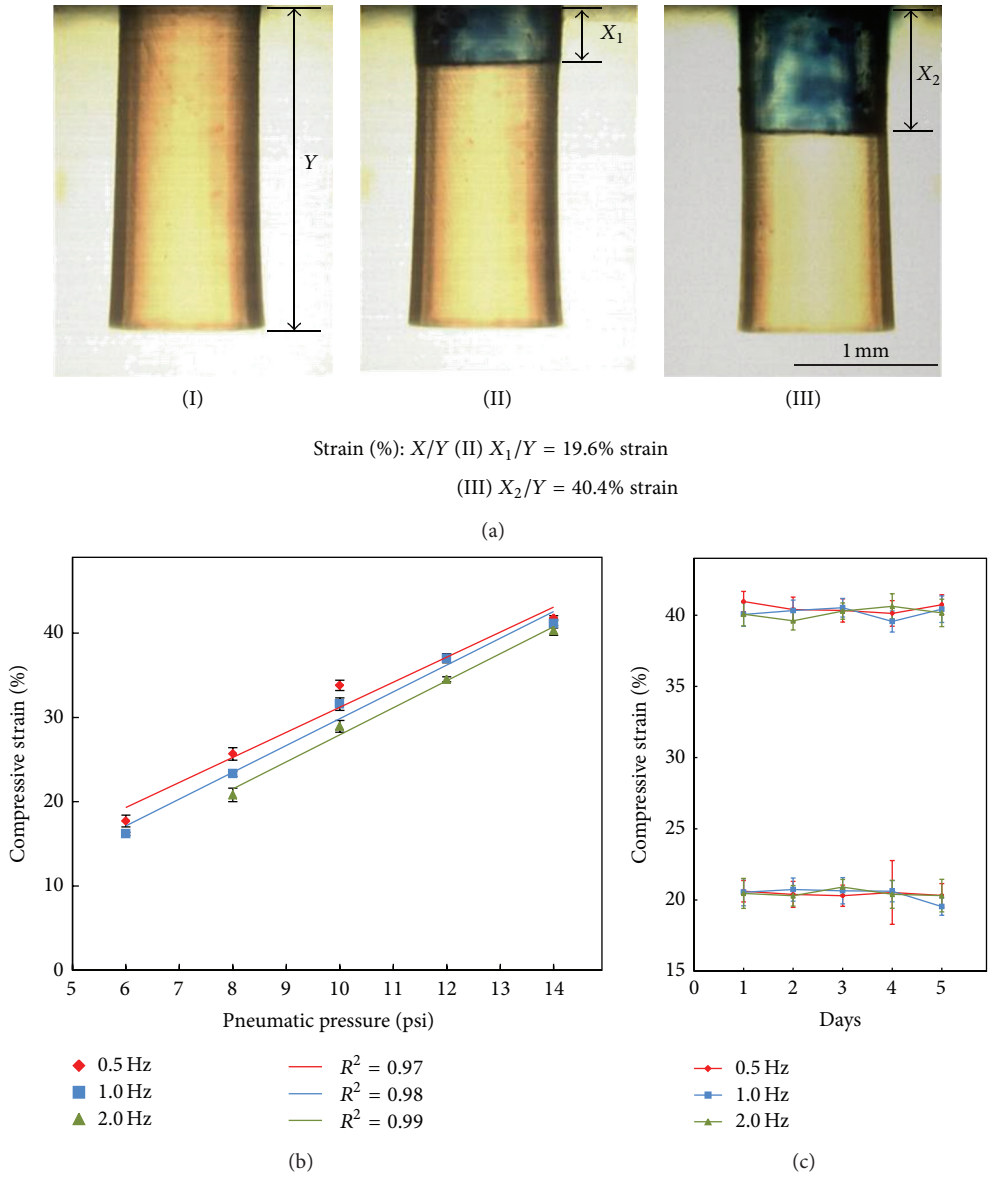

FIGURE 2: (a) Experimental quantification of the generated compressive strain by capturing the action images of micropillar using a high-speed CCD. The compressive strain (%) is measured by the equation: x (deformation length)/y (height of 3D cell culture construct; the photograph (I))∗100%. Photographs (II)-(III) showed the observed deformation lengths of 0.45 mm (X_1) and 0.93 mm (X_2) with the corresponding compressive strain of 19.6% and 40.4%, respectively. (b) The quantitative relationship between the compressive strain and the pneumatic pressure applied under different operating frequency conditions (0.5, 1.0, and 2.0 Hz). (c) Evaluation of long-term stability of the generated compressive strain (lower and higher level: 20% and 40%, resp.) under the operating frequencies of 0.5, 1.0, and 2.0 Hz.

x (the deformation length)/y (the height of 3D cell culture construct)∗100%. Figure 2(a) showed the microscopic images of the 3D cell culture constructs subjected to the dynamic compressive loading with magnitudes of 20% and 40% strain. Based on above approaches, the quantitative relationships between the magnitude (6–14 psi) and the frequency (0.5, 1.0, and 2.0 Hz) of the pneumatic pressures exerted and the resulting compressive strain (%) were experimentally determined. In this work, furthermore, the dynamic compressive stimulation was subjected to chondrocytes-encapsulating 3D culture constructs for up to 5 days. In order to examine the long-term stability of dynamic compressive loading, the daily measurements of the compressive strain (20% and 40%) generated under different operating frequencies (0.5, 1.0, and 2.0 Hz) were carried out, based on the approach aforementioned.

2.3. Perfusion 3D Articular Chondrocyte Culture under Different Dynamic Compressive Loading. Primary articular chondrocytes were isolated from the femorotibial joint as previously described [3]. The cell suspension thus obtained

was assessed microscopically for cell number and viability using 0.4% (w/v) trypan blue in phosphate buffered saline (PBS; Invitrogen, Taiwan). Only cell preparations with cell viability greater than 95% were then used. In this study, the primary articular chondrocytes were encapsulated in alginate hydrogel to form a 3D cell culture construct. Briefly, the isolated cells were then immobilized in 6% (w/v) alginate hydrogel at a cell density of 2.4×10^7 cells mL^{-1}. The mixture was subsequently loaded into the cylindrical cavity in the microbioreactors (Figure 1(a)). After sample loading and device assembling, each microbioreactor was perfused with 0.5 M calcium chloride solution at a flow rate of 1 μL min^{-1} for 25 min for the solidification of the alginate hydrogel. This was followed by perfusion articular chondrocyte culture under a serial compressive loading settings (strain: 20% and 40%; operating frequency: 0.5, 1.0, and 2.0 Hz; daily regimen: three consecutive cycles of 1 hour loading and 1 hour relaxation) for up to 5 days using the established experimental setup (Figure 1(b)). In this research, Dulbecco's Modified Eagle's Medium (DMEM) (with 1000 mg L^{-1} glucose, 25 mM HEPES, without sodium bicarbonate; unless stated otherwise all chemicals were purchased from Sigma, Taiwan) supplemented with 10% foetal bovine serum (Invitrogen, Taiwan), 2% antibiotic/antimycotic solution, and 50 μg mL^{-1} ascorbic acid was continuously perfused to the individual microbioreactors at a flow rate of 60 μL hr^{-1}. After a 5-day perfusion cell culture under compressive stimulation, the cell viability was observed microscopically through fluorescent staining. In addition, both culture medium and 3D cell culture constructs were collected to evaluate the proliferative, metabolic, and biosynthetic activities of articular chondrocytes by measuring the cellular DNA, lactic acid, GAGs, and hydroxyproline levels, respectively.

2.4. Bioassays

2.4.1. Evaluation of Cell Viability and Proliferation. The viability of the articular chondrocytes in alginate hydrogel under different compressive stimulation was evaluated using a fluorescent dye kit (LIVE/DEAD Viability/Cytotoxicity Kit L-3224, Molecular Probes). After cell culture, briefly, the remaining culture medium inside the microbioreactor chambers was removed. 10 μL of the dye reagent containing 1 μM calcein and 2 μM ethidium homodimer-1, prepared according to the manufacturer's instruction, was loaded into each microbioreactor chamber. After 20 min incubation, the images of live (green) and dead (red) cells were captured using a confocal microscope (LSM 510 META, Zeiss, Germany). Cell viability was then quantified by counting the live (green) and dead (red) cells using a software program (SimplePCI version 5.2.1, Compix Inc., PA, USA) [19]. In addition, the cell proliferation of articular chondrocytes was evaluated by quantifying the DNA contents of cells. The DNA content of cells was detected according to Hoemann et al. [20]. Calf thymus DNA (5 to 125 ng) was used as standard.

2.4.2. Lactic Acid. The lactic acid produced and released into culture medium was measured using a Lactate Reagent Kit (Trinity Biotech Plc., Ireland) [21]. The assay was carried out as directed by manufacturer's instructions. A lactate solution at a concentration of 50~500 mg L^{-1} made from dissolving lactate sodium salt in deionised water (DI) water was used as standard.

2.4.3. Glycosaminoglycans (GAGs) and Hydroxyproline. A colorimetric reaction based on Farndale et al. [22] was used to detect GAGs. The method used in this experiment was modified according to Hoemann et al. [20]. Absorbance at 540 nm was read using a microplate reader (Sunrise, Tecan Ltd, Taiwan) and chondroitin sulphate. A sodium salt in the range between 0.01 μg and 1.25 μg was used as standard. Moreover, total collagen production was assayed as hydroxyproline content after hydrolysis. The hydroxyproline content of insoluble collagen was determined according to Stegemann and Stalder [23]. In this evaluation, the hydroxyproline was assayed by a modified method by Urban and McMullin [24].

2.5. Statistical Analysis.

Data from at least three separate experiments were analyzed and presented as mean ± standard deviation. For a given experiment, each condition was tested in triplicate ($n = 9$). One-way ANOVA analysis with a statistical significance level of 0.05 was used to examine the effects of different compressive stimulation on the proliferative, metabolic, and biosynthetic activities of chondrocytes after 5 days of culture. The Tukey Honestly Significant Difference (HSD) post hoc test was used to compare the differences between two compressive loading conditions when the null hypothesis of ANOVA analysis was rejected.

3. Results and Discussions

3.1. Effect of Operating Conditions on the Generation of Dynamic Compressive Loading. In this study, a pneumatically-driven membrane-based actuation scheme was adopted to create compressive loading on 3D cell culture constructs (Figure 1(b)). This working mechanism has also been utilized in a wide variety of micropumps in various microfluidic systems [25, 26]. Different from the other approaches to generate such mechanical movements, pneumatically-driven mechanism is generally regarded to have lower fabrication cost and simpler fabrication and operation process [25, 26]. In the microcell culture system, the magnitude of the pneumatic pressure exerted in the pneumatic chamber (Figure 1(a)) and its operating frequency are two key parameters that can manipulate the dynamic compressive loading on a 3D cell culture construct. Figure 2(b) shows the quantitative relationships between the operating conditions and the resulting compressive loadings. For a given operating frequency, the generated compressive strain increased proportionally (R^2: 0.97, 0.98, and 0.99 for the 0.5, 1.0, and 2.0 Hz, resp.) with the increase of the applied pneumatic pressure within the experimental conditions investigated (Figure 2(b)). Neglecting the mechanical resistance of 3D cell culture construct, the above finding is due to the fact that the resultant compressive strain is directly proportional to the deformation magnitude of PDMS

membrane. The key moving component in the mechanism of compressive loading generation is the elastic PDMS membrane and its connected micropillar (Figure 1(a)). The pneumatically-driven deformation of a PDMS membrane is well described as follows [27]:

$$w_o = \frac{pa^2}{4\sigma_o h}, \quad (1)$$

where w_o, p, a, σ_o, and h represent the maximum magnitude of membrane deformation, applied pneumatic pressure, radius of PDMS membrane, intrinsic tensile stress, and thickness of membrane, respectively.

From above equation, it can be observed that the deformation magnitude of a PDMS membrane is proportional to the magnitude of pneumatic pressure applied. These could reasonably explain the proportional relationship between the applied pneumatic pressure and the resultant compressive strain as observed in Figure 2(b). Moreover, it was also found that the generated compressive strain decreased with the increase of operating frequency (Figure 2(b)). At a given pneumatic pressure, the dynamic process to load a pneumatic chamber with an air pressure is time-dependent [28, 29]. Higher operating frequency implies shorter imposition time (e.g., 2.0, 1.0, and 0.5 sec round^{-1} for the 0.5, 1.0, and 2.0 Hz, resp.) of pneumatic pressure input. This could accordingly lead to reduced PDMS membrane deformation and thus the lower level of compressive strain is generated. The experiments also found that the maximum frequency and strain that can be obtained in the system are 4 Hz and 50% stain, respectively. In the study, furthermore, a dynamic compressive stimulation was applied onto an articular chondrocytes-encapsulating 3D culture construct for 5 days. For a more accurate investigation, the long-term stability of the compressive loading was experimentally examined. This issue has been generally ignored in several studies based on the same pneumatically-driven membrane-based actuations [25, 26, 28]. Figure 2(c) exhibited the long-term variations of the compressive strain generated under different operating conditions. For the lower compressive strain range of around 20%, the measured compressive strains were found to have no significant difference ($P > 0.05$, ANOVA) during the 5 days operation under a given operating frequency tested. Furthermore, when the compressive strain generated under different operating frequencies were compared, they were measured to have no statistical difference ($P > 0.05$, ANOVA) at each time point investigated during the 5-day operation. Similar results were also found at the higher compressive strain range of about 40%. Taken together, the above findings might indicate that the proposed mechanism for dynamic compressive loading generation was capable of providing a stable compressive loading during the cell culture period.

3.2. Effect of Dynamic Compressive Loading on the Cell Viability, Proliferation, and Metabolic Activities of Articular Chondrocytes. In this study, the primary articular chondrocytes cultured in 3D alginate hydrogel constructs were subjected to various compressive stimulation conditions (strain: 20%, and 40%; frequencies: 0.5, 1.0, and 2.0 Hz) for up to 5 days. In addition, the dynamic compressive stimulation regimen was based on 3 consecutive cycles per day, (one cycle is defined as 1 hour of loading followed by 1 hour of relaxation), which was reported to be more physiologically relevant [1, 30, 31]. In this study, the impact of the compressive stimulation on the articular chondrocyte viability was observed using a fluorescent dye staining and quantified using an image analysis. Figure 3 showed the microscopic images of the articular chondrocytes treated with different compressive stimulation conditions, in which the green and red dots represent the live and dead cells, respectively. Overall, the articular chondrocytes cultured under dynamic compressive loading kept the average cell viability as high as 95%, without statistical difference ($P > 0.05$, ANOVA) among the experimental conditions tested. These outcomes were consistent with the previous findings showing that the cell viability of articular chondrocytes is not mechanically affected by the compressive strain being lower than 51.5% [11]. Articular cartilage is a tissue designed to withstand compression during joint movement, and thus the articular chondrocytes are normally subjected to a wide range of mechanical loadings *in vivo*. In normal physiological conditions, a human articular cartilage is subjected to the compressive strain ranging from 20% to 30% *in vivo* [1, 32, 33]. In this study, the higher compressive strain around 40% is regarded as the excessive loading of articular cartilage during vigorous exercise [33]. Taken together, the above findings could indicate that the articular chondrocytes might keep high cell viability under normal physiological condition or even under the excessive compressive strain as high as 40%–50%.

Furthermore, the DNA content of cells was measured as an indicator of articular chondrocytes proliferation after 5 days of cell culture in this study. As shown in Figure 4(a), there was no statistical difference ($P > 0.05$, ANOVA) between the control (no compressive stimulation) and the mechanical compression-treated cases, meaning that the stimulating frequency (0.5, 1.0, and 2.0 Hz) and the magnitude (20%, and 40% strain) of compressive stimulation play no role in the proliferation of articular chondrocytes within the experimental conditions investigated. The articular chondrocytes, accounting for less than 5% of tissue volume, are the only cell species existing in articular cartilage. It has been reported that articular chondrocytes could not significantly proliferate when they are cultured in 3D culture environment, whereas their proliferative activity might increase while cultured in 2D monolayer format [34]. The phenomenon of no positive effect on articular chondrocyte proliferation found in this study is also discovered in several primary articular chondrocyte 3D cultures no matter if they are treated with mechanical stimulation [8, 9] or not [16].

In addition, the metabolic activities of articular chondrocytes treated with various ranges of compressive loading were evaluated by measuring the lactic acid production. Regarding articular chondrocytes metabolism, anaerobic glycolysis is the major metabolic pathway [35], from which the lactic acid is the main metabolic product. Therefore, the production of lactic acid was utilized to indicate the chondrocytes metabolic activity in this study. Within the experimental conditions explored, results (Figure 4(b)) revealed that the stimulating

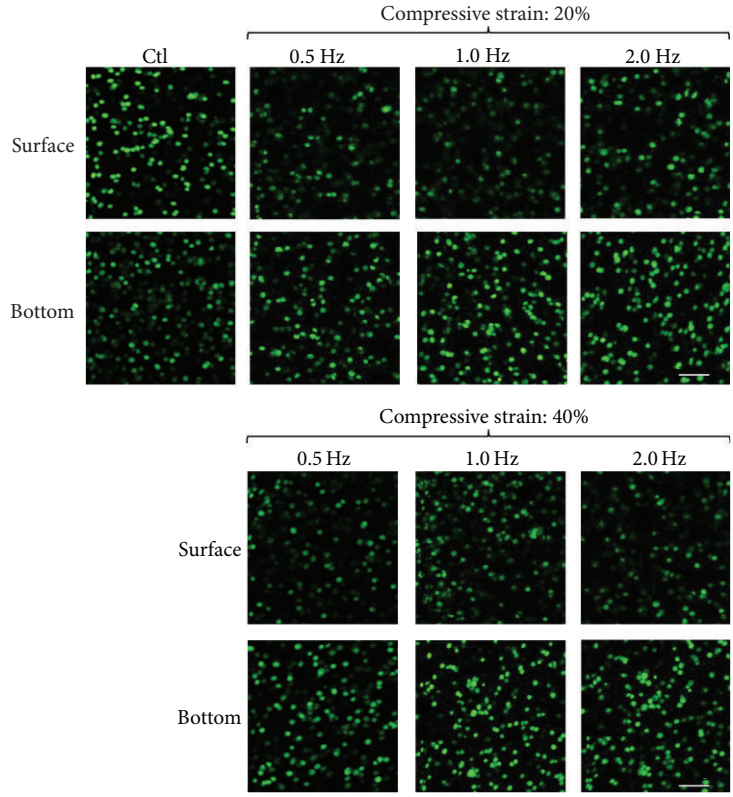

FIGURE 3: Microscopic observation of cell viability after 5 days of cell culture under different compressive stimulation conditions (strain magnitudes: 20% and 40%; stimulating frequencies: 0.5, 1.0, and 2.0 Hz) using the live/dead fluorescent dye. Green and red dots represent live and dead cells, respectively. The upper and lower images show the cells at the surface and the bottom of the 3D cell culture constructs, respectively.

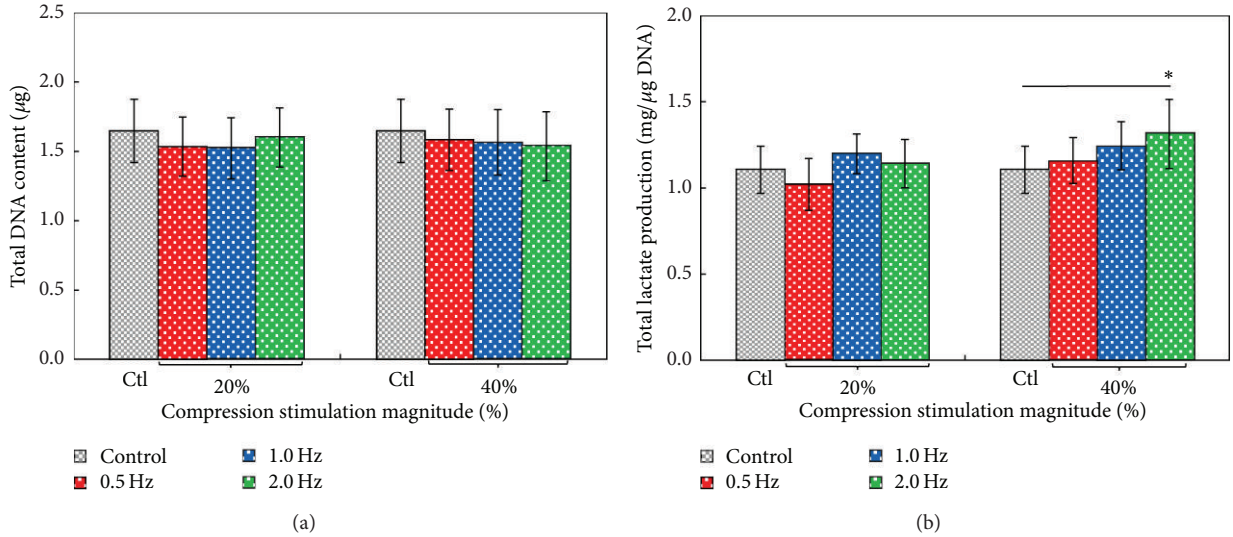

FIGURE 4: The evaluation of the (a) proliferative (DNA content measurement) and (b) metabolic (lactate production measurement) activities of the primary articular chondrocytes under different dynamic compressive loading conditions (as indicated) after 5 days of culture. The results are displayed as mean ± standard deviation of 3 separate experiments ($n = 9$). Significant differences are expressed as $^{*}(P < 0.05)$.

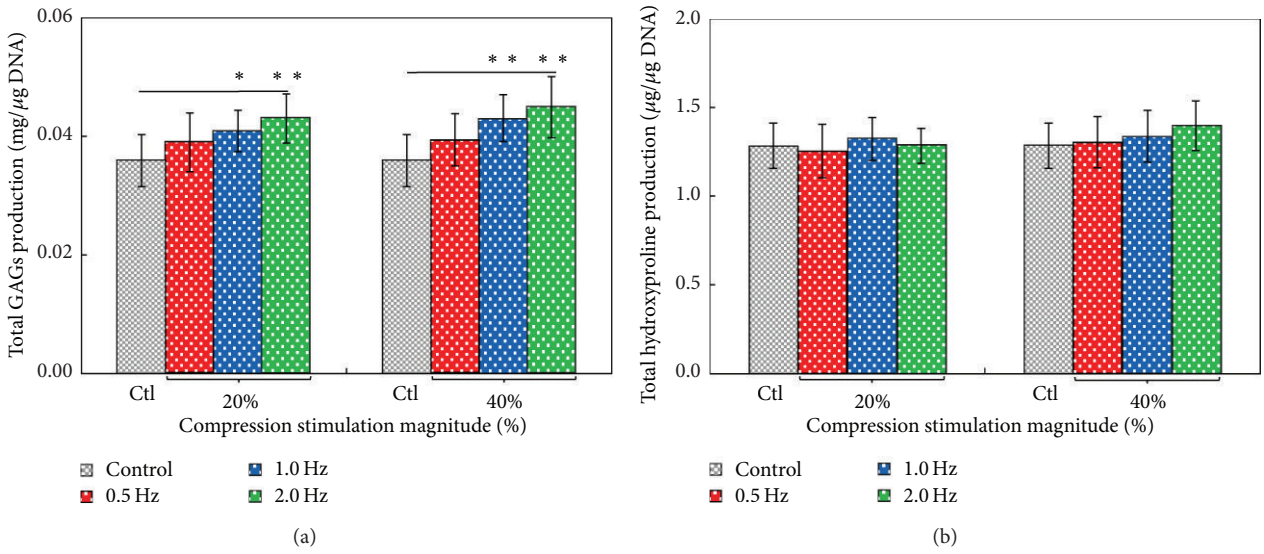

FIGURE 5: The evaluation of the biosynthetic activities ((a) GAGs and (b) hydroxyproline production) of the primary articular chondrocytes under different compressive loading conditions (as indicated) after 5 days of culture. The results are displayed as mean ± standard deviation of 3 separate experiments ($n = 9$). Significant differences are expressed as $^{*}(P < 0.05)$ and $^{**}(P < 0.01)$.

frequency of compressive loading did not significantly affect the metabolic activities of chondrocytes under the strain magnitude of 20%. At the higher strain magnitude of 40%, however, the frequency of compressive stimulation did have significant impact on the metabolic activities of articular chondrocytes ($P < 0.05$, ANOVA). The total lactic acid production of chondrocytes cultured under the stimulating frequency of 2 Hz (40% strain) was 18.77% statistically higher than that of the control case ($P < 0.05$). Nevertheless, the lactic acid production was not statistically different among the cells experiencing stimulating frequency lower than 2 Hz. The dynamic compression at the 40% strain and 2 Hz is close to the compressive condition that human articular cartilage experiences during high intense exercise [33, 36]. The finding disclosed in this study could indicate that the high frequency vigorous exercise might upregulate the metabolism of articular chondrocytes in comparison with the case without compressive stimulation.

3.3. Effect of Dynamic Compressive Loading on the Biosynthetic Activities of Articular Chondrocytes. Under compressive stimulation, several *in vitro* investigations revealed that the articular chondrocytes could rearrange their synthesis of ECM components [1, 5–11]. However, few of them have reported the role of stimulating frequency on the biosynthetic activities of articular chondrocytes [5, 6, 9]. In this study, results (Figure 5(a)) exhibited that the stimulating frequency could significantly influence the GAGs synthesis of articular chondrocytes ($P < 0.05$, ANOVA) both at the two strain magnitudes (20% and 40%) explored. In the ECM of articular cartilage, the GAGs are mainly responsible for the compressive stiffness of such tissue [10, 37]. It is reported that articular chondrocytes may synthesize more GAGs in responding to dynamic compressive loading [38]. For the two compressive strain groups tested, the total GAGs synthesis of articular chondrocytes cultured under the stimulating frequencies of 1 Hz, and 2 Hz were statistically ($P < 0.05$ for 1 Hz (20% strain) and $P < 0.01$ for 2 Hz (20% strain) and 1 and 2 Hz (40% strain)) higher than that of the control case. Nevertheless, such phenomenon was not found among the cells experiencing the stimulating frequency lower than 0.5 Hz. The stimulating frequencies of 1 Hz and 2 Hz are about the frequency range of compressive loading that the human articular cartilages are subjected to during walking [39] and running [36] conditions, respectively. Therefore, the findings revealed in Figure 5(a) might imply that the GAGs biosynthesis of articular chondrocytes might be upregulated under these physiological conditions. In terms of collagen biosynthesis of chondrocytes, results (Figure 5(b)) demonstrated that the formats of compressive loading including stimulating magnitude and frequency did not significantly ($P > 0.05$, ANOVA) influence the total hydroxyproline production within the experimental conditions investigated.

As a whole, the above findings demonstrated that the GAGs synthesis was mechanically upregulated while the collagen production was not affected when 3D cultured chondrocytes were subjected to dynamic compressive stimulation. Reports in literature have also revealed similar research outcomes. For example, some studies have disclosed that dynamic compressive or tensile loading might increase the GAGs biosynthesis of articular chondrocytes but these mechanical stimulations were found to have no positive effect on the synthesis of collagen [5, 8, 11, 21, 38]. Nevertheless, other studies have exhibited different results [1, 6, 31, 37]. For example, some studies have reported that dynamic compression has advantageous effect both on the production of GAGs and collagen [1, 6, 31]. Moreover, Hunter et al. [37] disclosed the adverse effect of dynamic compressive stimulation on GAGs and collagen production

of articular chondrocytes. The reasons behind the above discrepancies are complicated. It is well accepted that the regimen of compressive stimulation [31], as well as the scaffolding material [9, 37], can influence the ECM synthesis of articular chondrocytes. In this study, the daily regimen of dynamic compressive stimulation was based on 3 consecutive cycles of 1 hour loading and 1 hour relaxation, which was reported to be more physiologically relevant [1, 30, 31]. In the investigations, moreover, the primary articular chondrocytes were microencapsulated in an alginate construct. In addition to its excellent biocompatibility [40–42], alginate hydrogel is a commonly used scaffolding material for cartilage tissue engineering because the phenotypic or functional stability of articular chondrocytes in this material can be maintained [43–45]. Furthermore, mammalian cells are sensitive to extracellular microenvironments [16]. To precisely study the cellular responses to extracellular conditions, a stable and homogenous culture environment is crucial because it can provide a well-defined and quantifiable culture condition. Unlike the most of cell culture models (e.g., the static or larger scale cell culture devices [1, 5–7, 9, 10, 13]) adopted for the similar investigations, one of the technical highlights in this study is the use of a perfusion-based microscale cell culture platform capable of providing dynamic compressive stimulation to cells. It enables scientists to create more stable and well-controlled culture environments due to the continuous nutrient supply and waste removal [14, 17] and the phenomenon of low chemical gradients existing in 3D cell culture construct [14], respectively. As a whole, this study has utilized the microcell culture system to mainly explore the stimulating frequency effect of compressive loading on the articular chondrocytes functions. The use of the microcell culture system for more systematic researches will be required to reconcile the differences with data acquired through conventional methods.

4. Conclusions

In this study, the stimulating frequency (0.5, 1.0, and 2.0 Hz) effect of compressive loading (strain: 20 and 40%) on the cell viability and proliferation as well as the metabolic and biosynthetic activities of articular chondrocytes were investigated. It was found that the dynamic compressive loadings explored in this study did not have significant impact on the articular chondrocyte viability and proliferation, in which the cells kept the cell viability as high as 95%. As to the metabolic activity of articular chondrocytes, the frequency of compressive stimulation did have significant influence when the compressive strain was increased to 40%, in which the lactic acid production of cells treated with the stimulating frequency of 2 Hz (40% strain) was 18.77% statistically higher than that of the case without mechanical stimulation. This compressive loading is close to the condition that human articular cartilage experiences during high intense exercise. For the biosynthetic activities of articular chondrocytes, results showed that the GAGs synthesis was mechanically upregulated when the stimulating frequency of compressive loading was set at 1 Hz and 2 Hz. These are about the frequency range of compressive loading that the human articular cartilages subjected to during walking and running conditions, respectively. Nevertheless, the formats of compressive loading including stimulating magnitude and frequency did not have significant impact on the collagen production of articular chondrocytes within the experimental conditions explored. As a whole, the research findings above are found fundamentally important both for articular cartilage tissue engineering and articular cartilage rehabilitation.

Conflict of Interests

The authors declare that there is no conflict of interests regarding the publication of this paper.

Authors' Contribution

Wan-Ying Lin, Yu-Han Chang, Hsin-Yao Wang, Tzu-Chi Yang and Tzu-Keng Chiu contributed equally to this work.

Acknowledgment

The authors would like to thank the Chang Gung Memorial Hospital (CMRPD1C0121) for financial support.

References

[1] R. L. Mauck, M. A. Soltz, C. C. B. Wang et al., "Functional tissue engineering of articular cartilage through dynamic loading of chondrocyte-seeded agarose gels," *Journal of Biomechanical Engineering*, vol. 122, no. 3, pp. 252–260, 2000.

[2] L. A. McMahon, P. J. O'Brien, and P. J. Prendergast, "Biomechanics and mechanobiology in osteochondral tissues," *Regenerative Medicine*, vol. 3, no. 5, pp. 743–759, 2008.

[3] M. Brittberg, E. Sjögren-Jansson, M. Thornemo et al., "Clonal growth of human articular cartilage and the functional role of the periosteum in chondrogenesis," *Osteoarthritis and Cartilage*, vol. 13, no. 2, pp. 146–153, 2005.

[4] T. M. Griffin and F. Guilak, "The role of mechanical loading in the onset and progression of osteoarthritis," *Exercise and Sport Sciences Reviews*, vol. 33, no. 4, pp. 195–200, 2005.

[5] D. A. Lee and D. L. Bader, "Compressive strains at physiological frequencies influence the metabolism of chondrocytes seeded in agarose," *Journal of Orthopaedic Research*, vol. 15, no. 2, pp. 181–188, 1997.

[6] T. Davisson, S. Kunig, A. Chen, R. Sah, and A. Ratcliffe, "Static and dynamic compression modulate matrix metabolism in tissue engineered cartilage," *Journal of Orthopaedic Research*, vol. 20, no. 4, pp. 842–848, 2002.

[7] C. R. Lee, A. J. Grodzinsky, and M. Spector, "Biosynthetic response of passaged chondrocytes in a type II collagen scaffold to mechanical compression," *Journal of Biomedical Materials Research A*, vol. 64, no. 3, pp. 560–569, 2003.

[8] O. Schmidt, J. Mizrahi, J. Elisseeff, and D. Seliktar, "Immobilized fibrinogen in PEG hydrogels does not improve chondrocyte-mediated matrix deposition in response to mechanical stimulation," *Biotechnology and Bioengineering*, vol. 95, no. 6, pp. 1061–1069, 2006.

[9] I. Villanueva, D. S. Hauschulz, D. Mejic, and S. J. Bryant, "Static and dynamic compressive strains influence nitric oxide production and chondrocyte bioactivity when encapsulated in PEG hydrogels of different crosslinking densities," *Osteoarthritis and Cartilage*, vol. 16, no. 8, pp. 909–918, 2008.

[10] O. Preiss-Bloom, J. Mizrahi, J. Elisseeff, and D. Seliktar, "Real-time monitoring of force response measured in mechanically stimulated tissue-engineered cartilage," *Artificial Organs*, vol. 33, no. 4, pp. 318–327, 2009.

[11] M. H. Wu, H. Y. Wang, C. L. Tai et al., "Development of perfusion-based microbioreactor platform capable of providing tunable dynamic compressive loading to 3-D cell culture construct-Demonstration study of the effect of compressive stimulation on articular chondrocyte functions," *Sensors and Actuators B: Chemical*, vol. 176, pp. 86–96, 2013.

[12] A. Hasan, K. Ragaert, W. Swieszkowski et al., "Biomechanical properties of native and tissue engineered heart valve constructs," *Journal of Biomechanics*, 2013.

[13] M. M. G. Grafton, L. Wang, P.-A. Vidi, J. Leary, and S. A. Lelièvre, "Breast on-a-chip: mimicry of the channeling system of the breast for development of theranostics," *Integrative Biology*, vol. 3, no. 4, pp. 451–459, 2011.

[14] M.-H. Wu, J. P. G. Urban, Z. Cui, and Z. F. Cui, "Development of PDMS microbioreactor with well-defined and homogenous culture environment for chondrocyte 3-D culture," *Biomedical Microdevices*, vol. 8, no. 4, pp. 331–340, 2006.

[15] M.-H. Wu, J. P. G. Urban, F. C. Zhan, Z. Cui, and X. Xu, "Effect of extracellular pH on matrix synthesis by chondrocytes in 3D agarose gel," *Biotechnology Progress*, vol. 23, no. 2, pp. 430–434, 2007.

[16] A. Hasan, A. Memic, N. Annabi et al., "Electrospun scaffolds for tissue engineering of vascular grafts," *Acta Biomaterialia*, vol. 10, no. 1, pp. 11–25, 2014.

[17] P. M. Van Midwoud, E. Verpoorte, and G. M. M. Groothuis, "Microfluidic devices for in vitro studies on liver drug metabolism and toxicity," *Integrative Biology*, vol. 3, no. 5, pp. 509–521, 2011.

[18] J.-L. Lin, M.-H. Wu, C.-Y. Kuo, K.-D. Lee, and Y.-L. Shen, "Application of indium tin oxide (ITO)-based microheater chip with uniform thermal distribution for perfusion cell culture outside a cell incubator," *Biomedical Microdevices*, vol. 12, no. 3, pp. 389–398, 2010.

[19] M.-H. Wu, S.-B. Huang, Z. Cui, Z. Cui, and G.-B. Lee, "A high throughput perfusion-based microbioreactor platform integrated with pneumatic micropumps for three-dimensional cell culture," *Biomedical Microdevices*, vol. 10, no. 2, pp. 309–319, 2008.

[20] C. D. Hoemann, J. Sun, V. Chrzanowski, and M. D. Buschmann, "A multivalent assay to detect glycosaminoglycan, protein, collagen, RNA, and DNA content in milligram samples of cartilage or hydrogel-based repair cartilage," *Analytical Biochemistry*, vol. 300, no. 1, pp. 1–10, 2002.

[21] M.-H. Wu, H.-Y. Wang, H.-L. Liu et al., "Development of high-throughput perfusion-based microbioreactor platform capable of providing tunable dynamic tensile loading to cells and its application for the study of bovine articular chondrocytes," *Biomedical Microdevices*, vol. 13, no. 4, pp. 789–798, 2011.

[22] R. W. Farndale, D. J. Buttle, and A. J. Barrett, "Improved quantitation and discrimination of sulphate glycosaminoglycans by use of dimethylmethylene blue," *Biochimica et Biophysica Acta*, vol. 883, no. 2, pp. 173–177, 1986.

[23] H. Stegemann and K. Stalder, "Determination of hydroxyproline," *Clinica Chimica Acta*, vol. 18, no. 2, pp. 267–273, 1967.

[24] J. P. G. Urban and J. F. McMullin, "Swelling pressure of the intervertebral disc: influence of proteoglycan and collagen contents," *Biorheology*, vol. 22, no. 2, pp. 145–157, 1985.

[25] M.-H. Wu, S.-B. Huang, Z. Cui, Z. Cui, and G.-B. Lee, "Development of perfusion-based micro 3-D cell culture platform and its application for high throughput drug testing," *Sensors and Actuators B: Chemical*, vol. 129, no. 1, pp. 231–240, 2008.

[26] W.-B. Lee, Y.-H. Chen, H.-I. Lin, S.-C. Shiesh, and G.-B. Lee, "An integrated microfluidic system for fast, automatic detection of C-reactive protein," *Sensors and Actuators B: Chemical*, vol. 157, no. 2, pp. 710–721, 2011.

[27] R. Schellin, G. Hess, W. Kühnel et al., "Measurements of the mechanical behaviour of micromachined silicon and silicon-nitride membranes for microphones, pressure sensors and gas flow meters," *Sensors and Actuators A: Physical*, vol. 41, no. 1–3, pp. 287–292, 1994.

[28] S.-B. Huang, M.-H. Wu, Z. Cui, Z. Cui, and G.-B. Lee, "A membrane-based serpentine-shape pneumatic micropump with pumping performance modulated by fluidic resistance," *Journal of Micromechanics and Microengineering*, vol. 18, no. 4, Article ID 045008, 2008.

[29] S. B. Huang, S. S. Wang, C. H. Hsieh, Y. C. Lin, C. S. Lai, and M. H. Wu, "An integrated microfluidic cell culture system for high-throughput perfusion three-dimensional cell culture-based assays: effect of cell culture model on the results of chemosensitivity assays," *Lab on a Chip*, vol. 13, no. 6, pp. 1133–1143, 2013.

[30] C. T. Hung, R. L. Mauck, C. C.-B. Wang, E. G. Lima, and G. A. Ateshian, "A paradigm for functional tissue engineering of articular cartilage via applied physiologic deformational loading," *Annals of Biomedical Engineering*, vol. 32, no. 1, pp. 35–49, 2004.

[31] K. W. Ng, R. L. Mauck, C. C.-B. Wang et al., "Duty cycle of deformational loading influences the growth of engineered articular cartilage," *Cellular and Molecular Bioengineering*, vol. 2, no. 3, pp. 386–394, 2009.

[32] C. Herberhold, S. Faber, T. Stammberger et al., "In situ measurement of articular cartilage deformation in intact femoropatellar joints under static loading," *Journal of Biomechanics*, vol. 32, no. 12, pp. 1287–1295, 1999.

[33] J. T. Bingham, R. Papannagari, S. K. Van de velde et al., "In vivo cartilage contact deformation in the healthy human tibiofemoral joint," *Rheumatology*, vol. 47, no. 11, pp. 1622–1627, 2008.

[34] J. Diaz-Romero, J. P. Gaillard, S. P. Grogan, D. Nesic, T. Trub, and P. Mainil-Varlet, "Immunophenotypic analysis of human articular chondrocytes: changes in surface markers associated with cell expansion in monolayer culture," *Journal of Cellular Physiology*, vol. 202, no. 3, pp. 731–742, 2005.

[35] R. B. Lee and J. P. G. Urban, "Evidence for a negative Pasteur effect in articular cartilage," *Biochemical Journal*, vol. 321, no. 1, pp. 95–102, 1997.

[36] P. G. Weyand, D. B. Sternlight, M. J. Bellizzi, and S. Wright, "Faster top running speeds are achieved with greater ground forces not more rapid leg movements," *Journal of Applied Physiology*, vol. 89, no. 5, pp. 1991–1999, 2000.

[37] C. J. Hunter, J. K. Mouw, and M. E. Levenston, "Dynamic compression of chondrocyte-seeded fibrin gels: effects on matrix accumulation and mechanical stiffness," *Osteoarthritis and Cartilage*, vol. 12, no. 2, pp. 117–130, 2004.

[38] J. D. Kisiday, M. Jin, M. A. DiMicco, B. Kurz, and A. J. Grodzinsky, "Effects of dynamic compressive loading on chondrocyte biosynthesis in self-assembling peptide scaffolds," *Journal of Biomechanics*, vol. 37, no. 5, pp. 595–604, 2004.

[39] O. Gabay, D. J. Hall, F. Berenbaum, Y. Henrotin, and C. Sanchez, "Osteoarthritis and obesity: experimental models," *Joint Bone Spine*, vol. 75, no. 6, pp. 675–679, 2008.

[40] G. Klöck, A. Pfeffermann, C. Ryser et al., "Biocompatibility of mannuronic acid-rich alginates," *Biomaterials*, vol. 18, no. 10, pp. 707–713, 1997.

[41] C. L. Salgado, M. B. Oliveira, and J. F. Mano, "Combinatorial cell-3D biomaterials cytocompatibility screening for tissue engineering using bioinspired superhydrophobic substrates," *Integrative Biology*, vol. 4, no. 3, pp. 318–327, 2012.

[42] P. Dandoy, C. F. Meunier, C. Michiels, and B.-L. Su, "Hybrid shell engineering of animal cells for immune protections and regulation of drug delivery: towards the design of "Artificial Organs"," *PLoS ONE*, vol. 6, no. 6, Article ID e20983, 2011.

[43] H. J. Häuselmann, R. J. Fernandas, S. S. Mok et al., "Phenotypic stability of bovine articular chondrocytes after long-term culture in alginate beads," *Journal of Cell Science*, vol. 107, no. 1, pp. 17–27, 1994.

[44] M. F. Amilton, R. H. Sarah, A. K. Tommy, M. K. Axel, F. Yngvar, and E. B. Jan, "Similar properties of chondrocytes from osteoarthritis joints and mesenchymal stem cells from healthy donors for tissue engineering of articular cartilage," *PLoS ONE*, vol. 8, no. 5, Article ID e62994, 2013.

[45] M. F. Rai, T. Graeve, S. Twardziok, and M. F. G. Schmidt, "Evidence for regulated interleukin-4 expression in chondrocyte-scaffolds under *in vitro* inflammatory conditions," *PLoS ONE*, vol. 6, no. 10, Article ID e25749, 2011.

Hindawi Publishing Corporation
BioMed Research International
Volume 2014, Article ID 209469, 13 pages
http://dx.doi.org/10.1155/2014/209469

Research Article

Characterization of Silk Fibroin Modified Surface: A Proteomic View of Cellular Response Proteins Induced by Biomaterials

Ming-Hui Yang,[1,2,3] Shyng-Shiou Yuan,[2,3,4,5] Tze-Wen Chung,[6] Shiang-Bin Jong,[7,8] Chi-Yu Lu,[9,10] Wan-Chi Tsai,[11,12] Wen-Cheng Chen,[13] Po-Chiao Lin,[10,14] Pei-Wen Chiang,[7] and Yu-Chang Tyan[3,7,10,15]

[1] *Instrument Technology Research Center, National Applied Research Laboratories, Hsinchu 300, Taiwan*
[2] *Department of Medical Research, Kaohsiung Medical University Chung-Ho Memorial Hospital, Kaohsiung 807, Taiwan*
[3] *Translational Research Center, Kaohsiung Medical University Chung-Ho Memorial Hospital, Kaohsiung 807, Taiwan*
[4] *Department of Obstetrics and Gynecology, Kaohsiung Medical University Chung-Ho Memorial Hospital, Kaohsiung 807, Taiwan*
[5] *School of Medicine, College of Medicine, Kaohsiung Medical University, Kaohsiung 807, Taiwan*
[6] *Department of Biomedical Engineering, National Yang-Ming University, Taipei 112, Taiwan*
[7] *Department of Medical Imaging and Radiological Sciences, Kaohsiung Medical University, Kaohsiung 807, Taiwan*
[8] *Department of Nuclear Medicine, Kaohsiung Medical University Chung-Ho Memorial Hospital, Kaohsiung 807, Taiwan*
[9] *Department of Biochemistry, College of Medicine, Kaohsiung Medical University, Kaohsiung 807, Taiwan*
[10] *National Sun Yat-Sen University-Kaohsiung Medical University Joint Research Center, Kaohsiung 804, Taiwan*
[11] *Department of Medical Laboratory Science and Biotechnology, Kaohsiung Medical University, Kaohsiung 807, Taiwan*
[12] *Department of Laboratory Medicine, Kaohsiung Medical University Hospital, Kaohsiung 807, Taiwan*
[13] *Department of Fiber and Composite Materials, College of Engineering, Feng Chia University, Taichung 407, Taiwan*
[14] *Department of Chemistry, National Sun Yat-Sen University, Kaohsiung 804, Taiwan*
[15] *Center of Biomedical Engineering and System Biology, Kaohsiung Medical University, Kaohsiung 807, Taiwan*

Correspondence should be addressed to Yu-Chang Tyan; yctyan@kmu.edu.tw

Received 29 October 2013; Revised 18 January 2014; Accepted 20 January 2014; Published 25 March 2014

Academic Editor: Nihal Engin Vrana

The purpose of this study was to develop the pathway of silk fibroin (SF) biopolymer surface induced cell membrane protein activation. Fibroblasts were used as an experimental model to evaluate the responses of cellular proteins induced by biopolymer material using a mass spectrometry-based profiling system. The surface was covered by multiwalled carbon nanotubes (CNTs) and SF to increase the surface area, enhance the adhesion of biopolymer, and promote the rate of cell proliferation. The amount of adhered fibroblasts on CNTs/SF electrodes of quartz crystal microbalance (QCM) greatly exceeded those on other surfaces. Moreover, analyzing differential protein expressions of adhered fibroblasts on the biopolymer surface by proteomic approaches indicated that CD44 may be a key protein. Through this study, utilization of mass spectrometry-based proteomics in evaluation of cell adhesion on biopolymer was proposed.

1. Introduction

Biomaterials play important roles in regenerative medicine, tissue engineering, and drug delivery [1]. The construction of engineered scaffolds or matrices with chemical and physical surface properties that enable them to interact favorably with cells is important [2]. Cell proliferation, differentiation, and regeneration of tissues all depend upon the interactions between biomaterial surfaces and cells. For the responses of cells to biomaterials, both a cell-count method of counting nuclei stains and the MTT (3-(4,5-cimethylthiazol-2-yl)-2,5-diphenyl tetrazolium bromide) or BrdU (5-bromo-2′-deoxyuridine) assays are less accurate than usual studies, because small parts of cells adhere onto the biomaterial surfaces. Recently, using molecular expression-based methods such as flow cytometric analysis, immunofluorescent labeling

and immunoblotting of cells were developed for determining the responses at cellular levels in cell adhesion onto biomaterials [3]. In addition, the identification of proteins that are involved must be known to enable the assays to be properly carried out. The advantage of using the proteomic approach is that new proteins that influence the interactions of cells and biomaterials may be found.

Multiwalled carbon nanotubes (CNTs) have a large surface area and have been extensively studied for a variety of purposes, such as sensors, fuel cells, and device patterning [4, 5]. CNTs have good biocompatibility with cells and support cellular behavior proliferation as well as differentiation of cells in the presence of induction medium. Additionally CNTs substrates show good cell viability, spreading, and physical adhesion. Silk fibroin (SF) is a protein with bulky hydrophobic domains [6] and can be easily purified as sericin-free silk-based biomaterials. Such material is highly applicable due to its low immune response characteristics. SF-based biomaterials have been investigated in the form of files, fibers, hydrogels, particles, and scaffolds [7–10] and in applications of vascular, neural, skin, bone, and cartilage tissue regeneration [11–14]. Increasingly, SF is exploited in other areas of biomedical science, as a result of new knowledge of its processing and properties like mechanical strength, elasticity, biocompatibility, and controllable biodegradability [15]. These properties of SF are particularly useful for tissue engineering.

"Proteome" and "proteomics" are relatively new words, coined by Wilkins et al. in 1996 [16]. The proteome is the entire set of proteins expressed by the genome. Proteomic analysis means a comprehensive analysis of proteins, and proteomics is the science by which proteins are comprehensively investigated with regard to their roles as functional elements. Recently, characterization of these cellular proteins by proteomic approaches has revealed that the surface charge of biomaterials defines the protein reactivity and the protein-biomaterial interaction. In the previous studies, several reports utilized proteomic approaches to explain the biomaterials-cells interaction. Titanium (Ti) is used commonly in implants and biomaterials. The surface modification was grafted by poly(sodium styrene sulfonate) (poly NaSS). The mechanisms of titanium alloy inducing platelet activation, that causes cell adsorption and proliferation, were identified by using two-dimensional gel electrophoresis (2-DE) combined with mass spectrometry, which may be related to protein adsorption on biomaterial surfaces [17]. Nanomaterials may release trace substances, which may be toxic to the surrounding cells. Human lung epithelial cells and human monocyte-derived macrophages were used to examine the cellular uptake of several forms of titanium dioxide nanoparticles and carbon nanotubes by using proteomic approaches [18]. The direct analysis of extracellular matrix (ECM) proteins from vascular aortic smooth muscle cells using a Protein Chip Bioprocessor and combined with surface enhanced laser desorption ionization time-of-flight mass spectrometry (SELDI-TOF MS) was developed by Lavigne and coworkers [19]. Their method involved a protein chip to analyze ECM proteins without transferring.

To evaluate the responses of fibroblasts to a CNTs/SF polymer surface, a quartz crystal microbalance (QCM) technique was used to quantify the mass of adhesion cells and immunochemical stains to observe the morphological changes of the cells. To apply proteomic approaches to develop a new tool for characterization of the responses of cells to biomaterials, a mass spectrometry-based profiling system was adopted. This system was able to assess characteristic proteins that were expressed due to the interactions of fibroblasts with biopolymer surfaces. Through the investigation, proteins that influence the responses and later proliferations of fibroblasts on biopolymer surfaces were identified, and CD44 was found to be involved in cell adhesion when SF interactions regulate signaling pathways.

2. Materials and Methods

2.1. Fabricating CNTs and Dispersing CNTs on the Electrode of QCM. The multiwalled carbon nanotubes (CNTs, 6–13 nm outer diameter, 2.5–20 μm long) were treated by refluxing in concentrated nitric acid at 85°C for 3 h. When the CNTs were precipitated from the solution, the nitric acid was carefully removed. The mixture was then filtered through a 0.22 μm filter under a vacuum condition. The CNTs were rinsed with D.I. water, collected, and dried in an oven at 50°C. The surface of a 9 MHz QCM gold electrode (ANT Tech, Taiwan) was washed with 1 M HCl, rinsed with D.I. water, and dried at room temperature. The frequency of the electrode measured by the QCM (ADS, ANT Tech, Taiwan) was assigned as F_0 at the flow rate of 60 μL/min of phosphate buffered saline (PBS). To prepare an electrode with CNTs decoration, a solution of pluronic F68 was applied to disperse CNTs on the electrode surface. Briefly, a 1% F68 solution was dropped onto the QCM gold electrode and then dried under oscillation. The CNTs in solution were then deposited onto the surface of the electrode and dried for further applications.

2.2. Atomic Force Microscopy Image of QCM Chip Surface. The QCM chip surfaces were analyzed by atomic force microscopy (AFM). The AFM images were acquired with a Slover PRO (NT-MDT, Russia) atomic force microscopy under ambient pressure. The semicontact mode was used with a frequency of 0.5 μm/s to scan an area of 50×50 μm^2. The AFM probe was a golden silicon probe (NSG11, NT-MDT, Russia) with the length, width, thickness, resonant frequency, and force constant as 100 mm, 35 μm, 2.0 μm, 255 kHz, and 11.5 N/m^2, respectively.

2.3. Adsorption of SF onto CNTs Polymer Surfaces Determined by QCM Measurements and Characterized by FT-IR. Silk cocoons were purchased from a silk center in Taiwan (ShihTan, Miao-Li, Taiwan). Briefly, silk cocoons were boiled in Na_2CO_3 and extracted SFs were then dissolved in 9.3 M LiBr solution. The final concentration of the SF aqueous solution was 8% (w/v). This concentration was determined by weighing the residual solid in a known solution volume after drying at 60°C. For fabricating a CNTs/SF electrode, 1% of the SF solution was injected into the flow loop with

a CNTs dispersing electrode at the flow rate of 60 μL/min. Moreover, double injections of SF solution were performed to assure that the adsorption of SF on the electrode was saturated. The frequency shifts (ΔF) were determined by the QCM and the masses of SF adsorption were recorded and calculated. To determine that the CNTs/SF layers were stably coated onto the electrode, the frequency of the electrode was measured during the flow of PBS for several minutes. The surface characterizations of the electrode decorated with CNTs, CNTs/SF were also observed using a Fourier transform infrared spectrometer (FT-IR, Spectrum One system, PerkinElmer, USA).

2.4. Culturing Fibroblasts on the CNTs and CNTs/SF Electrode Surfaces. The fibroblasts were maintained at 37°C and 5% CO_2 in Dulbecco's Modified Eagle Medium (DMEM) supplemented with 10% fetal bovine serum (FBS, Hyclone Laboratories, Logan, UT), 1% penicillin/streptomycin (Gibco, Grand Island, NY, USA), and 44 mM $NaHCO_3$.

Before seeding fibroblasts, the electrodes were sterilized with 70% (v/v) ethanol and then exposed under ultraviolet light for 30 min. Serum-free medium containing 4×10^4 fibroblasts was added to each well in the presence of the aforementioned electrodes, and cells were incubated at 37°C with 5% CO_2 for 12 h for investigating the adhesion of the cells on those electrodes [20]. After incubation, the electrodes were rinsed with PBS, and then frequency shifts were measured by the QCM.

2.5. BrdU Assay. The viability of the adhered cells was determined by BrdU assay (BrdU Cell Proliferation Assay, Millipore, USA). The assay was performed according to the manufacturer's instructions. Briefly, fibroblasts were seeded into a sterile 96-well tissue culture plate with a density of 2×10^5 cells/mL in 100 μL/well of appropriate cell culture media and incubated for 72 and 120 h. Then, cells were incubated in the medium containing BrdU reagent for 2 h. Fixing solution was added before the absorbencies were measured at 520 nm using an ELISA reader (Multiskan EX, Thermo Scientific, Vantaa, Finland, reference wavelength: 450 nm).

2.6. Proteomic Analysis of Fibroblasts on Various Surfaces. After incubation on different material surfaces, the fibroblasts were lysed by cell lysis buffer (3500-1, Epitomics, Inc., USA), and cell lysates were centrifuged at 1500 ×g for 10 min at 4°C. The supernatants were filtered by 0.8 μm filters. The protein concentrations of the cell lysate samples were measured using a fluorescence-based protein quantification detection kit (Quant-iT Fluorometer, Qubit Protein Assay Kit, Q33212, Invitrogen), and the protein concentrations were adjusted to 1 mg/mL by 25 mM ammonium bicarbonate.

Cell lysate samples (100 μL) were transferred into 1.5 mL Eppendorf tubes and incubated at 37°C for 3 h after mixing with 25 μL of 1 M dithiothreitol (DTT, USB Corporation, 15397). Then the cell lysate samples were reduced and alkylated in the dark at room temperature for 30 min after the addition of 25 μL of 1 M iodoacetamide (IAA, Amersham Biosciences, RPN6302V) in 25 mM ammonium bicarbonate. Approximately 10 μL of 0.1 μg/μL modified trypsin digestion buffer (Trypsin Gold, Mass Spectrometry Grade, V5280, Promega, WI, USA) in 25 mM ammonium bicarbonate was added to the cell lysate samples, which were then incubated at 37°C for at least 12 h in a water bath. Two microliters of formic acid was added to each sample before mass spectrometric analysis for protein identification.

The complex peptide mixtures were separated by RP-nano-UPLC-ESI-MS/MS. The protein tryptic digests were fractionated using a flow rate of 400 nL/min with a nano-UPLC system (nanoACQUITY UPLC, Waters, Milford, MA) coupled to an ion trap mass spectrometer (LTQ Orbitrap Discovery Hybrid FTMS, Thermo, San Jose, CA) equipped with an electrospray ionization source. For RP-nano-UPLC-ESI-MS/MS analyses, a sample (2 μL) of the desired peptide digest was loaded into the reverse phase column (Symmetry C18, 5 μm, 180 μm × 20 mm) by an autosampler. The RP separation was performed using a linear acetonitrile gradient from 99% buffer A (100% D.I. water/0.1% formic acid) to 85% buffer B (100% acetonitrile/0.1% formic acid) in 100 min using the micropump at a flow rate of approximately 400 nL/min. The separation was performed on a C18 microcapillary column (BEH C18, 1.7 μm, 75 μm × 100 mm) using the nanoseparation system. As peptides were eluted from the microcapillary column, they were electrosprayed into the ESI-MS/MS with the application of a distal 2.1 kV spraying voltage with heated capillary temperature of 200°C. Each cycle of one full-scan mass spectrum (m/z 400–2000) was followed by three data dependent tandem mass spectra with collision energy set at 35%.

2.7. Database Search. For protein identification, Mascot software (Version 2.2.1, Matrix Science, London, UK) was used to search the Swiss-Prot human protein sequence database. For proteolytic cleavages, only tryptic cleavage was allowed, and the number of maximal internal (missed) cleavage sites was set to 2. Variable modifications of cysteine with carboxyamidomethylation, methionine with oxidation, and asparagine/glutamine with deamidation were allowed. Mass tolerances of the precursor peptide ion and fragment ion were set to 10 ppm and 0.5 Da, respectively. When the Mowse score was greater than 30, the protein identification was defined as positive and considered significant ($P < 0.05$). Proteins were initially annotated by similar search conditions using UniProtKB/Swiss-Prot databases.

2.8. Western Blotting of Protein Expression. Confirmation of protein expression was performed by Western blotting. Each cell lysate sample (1 μg/μL, 10 μL) was electrophoresed through a precast gel (NuPAGE Novex 4–12% Bis-Tris Gel, 1.5 mm, 10 wells, Invitrogen, Carlsbad, CA). Proteins were transferred from the gel to a polyvinyldifluoride (PVDF) membrane (Millipore, Bedford, CA) by means of the semidry technique using the Criterion Blotter (Bio-Rad) at 100 V for 60 min and blocked with 5% milk in PBS (adjusted to pH 7.4) containing 0.05% Tween 20. The membrane was then incubated overnight with primary rabbit antibody (1 μg/mL) of anti-CD44 (1998-1, Epitomics, Inc.).

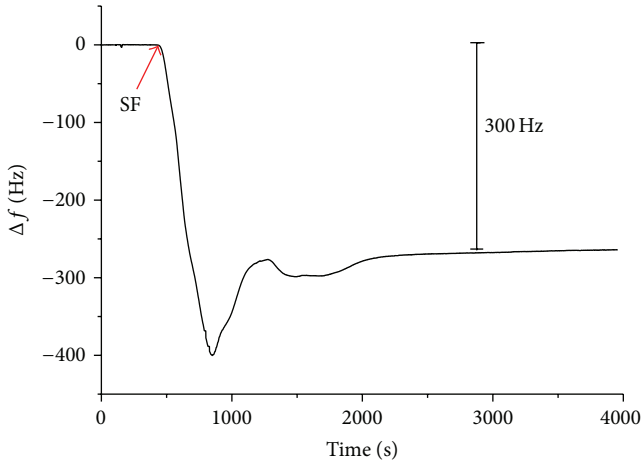

Figure 1: A representative of the frequency shift for preparing the electrodes decorated with CNTs/SF layer. The frequency shift of CNTs/SF exhibited the least frequency response around −335 ± 21 Hz, $n = 7$.

After washing, the membrane was incubated with alkaline peroxidase-conjugated AffiniPure goat anti-rabbit IgG (111-035-003, Immuno Research) for 1 h (1 : 10000). Proteins were detected with an enhanced chemiluminescent (ECL) system, and quantitative analysis of Western blotting was carried out using the ImageQuant-TL-7.0 software, version 2010 (Amersham Biosciences).

2.9. Cell Morphology Observed by Immunochemical Staining. For cell morphology of adhered fibroblasts on the aforementioned electrodes after incubation, the electrodes were washed and fixed with 4% formaldehyde at 4°C. The nuclei and cytoskeleton of the cells were stained with 4′-6-diamidino-2-phenylindole (DAPI, 32670, Sigma-Aldrich, USA) and vimentin (Vimentin DyLight 488 Antibody, Epitomics, USA), respectively. In addition to staining with DAPI and vimentin, the anti-CD44 antibody (1998-1, Epitomics, Inc) was incubated and followed by staining with Alexa Fluor 568 goat anti-rabbit IgG (A-11011, Invitrogen). The samples were blocked with 2% bovine serum albumin (BSA, A1933, Sigma-Aldrich, USA) at room temperature for 30 min. The cell images were observed by a microscope equipped with fluorescence light source (FLoid Cell Fluorescence Imaging Station, Invitrogen), and the cell micrographs were taken with a CCD camera.

2.10. Statistical Analysis. All calculations used the SigmaStat statistical software (Jandel Science Corp., San Rafael, CA). All statistical significances were evaluated at 95% of confidence level or better. Data are presented as mean ± standard error.

3. Results and Discussion

3.1. Characterizations of Electrodes of QCM Decorated with CNTs and CNTs/SF. To prepare CNTs/SF layer, SF was adsorbed onto a CNTs electrode surface using the layer-by-layer technique [21, 22]. For each tested biopolymer, the frequency shifts dropped sharply, as it was absorbed onto the electrode surface (Figure 1). The theory for QCM detections can be described by the Sauerbrey equation, Sauerbrey equation in gas phase. ΔF is the frequency shift (Hz); F is basic oscillation frequency of piezoelectric quartz (Hz); A is the active area of QCM (cm^2); ΔM is the mass change on QCM (g). Consider the following:

$$\Delta F = -2.3 \times 10^{-6} \frac{F^2 \Delta M}{A}, \quad (1)$$

which gives the mass change as proportional to the shift in the oscillation frequency of the piezoelectric quartz crystal [20]. QCMs with electrodes have been widely studied in several fields such as environmental protection, medicine, and biotechnology. Additionally, monitoring biomolecular interactions in immunology and investigating cell-substrate communications have been extensively studied [6, 7]. Recently, modifications of electrodes with various biopolymers of QCM have been used to detect the adhesion of cells [20]. The QCM frequency variation after CNTs-biopolymer formation was lowered to around 2.3 kHz. Table 1 presents the frequency responses and mass to the absorption of CNTs and CNTs/SF by using the Sauerbrey equation [23]. CNTs exhibited the strongest frequency responses upon deposition on the electrode (−2004 ± 33 Hz, 1377 ± 23 ng, $n = 7$) while CNTs/SF exhibited the least frequency response (−335 ± 21 Hz, 231 ± 30 ng, $n = 7$).

Table 1: Frequency shifts and mass for the adsorption of CNTs and CNTs/SF layers measured by the QCM and calculated by the Sauerbrey equation.

Adsorption polymer	ΔF (Hz)	Δm (ng)
CNTs	−2004 ± 33	1377 ± 23
CNTs/SF	−335 ± 21	231 ± 30

Data are expressed as mean ± standard error, $n = 7$.

To investigate the topology characteristics of the surface, AFM was used to observe the QCM chip surface. In Figure 2, the image of the topographical map taken in the semicontact mode of a 50 × 50 μm^2 zone is shown. Figure 2(a) is a surface image of the QCM chip, and Figure 2(b) shows the CNTs surface. This impressive image in Figure 2(b) shows the surface roughness with a mean depth of about 2.3 μm. Certainly, a rough surface may provide the opportunity to increase the reaction surface and the effectiveness of cell adhesion.

Modified surfaces of electrodes of QCM were also routinely characterized using FT-IR spectrum. Figure 3 displays the characteristics of the FT-IR spectra of the aforementioned polymers. In the absorption curve of CNTs, the broad band at 3400 cm^{-1} was attributed to the OH functional group from F68, a dispersing agent for CNTs, owing to its polyethylene oxide- (PEO-) polypropylene oxide structure [4]. The absorption bands at 1640 and 1460 cm^{-1} were assigned to C=O stretching and CH_2 deformation in carboxylic acid, which were attributed to the acid treatment of the CNTs

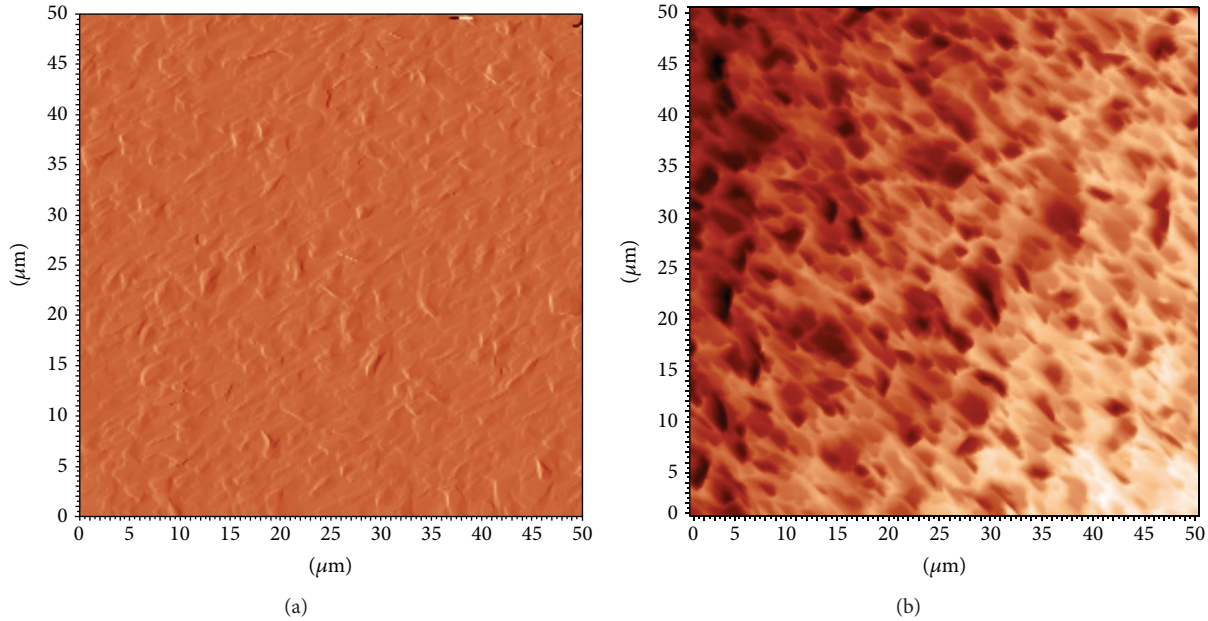

Figure 2: AFM images of the QCM chip. (a) Blank, 50 × 50 μm, (b) CNTs, 50 × 50 μm. AFM measurements could also be used for measuring the surface roughness of the QCM chip. The mean surface roughness was 1.0 and 2.3 nm for blank and CNTs surfaces, respectively.

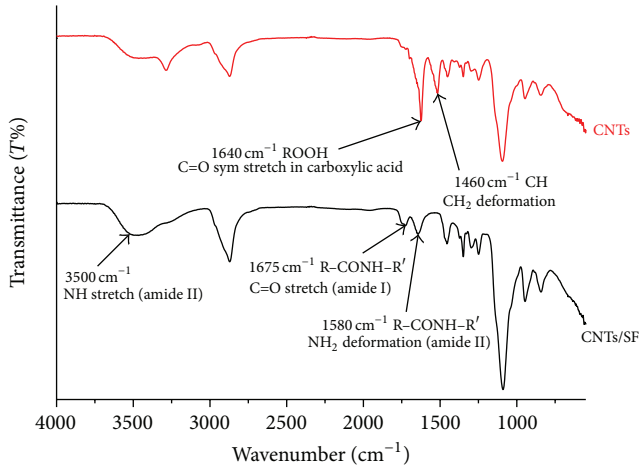

Figure 3: The ATR-FTIR transmission spectra of the CNTs and CNTs/SF layers decorated on electrodes of QCM. The peaks at 1580 cm^{-1} and 1675 cm^{-1} in the spectra were attributed to amide II and amide I, confirming the presence of amide I and II in SF modified surface.

[24]. The absorption band at 3500 cm^{-1} in the second curve corresponds to a NH stretch of SF. The peaks at 1580 cm^{-1} and 1675 cm^{-1} in the spectra of the SF surface were attributed to amide II (R–NHR′, NH_2 deformation, N–H bending, and C–N stretching) and amide I (R–CONHR′, C=O stretching), respectively, confirming the presence of amide I and II in SF [25]. These results indicate the presence of O=C–NH species, which are derived from carboxylic acid and amide structures. Accordingly, the polycomplex between CNTs and SF was formed when amino groups in SF formed complexes with carboxyl groups in CNTs [26]. The spectra indicated that the electrodes were successfully decorated with CNTs and CNTs/SF biopolymers.

3.2. Quantitative Analysis of Fibroblasts Adhesion on Electrodes. To investigate the adhesion of fibroblasts onto electrodes decorated by CNTs and CNTs/SF polymer surfaces, fibroblasts were incubated on the electrodes for 12 h. Since the adsorption of various proteins of bovine serum onto the aforementioned surfaces may influence cell adsorption behaviors, a serum-free medium was used in the cell culture. The cultivation of fibroblasts under serum-free conditions for 12 h herein prevented the apoptosis and proliferation of cells [27]. The results concerning the adhesion of fibroblasts onto the electrode of QCM that was decorated by CNTs or CNTs/SF were obtained from the frequency shifts [20]. The frequency shifts for nonmodified surfaces, CNTs-coated electrodes, and CNTs/SF-coated electrodes were -16.05 ± 0.44, -24.85 ± 0.30, and $-29.43 \pm 0.77 \times 10^3$ Hz; the attached cell masses corresponding to those surfaces were 11.02 ± 0.30, 17.07 ± 0.21, and $21.52 \pm 0.49 \times 10^3$ ng (Table 2, $P < 0.001$, $n = 10$), respectively. The amount of fibroblasts that adhered to the CNTs/SF-coated electrode significantly exceeded that coated with either of the other surfaces. The mass of the fibroblasts that adhered to the CNTs/SF-coated electrode was calculated markedly to exceed that of those that adhered to the other surfaces, such as the CNTs polymer surface. In this investigation, the results obtained using the QCM technique to examine the adhesion of fibroblasts to the polymer-coated surfaces of the electrodes were consistent with others [20].

3.3. BrdU Cell Proliferation Assay. The surface modifications were adopted to evaluate cell viability by BrdU cell proliferation assay. The BrdU cell proliferation assay is an artificial

Table 2: Frequency shifts of QCM and weights of adhered fibroblasts on the electrodes decorated with nonmodified surface, CNTs, and CNTs/SF layers for 12 h of cell incubation.

Cell adhesion	ΔF ($\times 10^3$ Hz)	Δm ($\times 10^3$ ng)
Nonmodified surface	-16.05 ± 0.44	11.02 ± 0.30
CNTs	$-24.85 \pm 0.30^*$	$17.07 \pm 0.21^*$
CNTs/SF	$-29.43 \pm 0.77^*$	$21.52 \pm 0.49^*$

Data are expressed as mean ± standard error, $n = 10$, $^*P < 0.001$ (t-test).

nucleoside that is an analogue of thymidine and used to detect *in vitro* cell proliferation rates [28, 29]. Figure 4 presents the result of the BrdU cell proliferation assay. On day one, no significant difference existed between the aforementioned nonmodified (polystyrene) and CNTs polymer surfaces, but the difference between the CNTs/SF and CNTs polymer surfaces was significant ($P < 0.05$). The number of adherent cells on the CNTs/SF polymer surface was 1.22 times that on the CNTs polymer surface (OD intensity: CNTs polymer surface, 0.0669; CNTs/SF polymer surface, 0.0816). This result of the BrdU assay is consistent with the shifts in the frequency of the QCM (different by a factor of 1.26-fold, Table 2, Δm). Since the number of absorbed cells may vary among plates, normalization is required. Therefore, data after three and five days were compared with those after one day. On day three, the amount of fibroblasts that adhered to the CNTs/SF polymer surface notably exceeded the numbers on the other surfaces. Almost 37% more cells were present on CNTs/SF polymer surface than on the original nonmodified surface, while only 9% of cells were increased on the nonmodified surface, and no significant difference was observed between the CNTs polymer surface and the nonmodified surface. On the fifth day, regardless of whether the number of cells had greatly increased, the percentage difference between the number of newly synthesized cells on the nonmodified surface and that on the CNTs polymer surface was the same as that on the third day (6%). Nevertheless, the difference between the number of cells on the CNTs/SF polymer surface and that on the nonmodified surface had increased from 28 to 41%. Hence, the results demonstrate that cells on the CNTs and nonmodified surface grew at similar rates while those on the CNTs/SF polymer surface grew more rapidly. These results provided the evidence that SF accelerated adult cell proliferation.

3.4. Results of Proteomic Analysis. To investigate the effect of CNTs/SF polymer surface on fibroblasts, a proteomic approach, such as RP-nano-UPLC-ESI-MS/MS analysis, was utilized to analyze cell lysates. The traditional method uses individual antibodies to evaluate the response of a cell to a surface, but the proteomic approach can be used to analyze an enormous number of proteins simultaneously. In this study, fibroblasts were incubated on various modified surfaces with serum-free medium. After 12 h, the cells were lysed, and the cell lysates were digested by trypsin, generating tryptic peptides that were subsequently analyzed by RP-nano-UPLC-ESI-MS/MS. The RP-nano-UPLC-ESI-MS/MS

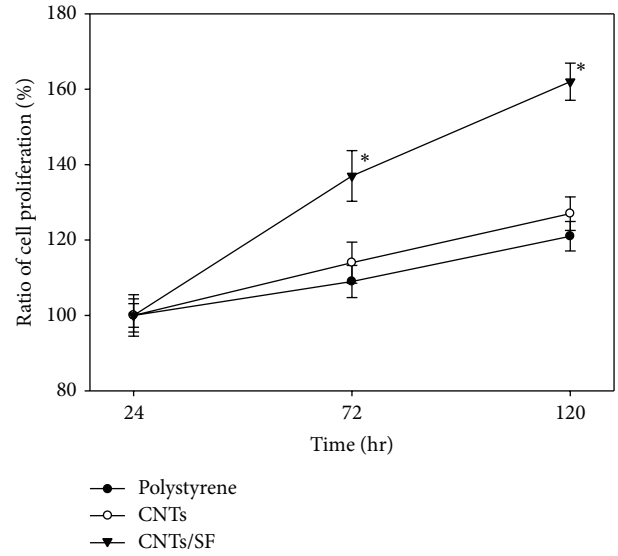

Figure 4: Proliferation (BrdU) test of fibroblasts on surfaces of polystyrene, CNTs and CNTs/SF. (polystyrene served as a control, $n = 10$, mean ± standard error, $^*P < 0.05$, t-test).

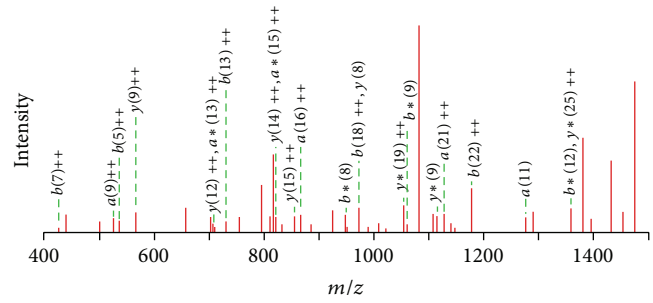

Figure 5: MS/MS spectrum of peptide from the fibroblasts incubated on CNTs/SF polymer surface. The amino acid sequence of the tryptic peptide is R.TPQIPEWLIILASLLALALILAVCIAVNSRRR.C (m/z = 1196.02, +3, from CD44). Interpretation of the complete y-ion and b-ion series provides the peptide sequences as shown.

approach is perhaps the most representative method in proteome research. The fragmentation spectra obtained by the RP-nano-UPLC-ESI-MS/MS analysis in gradient detection mode were compared with a nonredundant protein database using Mascot software. When a protein was identified by three or more unique peptides, no visual assessment of spectra was conducted and the protein was considered to be present in the sample. Figure 5 shows typical MS/MS spectrum of the identified peptides. The MS/MS spectrum represents the amino acid sequence of tryptic peptide, which is triply charged peptides with m/z of 1196.02. The amino acid sequence of the tryptic peptide is TPQIPEWLIILASLLALALILAVCIAVNSRRR. These peptides originated from CD44, and the interpretation of the complete y-ion and b-ion series provides the peptide sequence as shown.

The database search resulted in 127 proteins and most of these were identified at the minimal confidence level, which was only one unique peptide sequence matched.

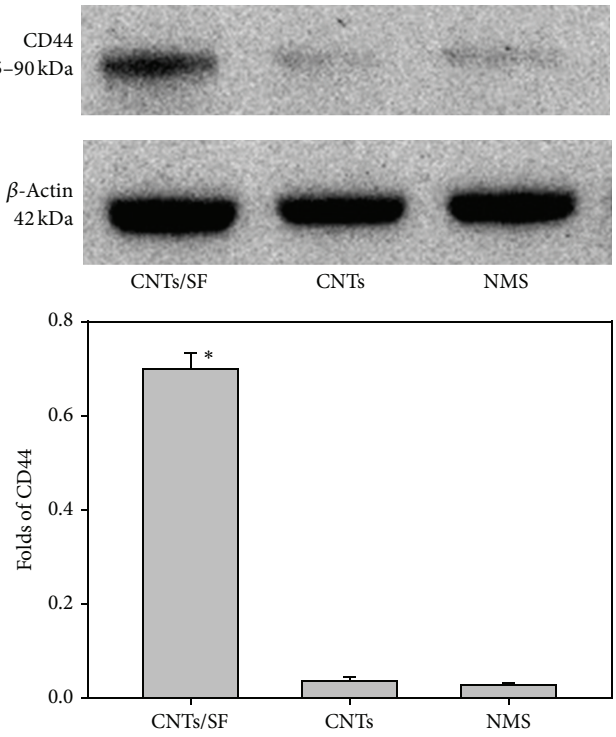

Figure 6: Immunoreactive bands of CD44 and β-actin from fibroblast cells cultured on surfaces of CNTs/SF, CNTs, and NMS (nonmodified surface). The quantitative analysis of Western blotting was carried out using the ImageQuant-TL-7.0 software. These values that refer to the expression of CD44 were normalized by the expression of beta-actin.

Experimental results reported a total of 17 protein identifications with higher confidence levels (Table 3, at least three unique peptide sequences matched), in which CD44 exhibited significant differences between the CNTs/SF and CNTs or nonmodified surfaces. CD44 was involved in cell differentiation, division, and cycle regulation, which was only found in the cell lysate samples from the CNTs/SF polymer surface and selected for validation by Western blot analysis and fluorescence image.

It has been well known that collagen plays important roles in cell adhesion progress [30–33]. In addition, other ECM proteins, such as lamina and fibronectin, were also involved in cell adhesion progress [33, 34]. The aim of this study was to develop a mass spectrometry-based analysis platform and to map the potential proteins and effective pathways associated with cell adsorption on a SF-surface. Thus, the influences of aforementioned proteins on cell adhesion were excluded in our study. Table 4 shows the identified peptides and ontologies of CD44. Proteins were initially annotated by similarity searches using Swiss-Prot/TrEMBL and Bioinformatic Harvester EMBL databases; then, the known functions of the protein could be examined.

CD44 forms a ubiquitously expressed family of cell surface adhering molecules. It is a cell surface glycoprotein that participates in cell-cell and cell-matrix interactions, cell adhesion, and migration. The CD44 gene has only been detected in the higher levels of organisms and the amino acid sequence of the molecule is conserved among mammalian species. CD44 participates in adhesion and migration by binding to SF and other molecules in the ECM [35]. The main ligand of CD44 is hyaluronic acid (HA), an integral component of the ECM. Other CD44 ligands include osteopontin, serglycin, collagens, fibronectin, laminin, SF, and matrix metalloproteinases (MMPs) [36]. The CD44 transmembrane glycoprotein family adds new aspects to these roles by participating in signal transduction processes, which include the establishment of specific transmembrane complexes, and signaling a cascade organizer associated with the actin cytoskeleton [37]. CD44 may function as cellular growth factors, which may be important in tumor metastasis [38].

To validate the influence of CD44 for fibroblast adhesion on the CNTs/SF polymer surface, the cells were blocked by a CD44 antibody and the cell adhesion on the CNTs/SF polymer surface was measured by the QCM technique. When fibroblasts were preincubated with the CD44 antibody, the frequency shift was reduced (from $-29.43 \pm 0.77 \times 10^3$ Hz to $-23.64 \pm 0.58 \times 10^3$ Hz). The result of significantly decreasing the weight of the blocked fibroblasts adhering to CNTs/SF polymer surface was obtained. Through this experiment, CD44 was confirmed to play roles on the cell adhesion which may be associated with the cell adsorption pathway on cell-CNTs/SF polymer surface interactions.

To confirm proteins identified by RP-nano-UPLC-ESI-MS/MS, Western blot analysis was applied to detect the candidate protein that may be associated with cell adhesion/growth pathways on the CNTs/SF polymer surface. Figure 6 presents representative results of the Western blot analyses of cell lysates. CD44 was detected strongly in the cell lysates from the CNTs/SF polymer surface, which is valuable in confirming the SF-induced cell adhesion. In Figure 6, the β-actin was used as a marker for concentration normalization. Compared with the results of Western blotting, the concentration of CD44 in cell lysates from the CNTs/SF polymer surface was 23-fold more than those from nonmodified and CNTs polymer surfaces. This comparison was made using the quantitative analysis software ImageQuant-TL-7.0, and the P value was less than 0.05.

3.5. Cell Morphology by Fluorescence Microscopy. Fibroblasts were cultured in the medium with CD44 antibody onto CNTs/SF polymer surfaces. The cells were observed by immunochemical staining under fluorescence microscopes to determine the morphology of the adhering fibroblasts. In Figure 7 ((a) CNTs polymer surface; (b) CNTs/SF polymer surface; DAPI, blue; vimentin, green; CD44, red; 600X, scale bar: 67 μm for panel A, 100 μm for panel B), the cell fluorescence images showed that CD44 was present in the cell nucleus and membrane. In the present work, we show that the CD44 protein localizes to the nucleus and colocalizes with actin in the external side of plasma membrane protrusions. The cell images showed that the adopted antibodies successfully entered into cells and have the right localization. The CD44 protein-protein interaction pathways were performed

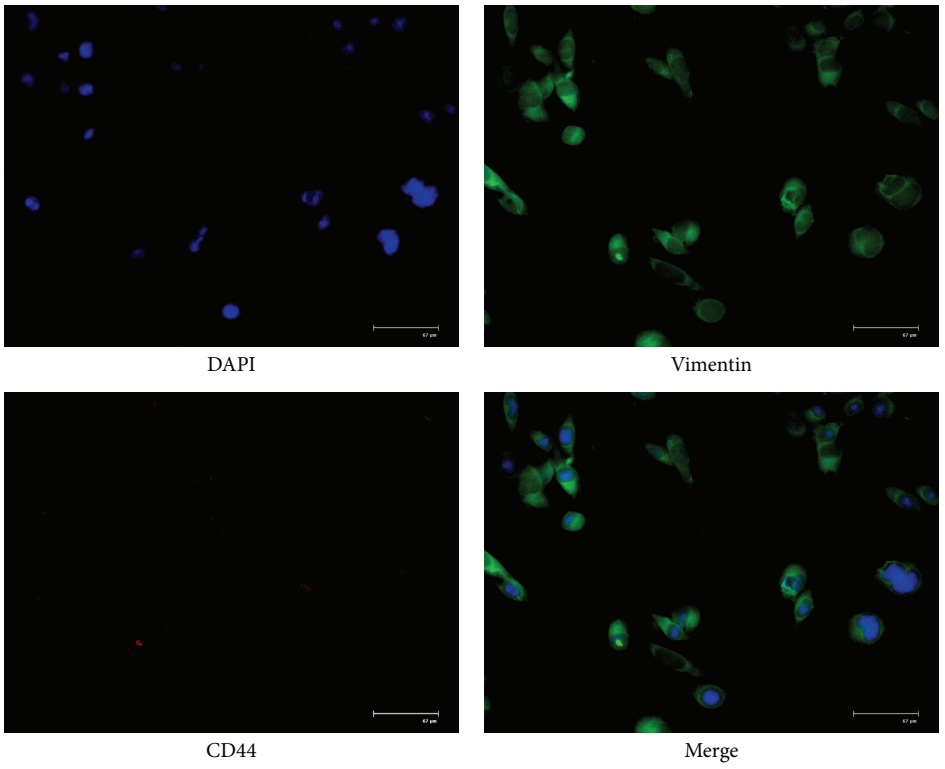

(a)

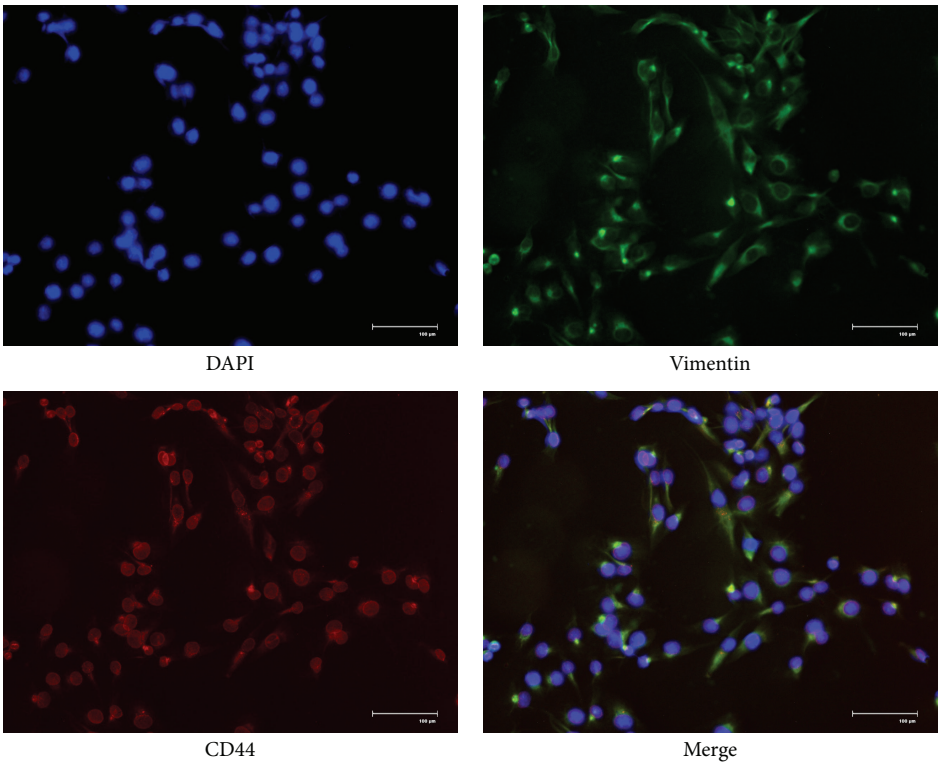

(b)

Figure 7: Immunochemical stains for DAPI (blue), vimentin (green), and CD44 (red) for adhered fibroblasts on CNTs and CNTs/SF polymer surfaces for 12 h of incubation to observe the morphology of the cells ((a) CNTs polymer surface; (b) CNTs/SF polymer surface; scale bar: 67 μm for panel (a), 100 μm for panel (b)).

Table 3: The 17 proteins identified with higher confidence level (at least three unique peptide sequences matched) in this study. The P17, CD44, was only identified on the SF modified surface.

Protein number	Swiss-Prot/ TrEMBL accession number	Protein name	MW (Da)	Score	Match queries	PI	Sequence coverage	Match peptide
P01	Q2M3C7	A-kinase anchor protein SPHKAP	186339	34	3	5.04	8%	R.EACAGEPEPFLSK.S + Carbamidomethyl (C); Phospho (ST) R.QSSMPDSRSPCSR.L + Carbamidomethyl (C); 4 Phospho (ST); Oxidation (M) R.SPVCHRQSSMPDSRSPCSR.L + Carbamidomethyl (C); Deamidated (NQ); 4 Phospho (ST); Oxidation (M)
P02	P05067	Amyloid beta A4 protein	86888	19	3	4.73	9%	K.WDSDPSGTKTCIDTK.E + 5 Phospho (ST) K.GAIIGLMVGGVVIATVIVITLVMLKK.K + Oxidation (M); Phospho (ST) R.ALEVPTDGNAGLLAEPQIAMFCGR.L + 2 Deamidated (NQ); Oxidation (M); Phospho (ST)
P03	Q9UKV3	Apoptotic chromatin condensation inducer in the nucleus	151771	19	3	6.08	2%	R.EREMER.R R.TSTSSSSVQAR.R + 7 Phospho (ST) K.QSADSSSSRSSSSSSSSR.S + Deamidated (NQ); 9 Phospho (ST)
P04	Q9NR09	Baculoviral IAP repeat-containing protein 6	529919	34	3	5.67	4%	R.SRGTPSGTQSSR.E + Deamidated (NQ); 3 Phospho (ST) R.TIPDKIGSTSGAEAANK.I + Deamidated (NQ) R.GRTIPDKIGSTSGAEAANK.I + Phospho (ST)
P05	P51685	C-C chemokine receptor type 8	40817	18	3	8.66	4%	R.ESCEKSSSCQQHSSR.S + Carbamidomethyl (C); Deamidated (NQ); 3 Phospho (ST) R.ESCEKSSSCQQHSSR.S + Carbamidomethyl (C); 2 Deamidated (NQ); 5 Phospho (ST) R.ESCEKSSSCQQHSSR.S + Carbamidomethyl (C); 2 Deamidated (NQ); 5 Phospho (ST)
P06	Q9BV73	Centrosome-associated protein CEP250	280967	19	3	5	5%	R.EPAQLLLLLAK.T K.GQLEVQIQTVTQAK.E + 4 Deamidated (NQ); Phospho (ST) K.AEHVRLSGSLLTCCLRLTVGAQSR.E R.SLFKRGPLLTALSAEAVASALHK.L + 3 Phospho (ST)
P07	O95067	G2/mitotic-specific cyclin-B2	45253	18	3	9	12%	R.KKLQLVGITALLLASK.Y K.VPVQPTKTTNVNKQLKPTASVKPVQMEK.L + Deamidated (NQ); Oxidation (M); Phospho (ST) K.AQNTKVPVQPTKTTNVNK.Q + 3 Deamidated (NQ); 2 Phospho (ST)
P08	Q16478	Glutamate receptor, ionotropic kainate 5	109195	42	4	8.54	7%	K.VSTIIIDANASISHLILRK.A + Deamidated (NQ); 2 Phospho (ST) R.LNCNLTQIGGLLDTK.G + 2 Deamidated (NQ); Phospho (ST) R.YQTYQRMWNYMQSK.Q + 4 Deamidated (NQ); Oxidation (M); 2 Phospho (ST); 2 Phospho (Y) R.LQYLRFASVSLYPSNEDVSLAVSRILK.S + 2 Deamidated (NQ)
P09	Q63HM2	Pecanex-like protein C14orf135	132616	36	7	5.88	9%	K.GDLIKVLVWILVQYCSK.R K.GDLIKVLVWILVQYCSK.R + Deamidated (NQ) K.HQLKDLPGTNLFIPGSVESQR.V K.HQLKDLPGTNLFIPGSVESQR.V + Deamidated (NQ) K.HQLKDLPGTNLFIPGSVESQR.V + 2 Deamidated (NQ) R.LMWIMILECGYTYCSINIK.G + 2 Carbamidomethyl (C); Deamidated (NQ) K.KYVANTVFHSILAGLACGLGTWYLLPNR.I + Carbamidomethyl (C)

Table 3: Continued.

Protein number	Swiss-Prot/ TrEMBL accession number	Protein name	MW (Da)	Score	Match queries	PI	Sequence coverage	Match peptide
P10	O14497	AT-rich interactive domain-containing protein 1A	241892	27	8	6.24	6%	K.SKKSSSSTTTNEK.I + Deamidated (NQ); 6 Phospho (ST) K.HPGLLLILGKLILLHHK.H R.NSMTPNPGYQPSMNTSDMMGR.M + 2 Deamidated (NQ); Oxidation (M); 2 Phospho (ST) R.EMAVVLLANLAQGDSLAARAIAVQK.G + Deamidated (NQ); Oxidation (M) R.ITATMDDMLSTRSSTLTEDGAK.S + 2 Oxidation (M); 4 Phospho (ST) K.APGSDPFMSSGQGPNGGMGDPYSR.A + 4 Phospho (ST); Phospho (Y) R.GYMQRNPQMPQYSSPQPGSALSPR.Q + Oxidation (M); Phospho (ST) K.RNSMTPNPGYQPSMNTSDMMGR.M + Deamidated (NQ); Oxidation (M); 3 Phospho (ST); Phospho (Y)
P11	P50224	Sulfotransferase 1A3/1A4	34174	23	4	5.68	6%	R.LIKSHLPLALLPQTLLDQK.V R.LIKSHLPLALLPQTLLDQK.V + Deamidated (NQ) R.LIKSHLPLALLPQTLLDQK.V + Deamidated (NQ) R.LIKSHLPLALLPQTLLDQK.V + 2 Deamidated (NQ)
P12	Q09666	Neuroblast differentiation-associated protein AHNAK	628699	39	3	5.8	2%	K.VHAPGLNLSGVGGKMQVGGDGVK.V + Deamidated (NQ); Oxidation (M); Phospho (ST) R.AGAISASGPELQGAGHSKLQVTMPGIKVGGSGVNVNAK.G + 2 Deamidated (NQ); Oxidation (M); 4 Phospho (ST) K.VKVPEVDVRGPK.V
P13	Q63HM2	Pecanex-like protein C14orf135	132616	35	3	5.88	5%	R.TSCMPSSKMK.E + Carbamidomethyl (C); 2 Oxidation (M); 2 Phospho (ST) K.HQLKDLPGTNLFIPGSVESQR.V + Deamidated (NQ) K.HQLKDLPGTNLFIPGSVESQR.V + 2 Deamidated (NQ)
P14	O43182	Rho GTPase-activating protein 6	105882	32	4	7	9%	R.EQQVTQK.K K.DPGMTGSSGDIFESSSLR.A + Phospho (ST) -.MSAQSLLHSVFSCSSPASSSAASAK.G + Deamidated (NQ); Oxidation (M); 3 Phospho (ST) R.EQQVTQKKLSSANSLPAGEQDSPR.L + 2 Phospho (ST)
P15	O76074	cGMP-specific 3′, 5′-cyclic phosphodiesterase	99921	39	5	5.74	10%	R.WILSVKKNYR.K + Phospho (ST) K.KIAATIISFMQVQK.C + Oxidation (M); Phospho (ST) K.ELNIEPTDLMNREKK.N + Deamidated (NQ) K.TQSILCMPIKNHREEVVGVAQAINK.K + 4 Deamidated (NQ); 2 Phospho (ST) R.GHTESCSCPLQQSPRADNSAPGTPTRK.I + 2 Deamidated (NQ); Phospho (ST)
P16	O60299	ProSAP-interacting protein 1	71747	35	5	7.56	9%	K.SRTMTPAGGSGSGLSDSGR.N + Oxidation (M) K.SRTMTPAGGSGSGLSDSGR.N + Oxidation (M); 4 Phospho (ST) R.IGTASYGSGSGGSSGGGSGYQDLGTSDSGR.A + 4 Phospho (ST); Phospho (Y) K.SRTMTPAGGSGSGLSDSGR.N + Oxidation (M); 4 Phospho (ST) K.QLQLSYVEMYQRNQQLER.R + 3 Deamidated (NQ); Phospho (Y)
P17	P16070	CD44	81487	79	3	5.13	16%	R.YGFIEGHVVIPR.I R.TPQIPEWLIILASLLALALILAVCIAVNSRRR.C K.SQEMVHLVNKESSETPDQFMTADETRNLQNVDMK.I

Table 4: The identified peptides and gene ontologies of CD44.

Accession number	Protein name	Subcellular location	Biological process	Molecular function
P16070	CD44	Membrane, cytoplasm, Golgi apparatus	Cell adhesion, cellular response to fibroblast growth factor stimulus	Blood group antigen, receptor, collagen binding

CD44 is the receptor for hyaluronic acid (HA) and mediates cell-cell and cell-matrix interactions through its affinity for HA and possibly also through its affinity for other ligands such as osteopontin, collagens, and matrix metalloproteinases (MMPs).

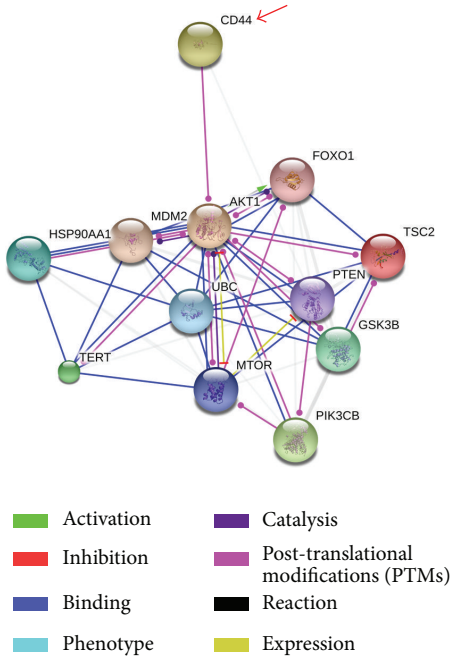

Figure 8: The CD44 protein-protein interaction pathways were performed by String 9.0 Web software. The CD44 can turn on the PI3 K/AKT/mTOR pathway, which is responsible for the proliferation and is required for survival of the majority of cells.

by String 9.0 Web software (Figure 8). The CD44 can turn on the PI3 K/AKT/mTOR pathway, which is responsible for the proliferation and is required for survival of the majority of cells. The hypothesis of the mTOR pathway is that it acts as a master switch of cellular catabolism and anabolism, thereby determining the growth and proliferation of the cells. Activation of PI3 K/AKT/mTOR signaling through mutation of pathway components as well as through activation of upstream signaling molecules occurs in the majority of cells contributing to deregulation of proliferation, resistance to apoptosis, and changes in the metabolism characteristic of transforming cells.

As expected, the CNTs/SF polymer surface caused larger frequency shifts than the CNTs polymer surface. Indeed, the presence of SF on the surface supported *in vitro* cell adhesion, and SF participates importantly in cell proliferation [39]. In this study, the results were mutually consistent when using the BrdU cell proliferation assay and QCM techniques which were utilized to investigate the adhesions of fibroblasts to polymer surfaces that coated the electrodes. However, these methods are limited to the quantitative analysis of cell amount. Proteomic analysis provides a means for the large-scale characterization of the differential expression of proteins from cells on modified surfaces. The mass spectrometry-based proteomics approach has many advantages, especially in identification of related proteins. Experimental results indicate that the CNTs/SF polymer surface may be able to activate several cell-material interaction pathways and promote cell adhesion. Consequently, previous unfamiliar proteins can be found and the interaction of cell-material may be established. The proteomic scheme was adopted to identify proteins with differential expression, which participate importantly in the adhesion of cells to material surfaces.

4. Conclusions

In this study, a biopolymer surface was formatted with SF. According to the results concerning fibroblasts that were stained with DAPI/vimentin/CD44, BrdU cell proliferation assay, and the frequency shifts that were determined using QCM, the numbers and mass of fibroblasts that adhered to the CNTs/SF polymer surface of electrodes were significantly higher than those of fibroblasts on other surfaces. The SF modified surface has been confirmed and improved the cell adhesion. To evaluate the responses of cellular proteins induced by SF-modified surfaces, mass spectrometry-based proteomics is adopted to analyze complex proteins of cell lysate and to profile proteins based on their associated cell-surface interactions. By utilizing proteomic approaches, it is indicated that the SF modified surface induces fibroblasts to express CD44 as an interactive protein between cell and material surface to enhance cell adhesion. Although the pathways of the interactions between CD44 and SF were unclear, the cell adhesion affected by CD44 was established. In summary, the functional groups of biomaterials may induce the secretion of proteins from cells. This study proposed a new approach for the detection of proteins to assess the response of fibroblasts to a material surface. Knowing the responses of cellular proteins induced by biomaterials may assist the development of applications in the immediate future.

Novelty of the Study

The preparation and characterization of silk fibroin modified surface were confined. The pathway of silk fibroin biopolymer surface induced cell membrane protein activation was identified by proteomic approaches. The silk fibroin biopolymer surface may induce and activate CD44 to enhance cell adhesion and proliferation.

Conflict of Interests

The authors declare that there is no conflict of interests regarding the publication of this paper.

Authors' Contribution

Ming-Hui Yang and Tze-Wen Chung contributed equally to this work as first authors.

Acknowledgments

The authors thank the Center of Excellence for Environmental Medicine, Kaohsiung Medical University, for the-assistance in protein identification, and S. Sheldon, MT(ASCP), of Oklahoma University Medical Center Edmond (retired), for fruitful discussions and editorial assistance before submission. This work was supported by research Grants NSC-102-3114-Y-492-076-023, NSC-100-2320-B-037-007-MY3, and NSC-099-2811-E-224-002 from the National Science Council, MOHW103-TD-B-111-05 from Ministry of Health and Welfare, and NSYSUKMU 102-P006 from NSYSU-KMU Joint Research Project, Taiwan.

References

[1] B. Kasemo, "Biological surface science," *Surface Science*, vol. 500, no. 1–3, pp. 656–677, 2002.

[2] M. P. Lutolf and J. A. Hubbell, "Synthetic biomaterials as instructive extracellular microenvironments for morphogenesis in tissue engineering," *Nature Biotechnology*, vol. 23, no. 1, pp. 47–55, 2005.

[3] E. Cenni, F. Perut, and N. Baldini, "*In vitro* models for the evaluation of angiogenic potential in bone engineering," *Acta Pharmacologica Sinica*, vol. 32, no. 1, pp. 21–30, 2011.

[4] H. Wang, "Dispersing carbon nanotubes using surfactants," *Current Opinion in Colloid and Interface Science*, vol. 14, no. 5, pp. 364–371, 2009.

[5] L. Su, F. Gao, and L. Mao, "Electrochemical properties of carbon nanotube (CNT) film electrodes prepared by controllable adsorption of CNTs onto an alkanethiol monolayer self-assembled on gold electrodes," *Analytical Chemistry*, vol. 78, no. 8, pp. 2651–2657, 2006.

[6] N. A. Ayoub, J. E. Garb, R. M. Tinghitella, M. A. Collin, and C. Y. Hayashi, "Blueprint for a high-performance biomaterial: full-length spider dragline silk genes," *PloS ONE*, vol. 2, no. 6, article e514, 2007.

[7] I. C. Um, H. Kweon, Y. H. Park, and S. Hudson, "Structural characteristics and properties of the regenerated silk fibroin prepared from formic acid," *International Journal of Biological Macromolecules*, vol. 29, no. 2, pp. 91–97, 2001.

[8] X. Zhang, M. R. Reagan, and D. L. Kaplan, "Electrospun silk biomaterial scaffolds for regenerative medicine," *Advanced Drug Delivery Reviews*, vol. 61, no. 12, pp. 988–1006, 2009.

[9] N. Guziewicz, A. Best, B. Perez-Ramirez, and D. L. Kaplan, "Lyophilized silk fibroin hydrogels for the sustained local delivery of therapeutic monoclonal antibodies," *Biomaterials*, vol. 32, no. 10, pp. 2642–2650, 2011.

[10] R. Rajkhowa, E. S. Gil, J. Kluge et al., "Reinforcing silk scaffolds with silk particles," *Macromolecular Bioscience*, vol. 10, no. 6, pp. 599–611, 2010.

[11] L. Soffer, X. Wang, X. Zhang et al., "Silk-based electrospun tubular scaffolds for tissue-engineered vascular grafts," *Journal of Biomaterials Science, Polymer Edition*, vol. 19, no. 5, pp. 653–664, 2008.

[12] Y. Yang, X. Chen, F. Ding, P. Zhang, J. Liu, and X. Gu, "Biocompatibility evaluation of silk fibroin with peripheral nerve tissues and cells *in vitro*," *Biomaterials*, vol. 28, no. 9, pp. 1643–1652, 2007.

[13] C. Li, C. Vepari, H.-J. Jin, H. J. Kim, and D. L. Kaplan, "Electrospun silk-BMP-2 scaffolds for bone tissue engineering," *Biomaterials*, vol. 27, no. 16, pp. 3115–3124, 2006.

[14] Y. Wang, D. J. Blasioli, H.-J. Kim, H. S. Kim, and D. L. Kaplan, "Cartilage tissue engineering with silk scaffolds and human articular chondrocytes," *Biomaterials*, vol. 27, no. 25, pp. 4434–4442, 2006.

[15] F. G. Omenetto and D. L. Kaplan, "New opportunities for an ancient material," *Science*, vol. 329, no. 5991, pp. 528–531, 2010.

[16] M. R. Wilkins, J.-C. Sanchez, K. L. Williams, and D. F. Hochstrasser, "Current challenges and future applications for protein maps and post-translational vector maps in proteome projects," *Electrophoresis*, vol. 17, no. 5, pp. 830–838, 1996.

[17] S. Oughlis, S. Lessim, S. Changotade et al., "Development of proteomic tools to study protein adsorption on a biomaterial, titanium grafted with poly(sodium styrene sulfonate)," *Journal of Chromatography B: Analytical Technologies in the Biomedical and Life Sciences*, vol. 879, no. 31, pp. 3681–3687, 2011.

[18] J. Sund, H. Alenius, M. Vippola, K. Savolainen, and A. Puustinen, "Proteomic characterization of engineered nanomaterial-protein interactions in relation to surface reactivity," *ACS Nano*, vol. 5, no. 6, pp. 4300–4309, 2011.

[19] D. Lavigne, L. Guerrier, V. Gueguen et al., "Culture of human cells and synthesis of extracellular matrix on materials compatible with direct analysis by mass spectrometry," *Analyst*, vol. 135, no. 3, pp. 503–511, 2010.

[20] M. H. Yang, S. B. Jong, C. Y. Lu et al., "Assessing the responses of cellular proteins induced by hyaluronic acid-modified surfaces utilizing mass spectrometry-based profiling system: overexpression of CD36, CD44, CDK9, and PP2A," *Analyst*, vol. 137, no. 21, pp. 4921–4933, 2012.

[21] T.-W. Chung, T. Limpanichpakdee, M.-H. Yang, and Y.-C. Tyan, "An electrode of quartz crystal microbalance decorated with CNT/chitosan/fibronectin for investigating early adhesion and deforming morphology of rat mesenchymal stem cells," *Carbohydrate Polymers*, vol. 85, no. 4, pp. 726–732, 2011.

[22] K. A. Marx, "Quartz crystal microbalance: a useful tool for studying thin polymer films and complex biomolecular systems at the solution-surface interface," *Biomacromolecules*, vol. 4, no. 5, pp. 1099–1120, 2003.

[23] A. Pomorska, D. Shchukin, R. Hammond, M. A. Cooper, G. Grundmeier, and D. Johannsmann, "Positive frequency shifts observed upon adsorbing micron-sized solid objects to a quartz crystal microbalance from the liquid phase," *Analytical Chemistry*, vol. 82, no. 6, pp. 2237–2242, 2010.

[24] M. Zhang, L. Su, and L. Mao, "Surfactant functionalization of carbon nanotubes (CNTs) for layer-by-layer assembling of CNT multi-layer films and fabrication of gold nanoparticle/CNT nanohybrid," *Carbon*, vol. 44, no. 2, pp. 276–283, 2006.

[25] E. L. Bakota, L. Aulisa, D. A. Tsyboulski, R. B. Weisman, and J. D. Hartgerink, "Multidomain peptides as single-walled carbon

nanotube surfactants in cell culture," *Biomacromolecules*, vol. 10, no. 8, pp. 2201–2206, 2009.

[26] S. J. Lee, S. Y. Kim, and Y. M. Lee, "Preparation of porous collagen/hyaluronic acid hybrid scaffolds for biomimetic functionalization through biochemical binding affinity," *Journal of Biomedical Materials Research—Part B Applied Biomaterials*, vol. 82, no. 2, pp. 506–518, 2007.

[27] R. R. Pochampally, J. R. Smith, J. Ylostalo, and D. J. Prockop, "Serum deprivation of human marrow stromal cells (hMSCs) selects for a subpopulation of early progenitor cells with enhanced expression of OCT-4 and other embryonic genes," *Blood*, vol. 103, no. 5, pp. 1647–1652, 2004.

[28] B. Lehner, B. Sandner, J. Marschallinger et al., "The dark side of BrdU in neural stem cell biology: detrimental effects on cell cycle, differentiation and survival," *Cell and Tissue Research*, vol. 345, no. 3, pp. 313–328, 2011.

[29] S. T. Becker, T. Douglas, Y. Acil et al., "Biocompatibility of individually designed scaffolds with human periosteum for use in tissue engineering," *Journal of Materials Science: Materials in Medicine*, vol. 21, no. 4, pp. 1255–1262, 2010.

[30] P. A. Harper, P. Brown, and R. L. Juliano, "Fibronectin-independent adhesion of fibroblasts to extracellular matrix material: partial characterization of the matrix components," *Journal of Cell Science*, vol. 63, pp. 287–301, 1983.

[31] W. M. Petroll, L. Ma, and J. V. Jester, "Direct correlation of collagen matrix deformation with focal adhesion dynamics in living corneal fibroblasts," *Journal of Cell Science*, vol. 116, no. 8, pp. 1481–1491, 2003.

[32] M. Miron-Mendoza, J. Seemann, and F. Grinnell, "Collagen fibril flow and tissue translocation coupled to fibroblast migration in 3D collagen matrices," *Molecular Biology of the Cell*, vol. 19, no. 5, pp. 2051–2058, 2008.

[33] T. J. Fuja, E. M. Ostrem, M. N. Probst-Fuja, and I. R. Titze, "Differential cell adhesion to vocal fold extracellular matrix constituents," *Matrix Biology*, vol. 25, no. 4, pp. 240–251, 2006.

[34] M. Dimitrijevic-Bussod, V. S. Balzaretti-Maggi, and D. M. Gadbois, "Extracellular matrix and radiation G1 cell cycle arrest in human fibroblasts," *Cancer Research*, vol. 59, no. 19, pp. 4843–4847, 1999.

[35] S. Goodison, V. Urquidi, and D. Tarin, "CD44 cell adhesion molecules," *Molecular Pathology*, vol. 52, no. 4, pp. 189–196, 1999.

[36] B. Ghosh, Y. Li, and S. A. Thayer, "Inhibition of the plasma membrane Ca^{+2} pump by CD44 receptor activation of tyrosine kinases increases the action potential afterhyperpolarization in sensory neurons," *Journal of Neuroscience*, vol. 31, no. 7, pp. 2361–2370, 2011.

[37] H. Ponta, L. Sherman, and P. A. Herrlich, "CD44: from adhesion molecules to signalling regulators," *Nature Reviews Molecular Cell Biology*, vol. 4, no. 1, pp. 33–45, 2003.

[38] H. Ponta, D. Wainwright, and P. Herrlich, "The CD44 protein family," *International Journal of Biochemistry and Cell Biology*, vol. 30, no. 3, pp. 299–305, 1998.

[39] J. R. E. Fraser, T. C. Laurent, and U. B. G. Laurent, "Hyaluronan: its nature, distribution, functions and turnover," *Journal of Internal Medicine*, vol. 242, no. 1, pp. 27–33, 1997.